Sugar surfactant based microemulsions at solid surfaces

vorgelegt von
M. Sc.
Salome Vargas Ruiz
geboren in Bogota, Kolumbien

von der Fakultät II - Mathematik und Naturwissenschaften
an der Technischen Universität Berlin
zur Erlangung des akademischen Grades

Doktor der Naturwissenschaften
(Dr. rer. nat.)

genehmigte Dissertation

Promotionsausschuss:

Vorsitzender:	Prof. Dr. Reinhard Schomäcker
1. Gutachterin:	Prof. Dr. Regine von Klitzing
2. Gutachterin:	Prof. Dr. Conxita Solans Marsa

Tag der wissenschaftlichen Aussprache: 15.02.2017

Berlin 2017

Acknowledgements

I would like to thank all the people, who in one way or another gave me their support and help to reach this goal. First, I would like to express my deep gratitude to Prof. Dr. Regine von Klitzing and Dr. Stefan Weller for giving me the opportunity to work in their research group and for offer me all the support and motivation to keep going in this interesting and challenging project. I would like also thank Prof. Thomas Hellweg and his group for their cooperation and continuous help in this project.

My work would not have been possible without the help of Samantha Micciulla, Olaf Soltwedel and Jana Lutzki. Their advice were essential for the characterization and study of the microemulsion, as well as, in the data analysis. I really enjoyed the shared time with the members Stranski group, who made my stay at the TU-berlin very pleasant.

I am thankful for the strength that God has given to my life, as well as for his infinite love and light to guided me through the best trails that I could go. I want to thank enormously my family, the engine of my life, for their unconditional love and support in this adventure. I thank with all my heart to Pietro Toriello for his advice and constant encouragement, without his company in this stage of my life, it would not have been the beautiful journey that has been so far. Finally, who can imagine being on this track without good friends? Thanks guys for such great moments, especially to Holman, Yazmin, Muriel, Martha, Karim, and Bita, who fill my life with wonderful memories.

Abstract

This study investigates the structural properties of sugar surfactant-based microemulsions at solid-liquid interfaces. In particular, this thesis attempts to correlate these structural properties at solid-liquid interfaces with the ability of microemulsions to wet the substrate and the mobility of model molecules from the wetted surface to the bulk of the microemulsion. The first part of this study is dedicated to studying the bulk structural properties of sugar surfactant based microemulsions prepared with tetradecane (nonpolar) and methyl oleate (polar) oils. The bulk structure of the two sugar surfactant microemulsion systems was characterized by means of small-angle neutron scattering, diffusion nuclear magnetic resonance spectroscopy, and cryo-scanning electron microscopy. The complementary results of the three employed methods revealed the formation elongated channels of oil and water, whose degree of connectivity depends on the oil and water contents. In the second part of this study, the wetting properties and the near-surface structure of the sugar surfactant based microemulsion on model surfaces were investigated. The near-surface structure was evaluated with neutron reflectometry and grazing-incidence small-angle neutron scattering. The scattering length density profiles estimated from the neutron reflectograms reveal that both tetradecane and methyl oleate based microemulsions develop a distinct structure in the perpendicular direction to the hydrophilic solid-liquid interface. In contrast, at the hydrophobic solid-liquid interface the structuring of the methyl oleate microemulsions is hindered, whereas the structuring of the tetradecane based microemulsion is preserved. The obtained results suggest that the adsorption of oil or surfactant molecules at the solid-liquid interface influences the interfacial structuring of microemulsions. Furthermore, these adsorption processes at the interface also had a strong implication on the wetting processes on the planar surfaces as demonstrated by dynamic contact angle measurements. In the last part of the study, the efficiency of microemulsions to extract test molecules from model surfaces were monitored by spectroscopic and chromatographic methods. The extraction and solubilization processes are strongly affected by the structure of the microemulsion, where an efficient extraction of the model molecules is achieved by the employment of symmetric bicontinuous microemulsions. In general, the presented results are of practical importance as the ability to identify the parameters that influence the interaction of the microemulsions with any surface could be a new powerful tool for the formulation of microemulsions to improve their performance in any desired application, such as the decontamination of surfaces.

Contents

List of symbols and abbreviations

α	Oil to water ratio
γ	Sugar surfactant content
δ	Co-surfactant content
κ	Bending elastic constant
$\bar{\kappa}$	Gaussian elastic constant
κ_{SANS}	Renormalized bending elasticity constant
κ_{bare}	Bare bending elasticity constant
f_a	Amphiphilicity factor
d_{TS}	Domain size estimated by Teubner-Strey model
ξ_{TS}	Correlation length estimated by Teubner-Strey model
θ_{Adv}	Advance contact angle
θ_{Rec}	Receding contact angle
θ_{hys}	Hysteresis of dynamic contact angle
θ_c	Critical angle
θ_i	Incident angle
Λ	Penetration depth
μ	Dynamic viscosity
E_c	percentage of extraction of the contaminant at the equilibrium stage
k	Overall extraction rate coefficient
H	Mean curvature
G	Gaussian curvature
H_0	Spontaneous curvature
R	Principal curvature
AFM	Atomic force microscopic
Ca	Capillary number
CEES	2-chloroethyl ethyl sulfide
GISANS	Grazing incidence small angle neutron scattering
MO	Methyl oleate
NR	Neutron reflectometry
NMR	Neutron magnetic resonance
OWRK	Owens-Wendt-Rabel-Kaelble method
SANS	Small-angle neutron scattering
SEM	Scanning electron microscopy
SLD	Scattering length density
TD	Tetradecane
TPM	Tilted plate method
WPM	Wilhelmy plate method

*Non-essential and empirical parameters are not included

Chapter 1

Introduction

Sugar surfactant based microemulsions are receiving considerable attention as tolerant and biological acceptable technologies, due to their gentle and green performance with structural stability in a wide temperature range.[1] These systems are becoming potential media for environmentally friendly cleaning and extraction technologies to decontaminate solid sorptive surfaces exposed to highly toxic and lipophilic compounds.[2,3] The advantage of microemulsions as decontamination media relies on the differences in polarity of their oil and water nanodomains and the high interfacial area between them.[4] Thanks to these properties, the lipophilic contaminants can be easily solubilized in the oil nanodomains, whereas their degradation into innocuous products takes place mostly at the interfaces by means of active ingredients located at the aqueous nanodomains (e.g., oxidizing agents, solid catalytic agents, enzymes, etc.).

A lot of effort has been carried out in the field of this environmentally friendly cleaning technology in order to determine the relationship between the microemulsion properties (composition and structure) and their efficiency to carry out the degradation of the contaminant in the bulk of the microemulsion.[3,5] However, before the degradation processes occur, a number of important steps that have not been extensively studied so far should take place. These steps include the wetting of the surface by the microemulsions and the subsequent extraction and solubilization of the contaminant. Both wetting and extraction take place near the solid-liquid interface. In this study, it is expected that the microemulsion composition and structural properties influence the wetting of the surfaces and that, the presence of the surface simultaneously influences the microemulsion composition and structure close to the interface. These complex interactions between microemulsions and solid surfaces also influence the extraction processes since the microemulsion structure close to the interface defines the pathways and potential barriers that the extracted contaminants have to overcome in order to reach the bulk of the microemulsions. Therefore, a fundamental knowledge of the interactions between microemulsions and solid surfaces is of a great importance.

In this context, this thesis attempts to gain a better understanding of the structural properties of sugar surfactant based microemulsions at the solid-liquid interface, and the correlation of those structural properties with the substrate wetting and contaminant mobility from the wetted surface to the bulk of the microemulsion. This knowledge not only allows to establish the parameters that influence the wetting and the extraction process but, most importantly, it could be used to develop a new approach for the formulation of

microemulsions, where their composition and structure can be tuned in order to optimize their contact with different types of surfaces. Thereby, allowing to enhance the efficiency of the microemulsion in any desired application.

In this project, sugar surfactant based microemulsions prepared by using tetradecane (nonpolar) and methyl oleate (polar) oils are studied. The first part of the results and discussion of this thesis is dedicated to the structural characterization in bulk of sugar surfactant based microemulsions (Chapter 5). The structural characterization of the sugar surfactant based microemulsions is carried out by means of three complementary techniques: small neutron scattering, diffusion nuclear magnetic resonance spectroscopy, and scanning electron microscopy. The complementary results allow us to clearly assess the influence of microemulsion composition on its structural properties in the bulk. Such characterization is relevant because it is the base to gain a fundamental understanding of the effect of the microemulsion composition and structure on their interaction with solid surfaces and their capacity to wet the surface, and to extract contaminants from solid substrates.

In Chapter 6, the structural properties of microemulsions at solid-liquid interfaces are investigated with neutron scattering techniques (neutron reflectometry and grazing-incidence small-angle neutron scattering). The extension of the structuring of the microemulsions at the interface is correlated to the structural properties of the microemulsion in the bulk and the polarity of the surface. The knowledge of microemulsion structure at the solid-liquid interface is the key to understand the wetting of solid surfaces by microemulsions. In this respect, the wetting of planar and porous surfaces of different polarities by microemulsions is addressed in Chapter 7. The wetting of model surfaces by sugar surfactant based microemulsion is evaluated by means of dynamic contact angle measurements carried out using the tilted plate, Wilhelmy plate, and Washburn methods. Differences in the wetting of the hydrophobic and hydrophilic surfaces by microemulsions are discussed in relation to the variation of microemulsion composition and structure near the interface.

In Chapter 8, the efficiency of the prepared microemulsions to extract lipophilic model molecules out of sorptive surfaces is presented. Spectroscopy and chromatography techniques are employed to monitor the extraction processes of the test molecules. In order to gain insight into the correlation between the structure and composition of the microemulsion and its extraction efficiency, the kinetics of the extraction process are studied by means of four different models.

Chapter 2

Scientific background

2.1 Microemulsions

Microemulsions are thermodynamically stable mixtures of water and oil nanodomains stabilized by a surfactant monolayer. They are microscopically a single phase and optically transparent liquid.[6–8] These thermodynamically stable systems were first identified by Schulman and Winsor,[9,10] where Schulman was the first person to denominate this kind of systems as microemulsions.[11] Nowadays, it is accepted that the term "microemulsions" is misleading as the actual size of the structure of these complex fluids is on the nanoscale. In order to emphasize the microemulsion properties, this section introduces the composition and phase diagrams of different microemulsion systems, followed by a description of microemulsion structures and their relationship to the mechanical properties of the surfactant membrane.

2.1.1 Composition and phase diagram of microemulsions

A simple microemulsion system can be composed of oil, water, and surfactant at specific temperature and pressure, meaning that the stability and properties of this simple microemulsion system would depend on five variables.[12] However, most microemulsion systems do not correspond to this simple case, as more additives are used to modify microemulsion properties. For instance, the tuning on the structural properties and phase boundaries of microemulsions can be achieved by the addition of salt, co-surfactant or polymer chains.[13–15] In microemulsions prepared with ionic or alkyl polyglycol ethers surfactants, the addition of salt influences the hydration sphere and the solubility of those surfactants; as a consequence, changes in the phase boundaries and mechanical properties of the surfactant membrane are produced.[13] Changes in the mechanical properties and curvature of the surfactant membrane are also induced by the addition of co-surfactants (e.g., short chain alcohols),[14] as the co-surfactant interpenetrates the surfactant membrane and enhances its flexibility. The addition of diblock copolymers into microemulsions leads to an increase in the size of surfactant membrane, which in turns favors the solubilization capacity of the microemulsion (lower amount of surfactant is required for the formation of one-phase microemulsions).[13–15]

This overview of multiple components, which can be used in the preparation of microemulsions, shows the complexity of their formulation. Therefore, the study of microemulsion systems is focused in the first place on determining the conditions in which these systems are formed. This can be achieved by studying their phase diagrams. The phase diagrams of microemulsion systems are usually presented as a Gibbs triangle.[16] Each corner of the triangle represents a pure component of the microemulsion, while the sides of the triangle account for the fraction of a specific component with respect to the others. The triangle extends to a Gibbs prism or tetrahedron when additional variables are introduced for tuning the properties of the microemulsions (e.g., temperature, co-surfactant).

In this section, exemplary phase diagrams of microemulsions based on non-ionic alkyl polyglycol ethers and sugar surfactants are presented and compared. The fraction of the components in the microemulsion are represented by the oil-to-water ratio (α), while the contents of sugar surfactant and co-surfactant are represented by (γ) and (δ), respectively.

$$\alpha = \frac{mass_{\text{oil}}}{mass_{\text{oil}} + mass_{\text{water}}} \tag{2.1}$$

$$\gamma = \frac{mass_{\text{surfactant}}}{mass_{\text{surfactant}} + mass_{\text{oil}} + mass_{\text{water}}} \tag{2.2}$$

$$\delta = \frac{mass_{\text{cosurfactant}}}{mass_{\text{cosurfactant}} + mass_{\text{surfactant}} + mass_{\text{oil}} + mass_{\text{water}}} \tag{2.3}$$

Ternary Microemulsion systems

In the case of microemulsion systems stabilized by non-ionic alkyl polyglycol ether surfactants (C_iE_j), the temperature as an external variable plays a significant role in the study of the phase diagrams, since the temperature rise causes a change in the conformation of the ethoxylate chains from the most polar conformation gauche to a less polar trans conformation trans.[17] The change of surfactant conformation results in a phase inversion of the microemulsion system and a change in the curvature of the surfactant membrane.[7] Typically, the phase diagrams of the C_iE_j-based microemulsions are presented as the Gibbs prism. This prism can be seen as the result of stacking Gibbs triangle isotherms of

their ternary components on top of each other, where the vertical component is associated with the change of temperature (Figure 2.1).[13,18]

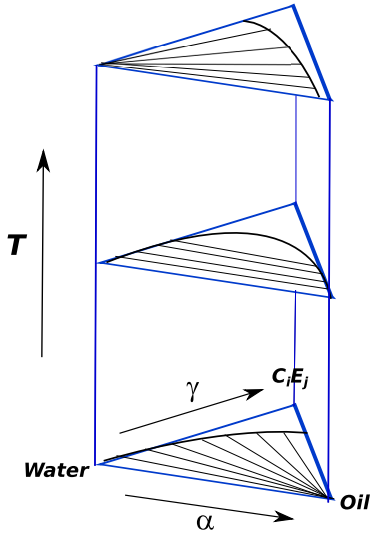

Figure 2.1: Scheme of the ternary phase diagrams of the microemulsions based on alkyl polyglycol ethers surfactants.

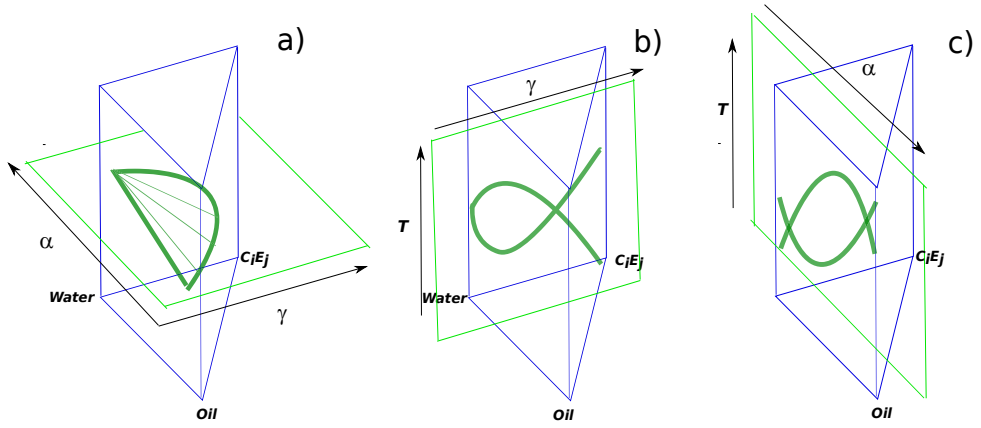

Figure 2.2: Two-dimensional cuts of the prism phase diagram. a) Δ-cut, b) γ cut and c) χ cut. Representation adapted from Ref.[19]

Due to the multiple variables presented in the determination of the Gibbs phase diagrams, these phase diagrams are usually cut in different sections to reduce the number of variables and thereby facilitate their evaluation.[19] The most common cuts in the Gibbs phase diagrams are the Δ-cut, the γ cut, and the χ cut (Figure 2.2a). The Δ cut is made at a constant temperature, whereas the oil-to-water ratio (α) and surfactant concentration (α) are varied. This is a typical ternary phase diagram, which gives information about the number of phases and their composition at a certain temperature. It is characterized by the demixing line and the tie-lines. The demixing line (curve) separates the number of

phases in the systems. Above the demixing line, one single phase microemulsion is found, whereas the formation of two or three phases is given below the demixing line. In the case of a two-phase region, the composition of each phase is given by the tie-lines (straight lines).[16]

In the γ cut, the temperature of the system and concentration of the surfactant (γ) are systematically varied, while the oil-to-water ratios (α) are maintained constant (Figure 2.2b). This cut is denominated as the "fish" phase diagram due to the shape of the phase boundaries. The most important feature of this phase diagram is the x point (i.e., the point where the body and the tail of the fish meet). This point provides information about the temperature and the surfactant concentration required to form a one-phase microemulsion.[12]

The χ cut is given at a constant surfactant concentration, and the temperature is plotted as a function of oil-to-water ratio (α). This cut allows for an estimation of the region where the O/W or W/O structures can be formed (Figure 2.2c).

Quaternary microemulsion systems

In contrast to the C_iE_j surfactant based microemulsions, the tuning of the structure and phases in sugar surfactant based microemulsions is independent of temperature, since temperature changes do not influence the curvature of the sugar surfactant membrane due to the strong hydrogen bonds between the hydroxyl groups of the head group of the sugar surfactant and the water molecules.[1,14] Thus, sugar surfactants contribute to the thermal structural stability of microemulsions across a wide temperature range, favoring their application in several scenarios with variable environmental conditions. Furthermore, the application of sugar surfactant based microemulsions as a decontamination medium is also preferred due to the fact that sugar surfactants are non-toxic, biodegradable, and economically viable.

Since temperature variation does not significantly alter the phases and the structural properties of sugar surfactant based microemulsion. Hence, these properties are tuned by adding a co-surfactant.[14] Typically, the co-surfactant employed in the sugar surfactant based microemulsions are alcohols with a medium to long chain length. Two main roles are played by the co-surfactant in the sugar surfactant based microemulsions: (I) the alcohol partially solubilizes in the oil phase, enhancing the hydrophilic character of the oil, and (II) the co-surfactant penetrates into the surfactant membrane, thus inducing a

change in its curvature. The addition of a co-surfactant into the system induces a change in the phase diagram in the form a tetrahedron,[16] where the variation of the co-surfactant content (δ) is presented in the vertical" direction (Figure 2.3 left).

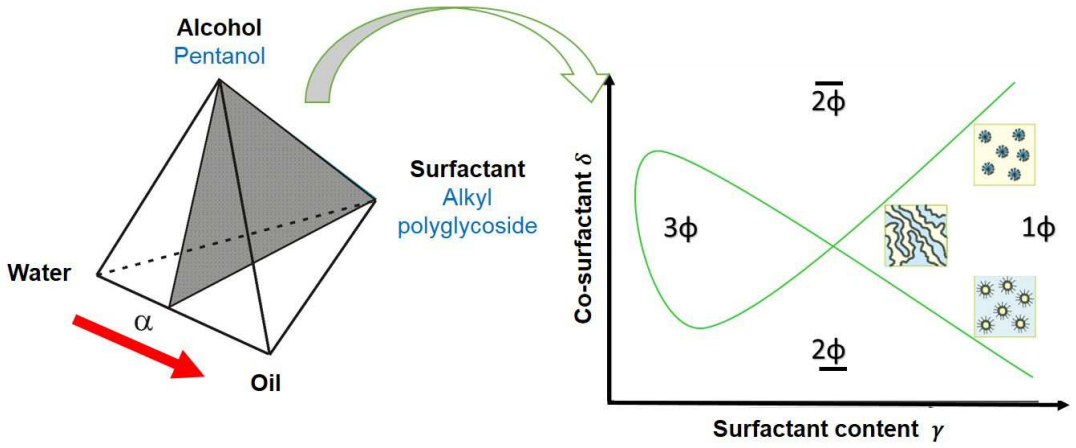

Figure 2.3: Scheme of the quaternary phase diagrams of the microemulsions based on sugar surfactants and the binary phase diagram obtained by the γ cut.

In this study, the phase tetrahedron is examined through γ cut (Figure 2.3 right), where the oil-to-water ratio is maintained constant (α), while the content of surfactant (γ) and co-surfactant (δ) is systematically varied. Similarly to the ternary microemulsion systems, the γ cut in the quaternary microemulsion system resembles the typical fish phase diagrams. At low δ content, outside of the fish body, the microemulsion separates into two phases: oil and microemulsion, phase denominated $\bar{2}$ or Winsor I. By increasing the surfactant content at low γ, a one-phase (1ϕ) microemulsion is formed (fish tail).

At an intermediate level of δ, the number of phases and the microemulsion structure highly depend on the surfactant content. At a higher surfactant content, highly viscous lamellar structures are formed (L_α). At an intermediate surfactant content, the structure of the microemulsion develops into a bicontinuous structure. This structure is characterized by the formation of oil and water channels (Winsor IV). At low surfactant content, the microemulsion separates into three phases: water, microemulsion, and oil. This region corresponds to the body of the fish and is commonly referred to as 3 phase or Winsor III microemulsions. As mentioned before, the point where the body and the tail of the fish meet is called the critical point or x-point. This is a reference point which indicates the efficiency of the surfactant in solubilizing both the oil and water under the given conditions.

A further increase of δ leads a change in the number of phases. Once more, the number of phases in this level of δ is highly dependent on the surfactant content. At low surfactant content, the microemulsion system will tend to separate into microemulsion and water phase denominated $\underline{2}$ or Winsor II, whereas at high surfactant content one-phase microemulsion (1ϕ) is present.

It is important to point out that the variation of δ not only leads to a variation in the number of phases, but it also influences the curvature of the surfactant membrane and thus the microemulsion structure. In the next section, the mechanical properties of the surfactant membrane and their role in the structural properties of microemulsions are presented.

2.1.2 Structure of microemulsions in bulk

The stability of the oil and water nanodomains in microemulsions is mainly defined by the properties of the surfactant membrane located at the interface between those nanodomains. The presence of the surfactant membrane drastically reduces the interfacial tension, which can be in the range from a few mN m^{-1} to 10^{-4} mN m^{-1} (this ultralow interfacial tension is typical for microemulsions with a bicontinuous structure).[20] Low interfacial tension is crucial for the thermodynamic stabilization of microemulsions and is achieved when the surfactant membrane reaches its optimal conformation. Importantly, the conformation and mechanical properties of the surfactant membrane has a direct impact on the structural properties of microemulsions.

The mechanical properties of the surfactant membrane can be described according to the Helfrich model.[21,22] In the Helfrich model, the surfactant membrane can be visualized as a flexible and fluctuating two-dimensional layer characterized by its curvature and bending energy (Figure2.4). The curvature of the surfactant membrane at a certain point is defined by two principal curvatures: K_1 and K_2. From these two main curvatures, one can define the mean curvature as the average of the principal curvatures $H = \frac{1}{2}(K_1 + K_2)$ and the Gaussian curvature as the product of the principal curvatures $G = (K_1 K_2)$. The free energy (F) of the system associated with the bending deformation of the membrane is given by:

$$F = \kappa (H - H_0)^2 + \bar{\kappa} (G) \tag{2.4}$$

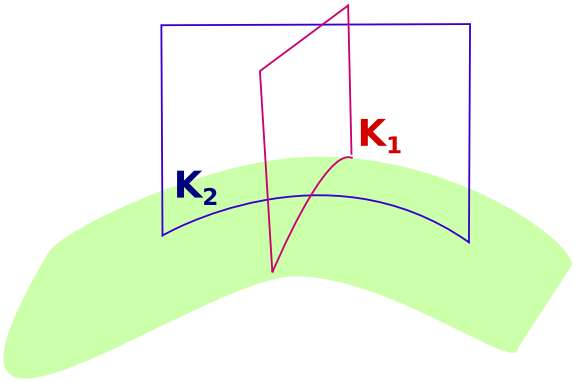

Figure 2.4: Scheme of the main curvatures K_1 and K_2 at a certain point on the surface.

where H_0 is the spontaneous curvature and κ and $\bar{\kappa}$ are the bending and Gaussian elastic constants, respectively. The spontaneous curvature of the surfactant membrane is set by the salinity, temperature, or co-surfactant, while the mean curvature is influenced by the volume fraction of the oil and water components of the microemulsions.[23] The bending elasticity constant (κ) is mainly influenced by the composition of the surfactant membrane. If the microemulsions are stabilized by a single chain non-ionic surfactant and short fatty alcohols, the κ values are commonly less than one. In contrast, when microemulsions are formulated by an ionic surfactant or a double-chain surfactant, the surfactant membrane is stiff and the κ values are larger than one.[24]

According to the Helfrich model, microemulsions adopt a structure that minimizes the energetic cost of membrane deformation. Based on this premise, the structure of the microemulsion has been modeled in the recent years by means of computer simulations. In the modeling processes carried out by Arleth and Duvail,[23–25] the preferred structure of the microemulsion can be estimated from a particular set of parameters such as composition, spontaneous curvature, bending, and the Gaussian elastic constants. The modeling of the microemulsion structure focused on two microemulsions systems: the symmetric microemulsions systems with a volume fraction of the polar (ϕ_p) and apolar (ϕ_a) domains equal to 0.5, and the diluted or asymmetric microemulsions systems, where the volume fraction of the apolar components was set to $\phi_a = 0.25$ (Figure 2.5). For microemulsions with a symmetrical composition, the model shows that positive values of H_0 (low co-surfactant content) induce the formation of well-defined oil droplets dispersed in water (O/W). The O/W structure transforms into highly interconnected channels of oil and water (bicontinuous structure) by decreasing H_0 to a value of zero. The zero value of H_0 is reached when the content of co-surfactant is at the same level as the x point (see Figure 2.3). A further decrease of H_0 into negative values (high co-surfactant content) leads to

the formation of water droplets dispersed in oil (W/O).

In contrast to the symmetrical microemulsions, the model shows that asymmetrical microemulsions present a structure of elongated and more irregular-shaped oil droplets dispersed in water when the H_0 is set to zero. Such structure has been denominated as "diluted bicontinuous". In this asymmetrical microemulsion, a positive H_0 induces the formation of the oil droplets in water, which tends to be monodispersed and regularly-shaped. When the H_0 becomes negative, a vesicle-like structure consisting of water droplets with a negative curvature inside oil droplets is formed. This structure is formed due to the interplay between the asymmetrical composition of the microemulsions, which imposes the formation of oil droplets and water, and the negative spontaneous curvature that favors the formation of water droplets in oil. In addition to the variation of the spontaneous curvature, the most noticeable changes in the microemulsion structure were also observed as a function of the elastic bending constant. The larger the elastic bending constant, the harder it is to bend the surfactant membrane. This implies that the large elastic bending constant induces the formation of the larger nanodomains, which also favors the formation of lamellar structures.

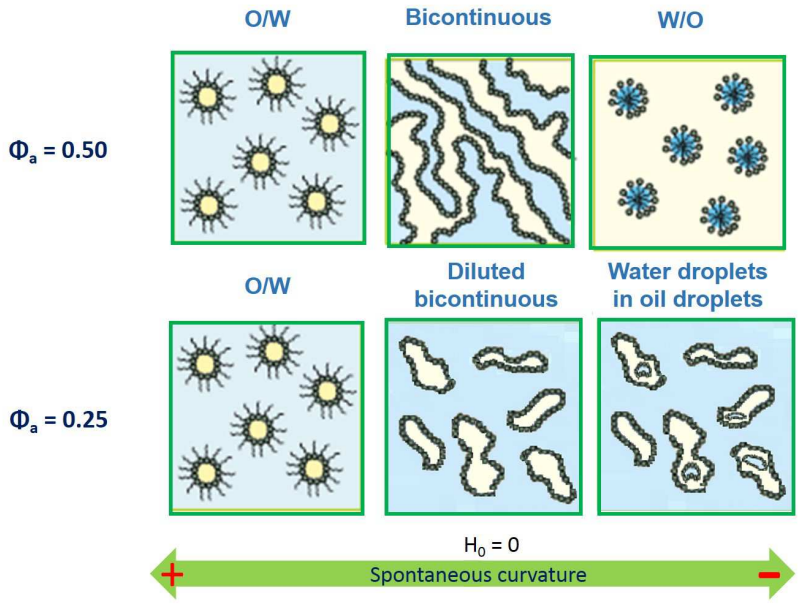

Figure 2.5: Structure of symmetrical and asymmetrical microemulsions with H_0 variations. Adapted from Ref.[23]

2.2 Decontamination Process

Decontamination is the process in which the chemical or biological threats are removed from the affected area and deactivated to a non-hazardous level.[26] In order to carry out the decontamination process, a medium is required to reconstitute personnel and equipment rapidly by removing or neutralizing surface hazards. Importantly, an ideal decontamination system should meet a few requirements such as:[26–28]

- Fast removal of toxic compounds from the surface
- Retaining and neutralizing the chemical agent into its structure (retaining the agents and converting them into harmless or innocuous products)
- Not discharging the vapors of the chemical agent or toxic compound during or after the cleaning process
- Stability under various environmental conditions
- Environmental compatibility
- Cost effectiveness and ease of use

The decontamination media that have been developed until now for cleaning surfaces exposed to highly toxic compounds are mainly based on four methods outlined below.[26]

Solid sorbent-based decontamination systems: Sorbents can remove chemical agents from the surface and degrade them by an active ingredient that is covalently attached to the surface of the solid sorbent or the matrix where they are dispersed.[26] Solid sorbents can be applied onto the solid surfaces in the form of a dispersion in organic solvents, dry powders, or granular pellets.[28] Some examples of solid sorbents employed as decontaminant media are zeolites, adsorptive carbon in dispersed solutions, or the M291 kit.[28] The M291 kit is based on the commercial particle resin XE-555 dispersed in a fiber matrix. The resin can absorb chemical contaminants and neutralize them via hydrolysis.[28] The main drawback of the solid sorbent decontamination media is that they cannot extract the chemicals entrapped in porous surfaces.[26]

Water-based decontamination systems: Water is the ideal environmentally compatible decontamination medium as it is inexpensive and non-toxic and. However, most toxic lipophilic contaminants show low solubility in water. The solubility and the hydrolysis

reaction of the chemical agents in aqueous systems can be improved by incorporating additives. For instance, the addition of surfactants increases the solubility of the chemical warfare agents, whereas the addition of an oxidation agent speeds up their degradation. Although the additives enhance the solubility and degradation of the contaminant in water, this medium has the disadvantage that it cannot wet and penetrate paints and hydrophobic coatings. Therefore, aqueous media are not efficient in extracting chemical warfare agents adsorbed on these materials. Moreover, the application of oxidation agents such as hypochlorite results in corrosion of the surfaces.[26]

Non-water based decontamination systems: Water-free systems or systems that are based on organic solvents provide the advantage of increasing the solubility of toxic compounds, and they can also penetrate painted surfaces or dissolve polymeric matrices, thus enabling a better extraction of contaminants. Nevertheless, their main disadvantages are associated with the intrinsic properties of the organic solvents such as their flammability, toxicity, and pollution of the environment. Another drawback of these systems is that the active reagent that permits the degradation of the contaminants has low solubility in organic media.[26]

Water/organic-based decontamination systems (macroemulsions): The advantages of both aqueous and non-aqueous systems can be brought together through the formation of macroemulsion systems, such as water in oil emulsions. In this case, the oil phase favors the extraction and solubilization of the contaminants, whereas the water phase acts as a reservoir of the active compounds.[26] For instance, the German macroemulsion C8, which consists of water, perchloroethylene as the non-polar phase, anionic surfactant, and only 8 % of hypochlorite as the active ingredient, presents all the advantages of the non-aqueous and aqueous decontamination systems.[27] Besides, this medium is not corrosive due to the low content of hypochlorite. However, macroemulsion systems still present some limitations. First, macroemulsions are kinetically stable colloids; as a consequence, they have to be prepared after the emergency case, therefore limiting the time of response. Second, high input energy is necessary to create macroemulsions. Third, the interfacial area between the oil and water domains is low due to the size of the droplets, which are in the range of micrometers. The low interfacial area reduces the transfer rate of the contaminant from the oil phase to the aqueous phase; therefore, the degradation of the contaminant is limited.[26]

In general, all these systems experience several limitations, ranging from the low efficiency to solubilize the contaminant to the total damage of the treated surfaces. For this reason,

the next section introduces microemulsions as a potentially new decontamination medium for solid surfaces.

2.2.1 Microemulsions and their potential as a new decontamination medium

Microemulsions have been considered in the last years as a promising technology for the decontamination of hard surfaces. In this application, the thermodynamical and structural stability of the microemulsions ensure their immediate use at different external conditions, therefore improving the time of response during an emergency event. Besides, the polarity difference between the nanodomains favors their wettability and penetration into different kinds of solid surfaces,[2,29] at the same time allowing the solubilization of lipophilic toxic substances and active ingredients into the same medium.[30] Importantly, the degradation speed of the toxic substances by the active ingredients is enhanced due to the large interfacial area between the polar and non-polar nanodomains, which is 100 larger than the interfacial areas obtained in macroemulsions.[4] Furthermore, microemulsions can be formulated with non-toxic and biodegradable components; hence, this novel technology can be in line with the actual environmental legislation.

Microemulsions have been employed as decontamination media in several areas, including solid washing and remediation, conservation of cultural heritage, and in-situ degradation of nerve agents. In solid remediation techniques, the low interfacial tension of the medium favors the mobilization of the contaminant and its solubilization.[31,32] For example, the desorption of organochlorine pesticides was improved using empty and oil-swollen micelles and optimized with respect to oil and surfactant type and concentration.[33]

To ensure environmental compatibility, the use of triglyceride oils in microemulsions designed for solid remediation has also been studied.[34] An interesting approach used rapeseed methyl ester and mixtures of anionic and non-ionic surfactants to form microemulsions that have been proven to extract polycyclic aromatic hydrocarbons from porous soil at low temperatures.[35] The approach of using microemulsions for the conservation of cultural heritage needs to solve problems similar to decontamination since sensitive surfaces require a microemulsion formulation for a soft performance. In this application, mild oil-in-water microemulsions have been used to remove hydrophobic material from hydrophilic surfaces of paintings.[36,37]

In particular, a model quaternary microemulsion system based on biodiesel, water, and sugar surfactant ($C_{8-10}G_{1.3}$) has been formulated as a decontamination medium.[3,5] In

this model microemulsion system, its efficiency to degrade the toxic organophosphate compounds (nerve agents) has been evaluated. The active ingredient is the enzyme diisopropyl fluorophosphate (Dfpase) from the squid Loligo vulgaris. This enzyme can detoxify the G-type nerve agents (e.g., Tabun (GA), Sarin (GB), and Soman (GD)) through the hydrolysis of their P-F bond.[38] The experimental results demonstrate that the enzyme maintains its catalytic activity in the complex environment of microemulsions and can therefore efficiently degrade the solubilized nerve agents in the bulk of the microemulsions. Furthermore, the environmental compatibility of this quaternary microemulsion system is provided by its formulation with non-toxic oil biodiesel and the biocompatibility of the sugar surfactant. Although it has been demonstrated that microemulsions are capable of degrading contaminants efficiently, the overall efficiency of the decontamination process is a complex interplay between three processes (wetting, extraction and solubilization, and in-situ detoxification). Detailed understanding of the performance of microemulsions in the decontamination process therefore requires a fundamental knowledge about the wetting of the surface by the microemulsion, the extraction kinetics at the solid substrate, and the reaction kinetics inside the microemulsion in terms of rate constant.

2.3 Microemulsions at solid surfaces

2.3.1 Wetting process

In the decontamination process, the wetting of the surface by the decontamination media is of great importance since a large contact area between the surface and the liquid media enhances the transport of the contaminant into the bulk .[4] The wetting of a particular solid surface by any liquid can be determined by evaluating the contact angle between a liquid drop and the solid surface. The magnitude of the contact angle depends on the interaction between the solid and the liquid and gas phases involved. The contact between the solid and the liquid can have one of two forms: either the drop can spread and form a very thin film (complete wetting) or the spreading of the liquid is limited such that a finite contact angle is established between the solid and the liquid.[39] In the latter case, a so-called three-phase contact line between the solid, the liquid, and the gas phase is formed. This three-phase contact line is the result of the force balance between the interfacial and surface tensions involved, which in turn defines the contact angle between the solid and the liquid. According to the force balance of the interfacial tension in the horizontal direction and the resulting contact angle (Figure 2.6), Young's equation can be applied to

describe the wetting of the surface:[40]

$$\gamma_s = \gamma_{sl} + \gamma_l \cos(\theta) \tag{2.5}$$

where γ_s is the surface tension solid-gas, γ_{sl} is the surface tension solid-liquid, γ_l is the surface tension liquid-gas, and θ is the contact angle between the solid and the liquid.

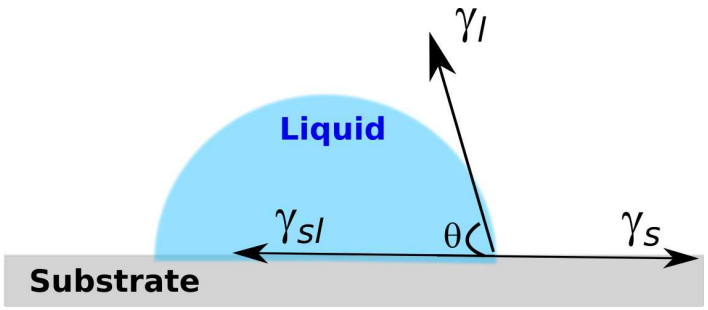

Figure 2.6: Schematic representation of the contact angle of a liquid on a solid planar surface.

Although Young's equation offers an easy way to describe the wetting of the solid surface, it is important to point out that this equation can only be applied to chemically homogeneous, rigid, and smooth surface.[41] Considering that these ideal conditions are not met by a real solid surface, the measurement of a single static contact angle for the characterization of the wetting process is no longer valid. For that reason, the advancing and receding contact angles of the liquid on the solid surface are the parameters that better describe the surface wetting.

The advancing and receding contact angles are denominated as dynamic contact angles. They are measured during the motion of the three-phase contact line. The advancing contact angle is defined as the angle given during the wetting of the surface, whereas the receding contact angle is measured during the retraction of the contact line from the wetted surfaces.[42] The differences between the advancing and receding contact angles is called contact angle hysteresis. Contact angle hysteresis is caused by the existence of different thermodynamic metastable states of the three contact line, where the maximum and minimum stable angles are associated with the advancing and receding contact angles, respectively. Furthermore, it has been established that the value of the contact angle hysteresis is dependent on three main parameters (I) chemical heterogeneity of the surface,

(II) roughness of the surface, and (III) reaction or adsorption of the molecules of the liquid onto the solid surface.[43–45] Although, it has been shown that there is a clear dependence of the contact angle hysteresis on the three parameters mentioned above, there are no models that can be used to predict the value of the hysteresis relative to the properties of the surface and the liquid. Nevertheless, the effect of the chemical heterogeneity or roughness of surfaces on the equilibrium contact angle has been described by the Cassie-Baxter and the Wenzel models.[46,47] Recently, the combination of Young's and Gibbs' adsorption equations has been proposed in order to predict the equilibrium contact angles on smooth and homogenous surfaces when the adsorption of the components of the liquid phase onto the solid surfaces takes place.[48,49]

(I) Effect of the chemical heterogeneity of the surface: The Cassie model predicts the contact angle of chemically heterogeneous surfaces when the contact angles of the pure components of the surface are known.[47] This model assumes that the heterogeneity is given as an array of patches of the different species on the surface. Moreover, the area of these patches should be small compared to the diameter of the drop and should be homogeneously distributed over the entire surface. Under these conditions, the contact angle on the chemically heterogeneous surface can be estimated by knowing the fraction area of the surface components (f_1 and f_2) and the corresponding contact angle of the pure species of the surface (θ_1 and θ_2):

$$\cos\left(\theta\right)_c = f_1 \cos\left(\theta_1\right) + f_1 \cos\left(\theta_1\right) \tag{2.6}$$

(II) Effect of the surface roughness: The Wenzel model predicts the contact angles on a rough surface. In this model, it is considered that the roughness of the surface increases the contact area between the solid and the liquid. Due to the larger contact area, the interfacial tension between the solid and the liquid as well as the surface energy of the solid are amplified when compared to a planar surface.[46] In general, the roughness of the surface enhances the wettability such that the hydrophilic surface becomes more hydrophilic and the hydrophobic surface becomes more hydrophobic. To account for the effect of the roughness on the contact angle, Wenzel introduced the roughness factor (r) to the Young's equation.

$$r = \frac{\text{real surface area}}{\text{projected area}} \tag{2.7}$$

$$\cos(\theta)_w = \frac{r.\gamma_s - r.\gamma_{sl}}{\gamma_l} = r.\cos(\theta) \tag{2.8}$$

(III) Effect of liquid molecule adsorption onto the solid surface: the solid-gas interface can be modified by the reaction or adsorption of the molecules in the liquid onto the solid surface. In this respect, Milne et al.,[48,49] have recently proposed a model that allows predicting the equilibrium contact angle when the adsorption of the liquid phase components onto the solid surface takes place. Particularly, the model focuses on understanding the wetting of surfaces by surfactant solutions as it is well known that the adsorption of the surfactant molecules on the solid-liquid interface has a strong impact on the wetting process. This model combines Young's equation with Gibbs' adsorption equation to predict the variation of the contact angle due to the adsorption process. The complete description of the model can be found in Refs.[48,49]

Effect of the adsorption of the complex fluids components on the wetting processes

In this work, the wetting of model surfaces by microemulsions was evaluated on planar silicon wafers homogeneously functionalized with silane reagents. Hence, it would be expected that the composition and structure of the microemulsion systems close to the solid-liquid interface have a significant impact on the dynamic contact angles. Nevertheless, to the best of our knowledge, a correlation between wetting processes and adsorption of microemulsions components or their structure at the solid-liquid interface has not been established. In the case of wetting by complex fluids, most researchers have focused on surfactant solutions. For these systems, it has been clearly shown than two main aspects play a role in this process: the degree of surface coverage by the surfactant, which in turn determines the role/efficiency of surfactant in reducing the contact angle, and their orientation and structure at the solid interface as it could modify the chemical nature of the surface.[50–54]

In general, the kinetics of adsorption of the surfactant molecules onto the solid/liquid interface is highly dependent on three aspects: the properties of the surface (roughness and polarity), the chemical structure of the surfactant (nature of the head group and the alkyl chain, and the pH and ionic strength of the aqueous solution. For example, Paria et al. have evaluated the kinetics of adsorption of anionic, cationic, and nonionic surfactants

from the aqueous solutions onto hydrophilic silicon solid surfaces.[54] It was found that the rate of adsorption of the cationic surfactant is higher than that of the anionic and nonionic surfactants at neutral pH. The fast adsorption of the cationic surfactant was attributed to the favorable electrostatic interaction between the positive charge of the head of the surfactant molecules and the negative charge of the surface.[55] Hence, the surface was wetted faster by the cationic surfactant solution in comparison to the anionic and nonionic surfactants.[56] However, after the fast wetting, a contraction of the three phase contact line was observed, which was associated with the hydrophobization of the solid surface due to the orientation of the alkyl chains of the surfactant molecules.

Moreover, the degree of covering and the structure of the surfactant aggregates near the solid/liquid interface also plays a role in the wetting process. On the hydrophobic surface, a general trend has been reported for different types of surfactants, where the speed of wetting increases by increasing the content of the surfactant in the aqueous solution.[51] Furthermore, the adsorbed surfactant molecules can arrange at the interface as hemimicelles or bilayers under certain conditions.[57] It has been proposed, that the formation of the hemimicelle structure is not efficient in lowering the interfacial tension of the solid/liquid interface, thus restricting the wetting process.[57] In contrast, the surfactant molecules capable of forming bilayers at the solid/liquid and liquid/vapor interface, for example, trisiloxane surfactant solutions (better known as superspreaders), can enhance the surface wetting process. The enhancement of the wetting processes has been attributed to the fact that the bilayer aggregates favor the transfer of the superspreader molecules from the air/liquid interface to the solid/liquid interface, thus inducing a fast spreading of the surfactant solution.[57]

Knowing that the adsorption and structure of the surfactant molecules at the solid/liquid interfacehave a strong influence on the wetting processes, it is necessary to understand the wetting of more complex systems, such as the quaternary microemulsion system, and their relation with the adsorption and structuring mechanisms of their components at the solid/liquid interfaces.

2.3.2 Structuring of complex fluids at solid/liquid interfaces

The contact between a solid surface and a fluid depends on their interaction potential and can result either in surface melting or the ordering of the fluid bulk phase in the vicinity of the surface. For example, these effects have been studied for metals, molecular crystals, and also colloidal systems, such as thermotropic liquid crystals,[58] particle suspensions,[59]

micellar solutions,[60–62] and microemulsions.[63] In these studies, surface sensitive scattering techniques (GISAXS, GISANS, neutron and X-ray reflectometry), atomic force microscopy, or surface force measurements are frequently applied.[64–67]

It has been demonstrated that the presence of a surface supports the ordering of colloidal liquid systems at the interface.[68,69] The ordering of colloidal systems have been described as a confinement effect. In this case, the confinement of the complex fluid induces an ordering of the dispersed medium into a layer in the lateral direction to the surface, which in turn favors their mobility in the normal direction of their alignment. The gain in mobility in the lateral direction compensates the loss of entropy of the system due to their organization into a layered structure.[70] In the research of structuring process at interfaces, our group has successfully investigated the confinement effect on silica nanoparticle suspensions and polyelectrolyte solutions by means of colloidal probe atomic force microscopy (CP-AFM) and small-angle X-ray scattering (SAXS).[71–73] Both systems showed a well-defined ordering in the vicinity of the confining surfaces. This ordering was indicated as an oscillatory change in the density of the dispersed medium in the perpendicular direction to the interface. In these investigations, it was demonstrated that characteristic structural lengths, inter-particle or interchain distances, and correlation lengths are in the same range in confined state as it is the bulk phase under different conditions (particle concentration, particle size and ionic strength of the silica suspensions, and the degree of polymerization and polymer concentration of the polyelectrolyte solutions). These results gave a clear indication that the structural properties of the colloidal systems are maintained under confinement and that this state only induces a break in the translational symmetry of the bulk system. Since colloidal systems suchas silica suspensions and polyelectrolyte solutions present the same structural behavior under confinement, it has been suggested that confinement effect could be a general phenomenon of complex liquids.[71,73]

The influence of the solid surface on the microemulsion structure is of particular interest because the surface also supports the ordering of the oil and water nanodomains at the interface. Previous research has focused on the near-surface structure of bicontinuous microemulsions on planar surfaces via neutron reflectometry, grazing incidence scattering, and computer simulations.[74–76] These studies have shown that the presence of the solid surface induces a structural transition in the microemulsion from bicontinuous to well-defined alternating channels of oil and water (lamellar structure) in the vicinity of the solid-liquid interface, where the characteristic length, domain size, and correlation length of the microemulsions at the surface and in bulk are preserved.[74,75] Importantly, it has been discussed that the structural changes of the bicontinuous microemulsions at the solid-liquid

interfaces could have a strong influence on the lubrication processes.[75,77] For instance, the surfactant membrane of the lamellar phase close to the interface showed faster relaxation than the membrane in the bulk of bicontinuous microemulsions. Here, the faster relaxation of the surfactant membrane could enhance the sliding of the microemulsions in the lateral direction of the surface, which in turn favors its lubrication. Recently, the effect of pressure on the structural transition of bicontinuous at hydrophilic solid surfaces has been studied.[78] It was shown that the presence of the surface itself induces the formation of a thin lamellar phase close to the interface and that this lamellar film persisted under pressure where only a small compression of the domain size was observed. It was suggested that the formation of more ordered structures at the interface is not favored by high pressure as the loss of conformational entropy of the surfactant membrane is not compensated by the high pressure in the system. Kraska et al.[79] studied the ordering of microemulsions based on oil droplets dispersed in water (O/W) at the air-liquid interface using X-ray reflectometry. It was observed that the presence of the air-liquid interface induces the ordering of oil droplets. The degree of ordering depends on their volume fraction in the bulk, whereas the structure of the oil droplets is preserved at the interface.[79] In general, these investigations demonstrate that the ordering of nanodomains of the microemulsions is present due to the confinement effect and, more importantly, the preservation of the structural lengths, domain size, and correlation length. These results are in line with the confinement effect observed for silica suspensions and polyelectrolyte solutions.[71–73]

It is important to point out that most experiments addressing confinement induced structures of microemulsions were carried out on non-ionic C_iE_j-type or ionic surfactants and alkane oils-based microemulsions. To the best of our knowledge, studies related to the structuring of microemulsions based on “green” surfactants and biocompatible oils have not yet been reported. Such investigations are crucial due to the increasing demands to develop biocompatible and biodegradable media for surface treatments. Hence, new model systems are required to understand the influence of microemulsion composition on its structural properties at solid-liquid interfaces.

Chapter 3

Materials and sample preparation

3.1 Materials

Material used in the preparation of microemulsions: The sugar surfactant Simulsol SL55 ($C_{12/13}G_{1.3}$) was provided by Seppic (Germany). Methyl oleate (MO) is acquired under the brand Synative ESMETI 05 (BASF, Germany), this oil is a synthetic equivalent of the main component of rapeseed methyl ester. Tetradecane oil (99 $\geq$ %) and pentanol (99 %) were purchased from Sigma-Aldrich (Germany). D_2O (heavy water) was purchased from Eurisotop (France) and a three-stage Milli-Q Plus 185 (Millipore) purification system was used for water purification. All chemicals, except the surfactant were used as received. The surfactant stock solution was freeze dried to a residual water content of $\ll$1 %. The chemical structure of the surfactant and oils employed in the preparation of the microemulsions are shown in Figure 3.1.

Material used in the preparation of the model surfaces: The epitaxial Si(100) wafers (Siltonic, Germany) with a thickness of (775 $\pm$ 15) μm cuted in dimensions of (20×20) mm were employed as model planar surfaces. Polished silicon blocks of ($8 \times 5 \times 1$) cm^3 with a surface roughness $<$ 1 nm were acquired from Siliciumbearbeitung Andrea Holm (Germany). Glass frits (VitraPOR, ROBU Geräte GmbH, Germany) of different porosity classes with a dimension of (18×18) mm and thickness of 2.5 mm were used as a model porous surfaces. Table 3.1 presents the structural properties of the glass filters, such as the pore size distribution, the mean value of pore diameter (R_{50}) and their porosity (ratio of the void volume to the total volume of the sample). Dichlorodimethylsilane (99 $\geq$ %), anhydrous toluene (99.8 %) and ammonium hydroxide solution ($28.0-30.0\%$ NH_4OH) were purchased from Sigma-Aldrich (Germany), and Hydrogen peroxide (30 %) was purchased from ChemSolute. All chemicals were used as recieved. The porous polymeric surfaces were prepared with butyl methacrylate (99 %), ethylene glycol dimethacrylate (99 %), 2,2-dimethoxy-2-phenylacetophenone (99 %), 3-(trichlorosilyl)propyl methacrylate (99%), 1-propanol (95 %), 1,4-butanediol (90 %). All these chemicals were purchased from Sigma-Aldrich (Germany) and used as received.

Material used as model contaminant: 2-chloroethyl ethyl sulfide (CEES), Sudan III (technical grade) methyl salicylate (99 $\geq$ %) were purchased from Sigma-Aldrich (Germany) and used as recieved.

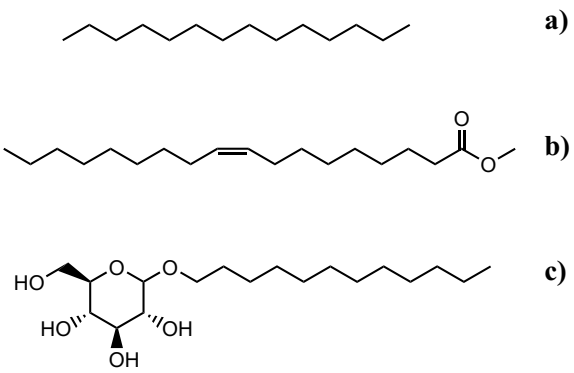

Figure 3.1: Scheme of the chemical structure of a) tetradecane (TD), b) methyl oleate (MO) and c) sugar surfactant $C_{12/13}G_{1.3}$.

Table 3.1: Structural properties of model porous glass filters

Type	**Pore size distribution (μm)**	R_{50} **(μm)**	**Porosity**
00	160 - 250	95	0.33
02	40 - 100	35	0.36
04	10 - 16	5.5	0.42

The values are taken from Ref.[80]

3.2 Sample preparation

3.2.1 Preparation of sugar surfactant based microemulsions

The phase tetrahedrons of the quaternary microemulsion systems water/ tetradecane/ $C_{12/13}G_{1.3}$(SL 55)/ pentanol (TD-microemulsion) and water/ methyl oleate/ $C_{12/13}G_{1.3}$(SL 55)/ pentanol (MO-microemulsion) were studied at different sections along the oil-water axis in the range of $\alpha = 0.1$ to $\alpha = 0.7$. The phase diagrams of these phase diagrams of this quaternary system were evaluated at constant oil to water ratio (α), while at constant α, the content of sugar surfactant (γ) and co-surfactant pentanol (δ) were varied.

Based on the phase diagrams of both microemulsions systems, TD-microemulsions and MO-microemulsions, the content of surfactant (γ) and (δ) were adjusted in order to obtain one phase microemulsions parallel to the inversion point. The composition of the TD-microemulsions and MO-microemulsions in this region is presented in Table 3.2. These samples were employed on the structural evaluation of the microemulsions in bulk via Cryo-SEM and diffusion NMR spectroscopy, as well as the evaluation of structuring and

wetting at solid surfaces. The MO-microemulsions were employed on the evaluation of the extraction processes of model contaminants.

Table 3.2: Composition of the investigated microemulsion samples based on tetradecane and methyl oleate oil

Microemulsions based on tetradecane		
α	γ	δ
0.1	0.24	3.00 x 10^{-2}
0.3	0.35	6.00 x 10^{-2}
0.5	0.40	8.00 x 10^{-2}
0.7	0.35	9.00 x 10^{-1}
Microemulsions based on methyl oleate		
α	γ	δ
0.1	0.22	6.80 x 10^{-3}
0.3[a]	0.22	4.00 x 10^{-2}
0.3[b]	0.30	4.00 x 10^{-2}
0.5	0.34	7.00 x 10^{-2}
0.7	0.34	8.50 x 10^{-2}

[a] MO-microemulsion sample employed on the evaluation of the structure of the microemulsions at the solid liquid interface. [b] MO-microemulsion sample employed on the bulk structural characterization via cryo-SEM and diffusion NMR spectroscopy, as well as in the study of wettting and extraction processes.

3.2.2 Preparation of planar solid surfaces

The silicon wafers and silicon blocks were cleaned with RCA solution (5:1:1 of water, 29 % NH_4OH and 30 % H_2O_2) at 72° C for 10 minutes, then rinsed several times with Millipore water and dried by nitrogen stream. The silicon wafers were hydrophobized by immersion in 10 mM solutions of dichlorodimethylsilane in anhydrous toluene for 4 hours at room temperature. Subsequently, the functionalized silicon wafers were rinsed three times with toluene and isopropanol. The functionalized silicon wafers were used as a hydrophobic surface, while freshly cleaned blocks were applied as a hydrophilic surface.

3.2.3 Preparation of porous solid surfaces

The glass filters were cleaned with RCA solution (5:1:1 of water, 29 % NH_4OH and 30 % H_2O_2) at 72° C for 15 minutes, then rinsed several times with Millipore water and dried by nitrogen stream and then under vacuum. The functionalization of the glass filters with

dichlorodimethylsilane was done by the vapor phase deposition method. In this method, batches of four glass filters were placed vertically in a desiccator. 120 μl of the silane reagent were placed in an open glass beaker lying on the desiccator. The desiccator was closed and connected to a vacuum pump. The pressure in the desiccator was reduced and maintained for 6 hours. The vapor phase deposition was repeated three times in each batch of glass filters to enhance their functionalization. In this study, the functionalized glass filters represent the hydrophobic model porous surfaces, while the clean glass filters represents the hydrophilic model porous surfaces.

3.2.4 Preparation of porous polymeric substrates

The porous surfaces were prepared by the photopolymerization of butylmethacrylate and ethylene dimethacrylate on (18 $\times$ 18) mm flat microscope cover glasses (Menzel−Gläser, Germany). In this procedure, the cover glasses were functionalized with 3-(trimethoxysilyl) propyl methacrylate to ensure the chemical fixation of the porous polymeric surface to a planar surface. The polymeric mixture consists of 0.24 wt. % butylmethacrylate, 0.15 wt. % ethylene dimethacrylate, 0.31 wt. % 1-propanol, 0.22 wt. % 1-Butanol, 0.06 wt. % water and 9.52 x 10^{-3} wt. % of initiator. The polymeric mixture was purged with nitrogen and injected between clean and functionalized glass covers, separated by a teflon mold of (0.50 ± 0.01) mm thickness. The polymeric mixture was irradiated with UV light for 15 minutes. After the photopolymerization process, the mold was disassembled and the obtained porous polymeric surface on the glass cover was washed several times with methanol and dried with nitrogen. The porous polymer coating was characterized via scanning electron microscopy.

Chapter 4

Methods and Data Evaluation

4.1 Neutron Scattering techniques

4.1.1 Small angle neutron scattering

Small-angle neutron scattering (SANS) measurements were performed on the KWS-1 instrument at the FRM II (Garching, Germany).[81,82] In this experiment, the bulk contrast was achieved by replacing all water by D_2O. The measurements were carried out at sample-to-detector distances of 2, 8 and 20 m, using a nonpolarized, monochromatic incident beam of a neutron wavelength λ =5 Å. In this configuration, q ranges between 0.003 $Å^{-1}$ and 0.3 $Å^{-1}$. The microemulsion samples were measured in bulk contrast in quartz cells with 1 mm neutron pathway at 25 °C. Raw scattering data were radially averaged and brought to absolute scale by the procedures provided by the JCNS using the QtiKWS10 software package.

Data evaluation by the Teubner-Strey model

The scattering data were analyzed according to the Teubner-Strey model using the Sasfit software (by J. Kohlbrecher from the Paul Scherrer Institut, Villigen, Switzerland). The Teubner-Strey model is a semi-empirical model used to describe the typical broad scattering peaks arising from bicontinuous microemulsion structures.[83,84] It yields the domain size d_{TS} and the correlation length ξ_{TS} of the microemulsion. The calculated domain sizes d_{TS} correspond to mean repeat unit lengths of the oil-water domains, whereas the correlation lengths is associated to the distance in the bulk phase at which the periodicity of the oil and water nanodomains is maintained.

$$I_{TS} = \frac{8\pi c_2 \langle \eta^2 \rangle / \xi}{a_2 + c_1 q^2 + c_2 q^4} \tag{4.1}$$

$$d_{TS} = 2\pi \left(\frac{1}{2} \left(\frac{a_2}{c_2} \right)^{1/2} - \frac{c_1}{4c_2} \right)^{-1/2} \tag{4.2}$$

$$\xi_{TS} = \left(\frac{1}{2} \left(\frac{a_2}{c_2} \right)^{1/2} + \frac{c_1}{4c_2} \right)^{-1/2} \tag{4.3}$$

Here, $\langle \eta^2 \rangle = \phi_w \phi_o (\Delta\rho)^2$ is the mean-squared fluctuation of the scattering length density of water and oil domains in the microemulsions, with volume fraction of ϕ_w and ϕ_o respectively, $\Delta\rho$ is the scattering length difference between water and oil, and I_{TS} is the scattering intensity. The parameters $a_2>0$, $c_1<0$ and $c_2>0$ are fitting parameters and q is the magnitude of the scattering vector. From the fit values and the structural parameters (domain size d_{TS} and correlation length ξ_{TS}) estimated from the Teubner-Strey analysis, the amphiphilicity factor f_a, the renormalized and the bare bending elasticity constants κ_{SANS} and κ_{bare} of the surfactant membrane in the microemulsions,[85,86] where l_c represents the thickness of the surfactant membrane.

The amphiphilicity factor (f_a) quantifies the amphiphilic strength of a surfactant, and its value also is related to the degree of organization of the microemulsions in the bulk phase.[87,88] A value of f_a close to 1 is characteristic for disordered systems and -1 for more organized systems (i.e. lamellar phases).[87,88] The renormalized bending modulus is the effective bending modulus of the membrane on the scale of the domain sizes. At this scale, the bending of the membrane is superposed by thermal fluctuations at smaller scales, such that the membrane can easily deform at larger thermal fluctuations.[85,89] Conversely, the bare bending modulus is associated with the high momentum cut off, given by the effective thickness of the amphiphilic films l_c (the smaller length scale).[86,90]

$$f_a = \frac{c_1}{\sqrt{4a_2c_2}} \tag{4.4}$$

$$\frac{\kappa_{SANS}}{k_BT} = \frac{10\sqrt{3\pi}}{64}\frac{\xi_{TS}}{d_{TS}} \tag{4.5}$$

$$\frac{\kappa_{bare}}{k_BT} = \frac{\kappa_{SANS}}{k_BT} + \frac{3}{4\pi}\ln\left(\frac{d_{TS}}{2l_c}\right) \tag{4.6}$$

4.1.2 Neutron reflectometry

Neutron reflectometry (NR) measurements were carried out on the NREX reflectometer at the Heinz Maier-Leibnitz Zentrum (Garching, Germany). The neutron reflectometry measurements are based on the determination of the ratio between the intensity of the specularly reflected beam from the solid-liquid interface and the intensity of the incident neutron beam (λ = 4.3 Å). Such a ratio is defined as reflectivity, R =I/I_0, and R is evaluated as a function of the momentum transfer vector Q_Z.

Figure 4.1 sketches the scattering geometry in the neutron reflectometry and GISANS type measurements.

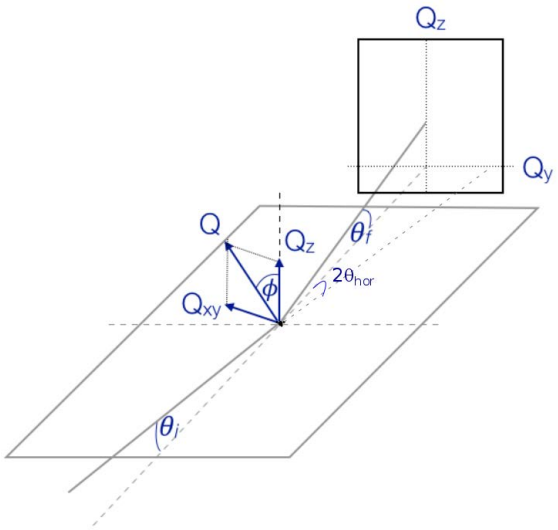

Figure 4.1: Scheme of the scattering geometry in the neutron reflectometry and GISANS measurements.

Importantly, below the critical edge of total external reflexion only mirror like reflectivity occurs, while above it the intensity drops with the 4^{th} power of the incidence angle, as described by the Fresnel reflectivity. This restricts the accessible Q_z-range from the critical edge up to the angle where the signal to noise ratio has the same order of the reflectivity. Thus a background correction is mandatory. In fact, the specular reflected signal to noise ratio depends not only on Q-independent factors like intrinsic background level in the surroundings, incoherent scattering generated by sample and sample holder, but also on Q-dependent factors like the footprint of the direct beam and diffuse scattering at sample and its holder.[91] A general prediction of the background is therefore hopeless, hence has to be done for each reflectivity curve individually.

The investigated microemulsions generate individually strong off-specular scattering. In that case, the most promising strategy estimating the background is using the off-specular reflected intensity in the vicinity of the specular condition. This method has two major advantages: (i) the background is Q_z-depended estimated and (ii) if a second detector is present in the vicinity of the specular reflected beam, the required data can be collected while the specular signal is measured. In this experiment, we made use of a position sensitive detector. It allows shaping the sensitive detector area arbitrarily. Practically, two rectangular ranges of interests (ROIs) with the identical area were applied to mime

the detectors. While the ROI for the specular reflectivity matches the condition $\theta_f = \theta_i$, the off-specular signal is recorded below and above this region ($\theta_f = \theta_i \pm 0.12°$). The geometry is in general described by:

$$Q\left(\theta_i, \theta_f\right) = \begin{pmatrix} Q_x \\ Q_z \end{pmatrix} = \frac{2\pi}{\lambda} \begin{pmatrix} \cos\left(\theta_f\right) - \cos\left(\theta_i\right) \\ \sin\left(\theta_f\right) + \sin\left(\theta_i\right) \end{pmatrix} \cong \frac{\pi}{\lambda} \begin{pmatrix} {\theta_i}^2 - {\theta_f}^2 \\ 2\theta_f + 2\theta_i \end{pmatrix} \quad (4.7)$$

Data evaluation

Data analysis was done by applying the Parratt recursion algorithm (Parratt 32 software, by J. C. Braun from Helmholtz-Center Berlin, Germany), and using a scattering length density profile (SLD) of the form

$$SLD = Ae^{(-z/\xi_z)} \cos\left(\left(\frac{2\pi z}{d_z}\right) + \phi\right). \quad (4.8)$$

which results from an oscillatory one-dimensional order parameter profile in the microemulsion. Based on Ginzburg-Landau theory, this order parameter profile was obtained by including additional surface fields in the free energy functional.[92–94]Similar theoretical concepts are used for the description of planar amphiphilic membranes adhered to a planar solid substrate.[95] The scattering length density profile of the near surface structure of the bicontinuous microemulsion contains an oscillatory contribution describing the alternating scattering length densities of the layered oil and water domains. The exponential term describes the transition of this layered structure into the randomly oriented bicontinuous bulk structure, represented by a mean scattering length density of the bulk medium. The parameters A and φ are the amplitude and phase of the oscillation, while d_z and ξ_z are the mean repeat distance of oil and water domains and the correlation length of this layered structure. As a consequence of the theoretical approach, both parameters should be identical to the corresponding parameters d_{TS} and ξ_{TS} in the bulk phase.

In the fitting process, the A, φ, d_z and ξ_z are taken as free parameters, while the SLD of the pure silicon, the silicon oxide layer (20 Å), and the bulk of the microemulsions were kept constant (Table 4.1). This approach leads to the best fit results, especially in the peak region and at higher Q values. The SLD of the bulk microemulsions was calculated according to their composition.

Table 4.1: Scattering length density of the pure components of microemulsion and solid surfaces

Component	**SLD** ($Å^{-2}$)
Si	2.07 x 10^{-6}
SiO_2	3.47 x 10^{-6}
D_2O	6.36 x 10^{-6}
SL55 surfactant	-1.16 x 10^{-6}
Pentanol	-3.29 x 10^{-7}
Methyl oleate	2.39 x 10^{-7}
Tetradecane	-4.38 x 10^{-7}

Before the measurements, the treated hydrophilic and hydrophobic silicon blocks were placed in a liquid cell trough made of poly(tetrafluoroethylene) with stainless steel inlet and outlet tubes. The contact between the silicon blocks and the trough was sealed by using a Viton O-ring. Approximately 10 ml of microemulsion samples were injected into the cell. The inlet and outlet line were closed, and the sample inside the cell was equilibrated for one hour. Subsequently, the neutron reflectometry measurements of the solid-liquid interface were carried out at 25° C.

4.1.3 Grazing incidence small angle neutron scattering

Small angle neutron scattering under grazing incidence was measured at NREX (MLZ, Garching, Germany). Compared to the setup described for measuring the neutron reflectivity, the resolution in the in-plane direction Q_y had to be increased. Therefore the incoming beam was collimated by two slits (separated 2m from each other) down to 1x1 mm^2. Since the scattering length density of the sub-phase differs with the oil/water ratio and the incoming beam strikes the interface through the silicon substrate, a critical edge (θ_c) occurs only for high D_2O content in the microemulsions, namely for $\alpha = 0.1$ and $\alpha = 0.3$ of the tetradecane based microemulsions. Thus an evanescent wave is only present for the two most diluted systems. To maximize the neutrons in the vicinity of the solid-liquid interface the incidence angle θ_i was fixed to 0.18° for $\alpha = 0.1$ and $\theta_i = 0.15°$ for all other oil/water ratios investigated. The resulting penetration depths Λ of the evanescent wave are calculated according to

$$\Lambda = \frac{\lambda}{4\pi\sqrt{\theta_c^2 - \theta_i^2}}. \tag{4.9}$$

Table 4.2 summarizes the parameters of the grazing incidence measurements.

Table 4.2: Critical angle (θ_c), incident angle (θ_i) and penetration depth (Λ) of the neutron beam at the solid/liquid interface for tetradecane based microemulsions at different oil contents (α)

α	θ_c [°]	θ_i [°]	Λ [Å]
0.1	0.19	0.18	320
0.3	0.16	0.15	190
> 0.3	-	0.15	∞

The position sensitive detector (20 x 20) cm^2 placed 2.5 m behind the sample counts vertical and horizontal scattered neutrons within 4.5° solid angle. In order to enlarge the covered Q-space during a single measurement, we focused on the first quadrant (only positive Q-vectors). Therefore the detector was moved out of the scattering plane by $2\theta_{hor}$ = 1.6° and in the scattering plane to θ_f = 1.6°. As a result, direct and reflected beam are located in a detector corner, and a maximum Q-space is covered. The highly collimated beam decreased the incoming neutron flux dramatically. To account for this, each GISANS pattern was summed over 12 h of counting time. The position sensitive detected events where then transformed into a lateral component Q_{xy}

$$Q_{xy} = \sqrt{{Q_x}^2 + {Q_y}^2} \tag{4.10}$$

where

$$Q_x = \frac{2\pi}{\lambda}\left(\cos\left(\theta_f\right).\cos\left(2\theta_{hor}\right) - \cos\left(\theta_i\right)\right) \tag{4.11}$$

$$Q_y = \frac{2\pi}{\lambda}\left(\cos\left(\theta_f\right).\sin\left(2\theta_{hor}\right)\right) \tag{4.12}$$

and a vertical component

$$Q_z = \frac{2\pi}{\lambda}\left(\sin\left(\theta_f\right) + \sin\left(\theta_i\right)\right) \tag{4.13}$$

Since the diffuse scattering is Debye-Scherrer-Ring like distributed the data were finally radially $\left(Q = \sqrt{{Q_{xy}}^2 + {Q_z}^2}\right)$ sorted and binned (ΔQ = 0.001 Å^{-1}).

4.2 Evaluation of static and dynamic contact angles

4.2.1 Goniometer method

Static contact angles were measured with a Goniometer OCA20 (Dataphysics, Germany). The surfaces were placed on a sample stage in a closed cell. The cell was filled with the probe liquid to have a saturated atmosphere. The cell was set in equilibrium for 30 minutes before the measurements. Afterwards, a drop of the probe liquid (4 μl) was placed on the surface via syringe. The contact angle was determined using the tangent fitting method. At least five drops of each probe liquid were placed on different spots of the substrates and the resulting contact angle is given as the average of the five measurements.

The measurements of the static contact angles on test surfaces allows to characterize the surface energy of the planar solid surfaces by means of Owens-Wendt-Rabel-Kaelble method (OWRK). In this method, the polar γ_s^p and dispersive γ_s^d components of the surface energy γ_s of the surface are determined by using a series of probe liquids with known surface energy (polar γ_l^p and dispersive γ_l^d components). The determination of the surface energy of the solid is given through the following equation:

$$\frac{(1+\cos(\theta))}{2}\frac{\gamma_l^p}{\sqrt{\gamma_l^d}} = \frac{\sqrt{\gamma_s^p}}{\sqrt{\gamma_l^p}}\sqrt{\gamma_l^d} + \sqrt{\gamma_s^d} \quad (4.14)$$

The probe liquids employed on determination of the surface energy of the model planar surfaces and their corresponding polar γ_l^p and dispersive γ_l^d components are listed in Table 4.3

Table 4.3: Total surface energy, including dispersive and polar components, of the probe liquids

Probe liquid	**Total energy** (γ_s) $mN\ m^{-1}$	**Dispersive component** (γ_s^d) $mN\ m^{-1}$	**Polar component** (γ_s^p) $mN\ m^{-1}$
Water	72.8	21.8	51.0
Glycerol	63.3	20.2	43.15
Ethylene glycol	48.2	29.3	18.9
Diiodomethane	50	47.4	2.6
1-Bromonaphthalene	44.4	44.4	0
Ethylene glycol	56.9	23.5	33.4

The values are given according to the Refs.[96,97]

4.2.2 Tilted Plate Method

The dynamic contact angles were evaluated by the tilted plate method using the Goniometer OCA20 (Dataphysics, Germany), equipped with an autimated tilting stage. In this method, 4 μl of the tested liquid were placed on the planar solid surfaces by means of a microsyringe. After the deposition of the liquid on the solid planar surface, the plate was tilted at 1.02°/sec until the drop starts to roll off from the surface. The advancing (right angle) and receding (left angle) contact angles were defined as the angles between the tilted sample and the horizontal plane before the roll off of the liquid from the inclined surface (Figure 4.2).[42] Importantly, five measurements were take in a different position of the solid planar surface and they were averaged to give the deviation of the measurements.

Figure 4.2: Example of the determination of the dynamic contact angles of micromeulsion on a tilted plate. At this point the plate has been tilted by 20°.

4.2.3 Wilhelmy Plate Method

The dynamic contact angles evaluated by the Wilhelmy plate method were measured at the KRÜSS force tensiometer K11 (Germany). Advancing and receding contact angles are calculated according to the force measured during the immersion and emmersion stages, respectively.[98–100] Here, the force acting on the solid surface during the measurement are given by the following force balance:

$$F = mg - \rho_l hwtg + 2(w + t)\gamma_l \cos(\theta) \tag{4.15}$$

where F is the resulting force, mg the force related to the mass of the plate and gravitational forces. The term $\rho_l hwtg$ is associated to the buoyancy force, where h is the length of the plate submerged into the liquid, w is the width of the plate and t is the thickness of the plate. The last term of the equation represents the capillary forces associated to the wetting of the plate, where γ is the surface tension of the liquid and θ is the contact angle between the liquid and the solid. Before the measurement starts, the balance of the tensiometer is set to zero such that the weight of the solid planar surface does not contribute to the total force during the measurements. The buoyancy force can be excluded by extrapolation of the force curves to the zero immersion step as it is schematically shown in Figure 4.3. Hence, the advancing and receding contact angles can be calculated by knowing the dimensions of the solid planar surface and the surface tension of the test liquid. In this method, the immersion and emmersion speed of the solid surfaces was set to 0.5 mm/min with a total immersion depth of 5 mm.

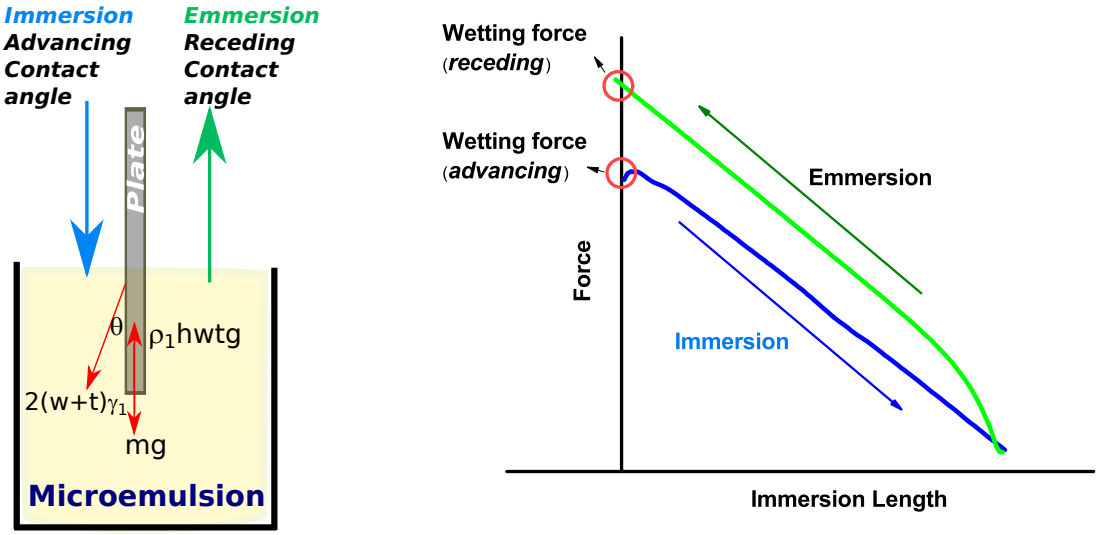

Figure 4.3: Schematic representation of the Wilhelmy plate method (left) and the corresponding measured forces (right) during the immersion and emmersion steps of the plate in the microemulsion

4.2.4 Washburn method

The contact angles evaluated by the Washburn method were measured at the KRÜSS force tensiometer K11 (Germany). The Washburn method is based on the capillary rise principle, in which the porous surfaces is modeled as an array of parallel capillaries with an average radius.[80,101,102] According to this method, the square of the liquid height h imbibed in the porous surfaces as a function of the time will depend on the properties of the liquid (surface tension γ, density ρ and kinematic viscosity η), the properties of the surface (average pore size R_s, porosity ϕ and permeability K), as well as, the interaction between the porous surface and the fluid give represented by contact angle (θ).

$$h^2 = \frac{4\gamma \cos(\theta) K}{R_s \phi \eta} t \tag{4.16}$$

The evaluation of the height is difficult due to the development of an inhomogeneous front of the rising liquid, hence it is more accurate to evaluate the mass of the imbibed liquid as a function of time. Here, the mass and the height of the imbibed liquid have a linear relation, which depends on the porosity ϕ of the porous solid, the cross-sectional area A_b of the porous solid and the density of the liquid ρ.

$$m = hA_b\phi\rho \tag{4.17}$$

By the substitution of equation 4.17 in 4.16, a relation of the square of the mass of the imbibed liquid into the porous surface as a function of the time is obtained (Eq.4.18.

$$m^2 = \frac{4\gamma\rho^2\cos(\theta)}{\eta}\frac{A_b^2K\phi}{R_s}t \tag{4.18}$$

In the Washburn method, the porous surface is brought into the liquid until it touches the surface of the liquid. Subsequently, the mass of the liquid wicked by the porous solid surface is recorded as a function of time. The contact angles of the test liquid can be then calculated by applying the equation 4.18 to the linear part of the obtained curve. However, some of the parameters of the porous surfaces are not known (particularly K), hence a reference liquid capable to completely wet the porous surface ($\cos(\theta) = 0$) has to be employed in order to estimate the constant associated with the properties of the porous surface (constant = $\frac{A_b^2K\phi}{R_s}$) Here, we employ decane as reference liquid and the constant values obtained for the hydrophilic and hydrophobic model porous surfaces are reported in table 4.4.

Table 4.4: Constants of the model porous surfaces evaluated with decane

Pore size	**hydrophilic porous surfaces** (cm^5)	**hydrophobic porous surface** (cm^5)
$10-16$	1.77×10^{-4}	1.70×10^{-4}
$40-100$	7.65×10^{-4}	6.99×10^{-4}
$160-250$	9.19×10^{-4}	7.32×10^{-4}

4.3 Spectroscopic and chromatographic methods

4.3.1 UV-vis Spectroscopy

UV-Visible spectroscopy is used in this study to quantified the extraction of Sudan III deposited on the porous polymeric substrates by microemulsions. In order to evaluate the extraction processes by UV-vis spectroscopy, 30 μl of Sudan III solution in ethyl acetate (1 mg ml^{-1}) were deposited homogeneously on the porous polymeric surface. The Sudan III solution rapidly penetrates into the surface. After 15 minutes the solvent was removed by

blowing the surface with nitrogen. To evaluate the extraction process, the contaminated porous polymeric surface was inserted into a glass cell with a size of (2 x 2 x 2) cm^3. Subsequently, 5 ml of the microemulsion was poured on the top of the surface and it was continuously stirred at 250 rpm. The extraction of the Sudan III dye from the porous surface by microemulsions was on-line monitored by recording the absorption of the Sudan III in the microemulsions at 543 nm wavelength by a Lambda 35 Perkin Elmer UV-Visible spectrometer. The amount of dye removed by the microemulsion was estimated by means of calibration curves of solutions of Sudan III dye in the respective microemulsion. Three repeated measurements were done on each microemulsion to evaluate the reproducibility of the removal process.

In the UV-Visible spectroscopy, the light radiation in the region from 100 to 800 nm induces electronic transitions in the molecules. These transitions are quantified and consist in the excitement of an electron from the highest occupied molecular orbital HOMO to the lowest unoccupied molecular orbital LUMO.[103,104] The relationship between the energy absorbed ΔE and wavelength λ of light radiation is given by:

$$\Delta E = \frac{hc}{\lambda} \tag{4.19}$$

where h is the Planck's constant and c the velocity of light.

Since the energy absorbed is quantized, the absorption spectrum should be a discreet and simple line. However, the spectrum is a band due to the overlapping of the rotational and vibration levels of the molecule. The main characteristics of an absorption band are its position and intensity. The position of the absorption corresponds to the wavelength of the radiation, whose energy is equal to that required for the electronic transition.[103,104] Whereas the intensity of the absorption depends mainly on the probability of interaction between the radiation energy and the electronic system. This intensity can be expressed as transmittance (T) defined as the ratio of incident light and the transmitted light by the sample. Importantly, the monitoring the transmittance as a function of the time allow us to detect changes in the concentration of Sudan III in the microemulsions by means of Beer-Lambert law:[104]

$$-\log(T) = A = bc\epsilon$$

where A is the absorbance, b is the path length, c the concentration of the solute and ϵ is the absorption molar coefficient.

4.3.2 Fourier Transform Infrared Spectroscopy-Attenuated Total Reflectance

Fourier Transform Infrared Spectroscopy-Attenuated Total Reflectance (FTIR-ATR) spectroscopy was employed to on-line monitored he removal of thickened 2-Chloroethyl ethyl sulfide (CEES) from the crystal interface by microemulsions. The FTIR-ATR spectroscopy is a ReactIR4000 instrument with a DiComp diamond probe (Mettler Toledo AutoChem ReactIR with a 24MID MCT module and a laser frequency of 7901.42 Hz with HappGenzel apodisation). The ReactIR was connected to a PG 14 L CMC-instruments purge Gas generator (CO_2 content $<$ 1 ppm and water content $<$ 0.1 ppm. Here, 5 μl of CEES were deposited directly on the DiComp probe by covering the entire surface of the diamond. After that the DiComp probe was sealed within a stainless steel reaction chamber, followed by the addition of 10 ml of microemulsion. The IR spectra were recorded continuously in the range of 4000 to 650 cm^{-1} and analyzed using the iC IR 4.2 software (Mettler Toledo). The signal of the pure CEES was used as reference. The change of this signal with time permits to evaluate the extraction efficiency of the CEES by the microemulsions. Three repeated measurements were done on each microemulsion in order to evaluate the reproducibility of the extraction process.

FTIR-ATR is a technique that involves an optically transparent transmitting element with high refractive index (e.g., diamond, silicon). In this technique, the infrared light is directed through the transmitting element that is in contact with the sample (Figure 4.4).[105,106] At the interface, a total internal refraction of the light is generated, as the refractive index of the samples is lower than the refractive index of the transmitting element, and the angle of incidence of the light is larger than the critical angle.

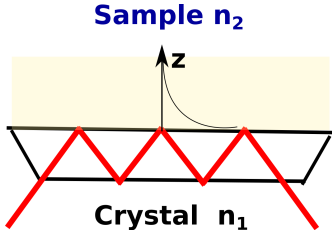

Figure 4.4: Scheme of the FTIR-ATR.

Due to the total internal reflection, an evanescent wave is generated near the interface. The amplitud of this wave decays exponentially as a function of the vertical distance (z)

from the interface into the sample, according to the following equation:

$$E = E_0 \exp(\frac{-z}{d_p}) \tag{4.21}$$

where E_0 is the electric field amplitude at the interface, which depends on the angle of incidence, the refractive indices, and the polarization of the field . d_p is the depth of the penetration of the evanescent wave into the sample and it is in the range from 0.5 to 5 μm.[107] The depth of penetration depends on wavelength, angle of incidence and refractive incidence of crystal and sample. The depth of penetration can be calculated by :

$$d_p = \frac{\lambda_1}{2\pi\sqrt{\sin^2\theta - n_{21}^2}} \tag{4.22}$$

Because of the absorption of the sample near to the interface, the intensity of the internal reflected light is attenuated, therefore an infrared spectrum can be obtained. The infrared spectrum provides information of the molecular structure of the molecules of the sample located near to the interface. Hence, the continuous monitoring of the attenuation the infrared light can be used to quantified the adsorbed amount of each molecule at the interface.

4.3.3 High Performance Liquid Chromatography

High Performance Liquid Chromatography was employed to monitor the extraction of methyl salicylate from porous surfaces by microemulsions. Here, 3 μl of methyl salicylate were homogeneously distributed on the porous polymeric surface. Subsequently, the surface was transferred to the glass cell. After 15 minutes of the deposition of the methyl salicylate on the surface, 5 ml of the microemulsion were poured in the glass cell and it was continuously stirred at 250 rpm. To determine the concentration of methyl salicylate in the microemulsion, aliquots of 20 μl microemulsion were taken at different intervals of time and diluted in 320 μl of methanol containing 137 mg l^{-1} of ethyl salicylate. The diluted samples were filtered to remove the precipitated surfactant. The concentration of the methyl salicylate in the diluted samples was determined by liquid chromatography coupled to a UV detector. A reversed phase column (Grom-Sil ODS-4 HE, 5 μm, 8.0 $\times$ 250 mm) and a gradient eluent of water and acetonitrile containing 0.01 % of acetic acid

were employed. The concentration of methyl salicylate in the samples is calculated by the comparison with the signal of the internal standard ethyl salicylate.

High Performance Liquid Chromatography (HPLC) is a separation analytical technique based on the difference of solubility of the analytes of interest between the liquid mobile phase and solid stationary phase. In HPLC technique, the dissolved sample is injected into a stream of the mobile phase pumped at high pressure through the stationary phase which is a solid porous packed column.[108] The distributions of the analytes between the mobile and the stationary phase depend on the polarity of the analytes and the column, as well as the composition of the mobile phase. For instance, in a reverse stationary phase (hydrophobic column), a polar analyte is eluted faster from the stationary phase when a polar mobile phase is employed. On the contrary, a non-polar analyte is retained stronger in the column incrementing, therefore, the time at which the analyte is eluted is also increased. The elution of the analytes from the stationary phase can be detected by different methods (e.g, UV-vis detectors, refractive index detector, fluorescence detectors, among others). The selection of the detector will depend on the properties of the analytes and the solvent. Ideally, the detector should show a higher response to the analyte over the mobile phase and it should allow estimating the concentration of the analyte in this particular case.

4.4 Additional experimental techniques

4.4.1 Diffusion Neutron Magnetic Resonance Spectroscopy

The self-diffusion coefficients of microemulsion components were determined by Diffusion Neutron Magnetic Resonance (NMR) Spectroscopy at 25° C using a Bruker AVII 500 spectrometer equipped with a broad band fluorene observation (BBFO) probe. In order to lock the frequency on the magnetic field, the composition of the microemulsions was varied by interchanging 50 wt. % of water by D_2O. The measurements were performed under a stimulated spin-echo sequence with magnetic field gradients. An increasing gradient strength with a duration of 1 to 2 ms was applied. Importantly, the gradient strength and the diffusion time was varied for each sample in order to obtain well defined diffusion curves. The obtained data were fitted and analyzed with the Topspin 2.3 software.

4.4.2 Cryogenic-Scanning Electron Microscopy

The Cryogenic-Scanning Electron Microscopy (cryo-SEM) allows to characterize and visualize the structural changes of the microemulsions caused by the variation on their composition.[109–111] The structure of the bicontinuous microemulsion was examined by cryo-high resolution scanning electron microscopy (cryo-SEM). Each sample was cooled by plunging into nitrogen slush at atmospheric pressure. Afterwards, the samples were freeze-fractured at -180°C, etched for 45 sec at -98°C and sputtered with chromium in the GATAN Alto 2500 cryo-preparation chamber and then transferred into the cryo-SEM (S-4800, Hitachi).

4.4.3 Atomic Force Microscopy

The planar solid surfaces were scanned by means of Atomic Force Microscopy (AFM) in order to determine their roughness. The scanning of the surface was done in air and tapping mode, using a AFM Cypher Scanning Probe Microscope (Asylum Research, USA) and Olympus AC160TS cantilevers. Data analysis was performed with the program Igor Pro 6.1.2. Through this program, the surface roughness was calculated according to the following equation:

$$\sigma = \frac{1}{N}\left(\sum y_i^2\right)^{1/2} \tag{4.23}$$

where σ is the root-mean-square roughness of the scan area, N is the number of pixels of the area and y_i is the distance of the corresponding pixel.

4.4.4 Ellipsometry

The thickness of the layer on the functionalized model planar surfaces was evaluated by means of ellipsometry. The ellipsometric measurement was carried out with PCSA ellipsometer (Optrel Gbr, Germany) in Null ellipsometry mode. The measurement was performed at ambient conditions and room temperature. The measurements were performed with a PCSA (polarizer- compensator- sample- analyzer) ellipsometer (Optrel GbR, Sinzing, Germany). The laser is a NeHe-Laser with a fixed wavelength of $\lambda = 632.8$ nm. The data were analysed by the program: "Ellipsometry, simulation and data evolution", where the thickness of the silicon oxide layer (hydrophilic model planar surface) and the

dichlorodimethylsilane layer (hydrophobic model planar surface) are estimated. Table 4.5 shows the used model for the thickness evalaution of the planar surfaces.

Table 4.5: The layer model for ellipsometry evaluation. Air and silicon are the surrounding media (infinite thickness)

Hydrophilic planar surface

Layer	**Thickness (nm)**	**Refractive index**	**K**
Air	Infinite	1.000	0.000
Silicon oxide	fit	1.4598	0.000
Silicon	Infinite	3.885	-0.018

Hydrophobic planar surface

Layer	**Thickness (nm)**	**Refractive index**	**K**
Air	Infinite	1.000	0.000
dimethylsilane	fit	fit	0.000
Silicon oxide	fit	1.4598	0.000
Silicon	Infinite	3.885	-0.018

4.4.5 Density Measurements

Density of the pure components and microemulsions was measured by using a precision Density Meter Anton Paar DS 5000 at 25 °C. The densimeter was calibrate with Millipore water and air. Precision of the densimeter corresponds to 1 $\times 10^{-6}$ g l^{-1}. Three repeated measurements were carried out for each sample.

4.4.6 Tensiometry

The surface tension of liquids were determined with a KRÜSS force tensiometer K11 (Germany) using the du Noüy ring method. Prior the measurements, the ring was flamed to eliminate the organic contaminants. Three repeated measurements for each sample were carried out at 25 ° C.

4.4.7 Viscosimetry

The viscosity of liquids was measured in the PC-controlled Lauda processor viscosity system PVS1 (Lauda, Germany) and Ubbelohde glass capillary viscometer with constants 1.03 and 1.36 $mm^2\ s^{-1}$ (Schott, Germany). The temperature was controlled with a Lauda E200 thermostat with ± 0.01 K control and Lauda 015T water bath. Three repeated measurements were carried out for each sample at constant temperature of 25 ° C.

4.5 Empirical models for the evalutaion of extraction kinetics

In literature, one can find different models applied to describe extraction processes and for the optimization of the extraction efficiency. Differences in the applicability of models can be attributed to the variations in target compounds as well as type of the extraction processes. Therefore, it is important to evaluate, which kinetic model describes best the experimental data. Here, we discuss the four most prominent models by fitting them to the data and compare the goodness of the fits using the Pearson correlation coefficient.

4.5.1 First-order model

To model the kinetics of transfer of extracted solute from the solid surfaces to the bulk liquid phase, a kinetics model based on the first Fick diffusion law can be used.[112] Formally, by integrating Fick's differential equation with boundary conditions of zero extraction of the contaminant, at the extraction time t=0, one obtains the exponential function:

$$E(t) = E_c(1 - exp(-(kt))) \tag{4.24}$$

The constant k denotes the overall extraction rate coefficient of the contaminated surface to the microemulsion, E_c indicates the percentage of extraction of the contaminant at the equilibrium stage.

4.5.2 Peleg's model

The semi-empirical extraction kinetic model of Peleg has been widely used to describe the sorption isotherms of food materials.[113] Since the extraction process corresponds reciprocally to the sorption process, the Peleg equation with some modifications can be applied to describe extraction curves:[114]

$$E(t) = \frac{t}{k_1 + k_2 t} \tag{4.25}$$

where k_1 is Peleg's rate constant given as the extracted percentage as a function of time, and k_2 is Peleg's capacity constant at the equilibrium stage.

4.5.3 Modified Gompertz model

The Gompertz model is a kinetic model employed to describes asymmetrical sigmoidal curves. This model has been mainly used to describe the exponential growth of microorganism,[115] and it has been also successfully applied to describe the extraction of bio-active compounds from natural sources:[116]

$$E(t) = E_c exp\left(-exp\left(\frac{E_{max}}{c_0}(\lambda - 1) + 1\right)\right) \tag{4.26}$$

The term E_c corresponds to the percentage of compounds extracted at the equilibrium stage, E_{max} represents the maximum extraction rate and λ is the delay time.

4.5.4 Two-site kinetics model

The two-site kinetics extraction model is applied to evaluate the solid-liquid extraction process in which the external elusion of the compound is faster than its internal diffusion in the solid phase, such that the rate of extraction is limited by the internal diffusion.[116] In general, the two-site kinetics model consists on the association of two exponential functions corresponding to two first order processes:

$$E(t) = E_c\left(1 - (x \cdot exp\left(k_1 t\right)) - ((1 - x)\, exp\left(k_2 t\right))\right) \tag{4.27}$$

The term E_c corresponds to the extracted percentage at the equilibrium stage. x represents the fraction of substance extracted by the external elusion process with rate constant k_1 (min^{-1}). (x-1) represent the fraction of substance within the slower process (internal diffusion) with rate constant k_2 (min^{-1}).

4.5.5 Evaluation of the models

The four conventional kinetic models have been fitted to the experimental data using the least squares fit algorithm of the Mathcad Prime 2.0 software. The goodness of the description of the experimental data by the models was analyzed using the Pearson correlation coefficient r and the normalized root mean square error value (NRM):

$$NRM = \frac{1}{max(dat_i)} \sqrt{\frac{1}{n-1} \sum_{i=1}^{n} (fit_i - dat_i)^2} \tag{4.28}$$

where $\max(dat_i)$ is the maximum value of the data points dat_i, and fit_i refers to the respective functional value of the modeling curve. The normalization of the mean square error value compares the goodness of the fits for extraction kinetics of different amplitudes

Chapter 5

Structural characterization of microemulsions in bulk*

Abstract

Sugar surfactant based microemulsion systems were prepared by using tetradecane (non-polar) and methyl oleate (polar) oils. The influence of the oil type employed in the preparation of the microemulsion systems on their structural properties in the bulk was evaluated. The bulk structure of the microemulsion systems was characterized by means of small-angle neutron scattering, diffusion neutron magnetic resonance spectroscopy, and scanning electron microscopy. The complementary results of the three employed methods revealed the formation of a bicontinuous structure in the whole range of oil-to-water content (α) in both sugar microemulsion systems. These results also demonstrated that the range of ordering of the bicontinuous structure depends on the type of oil used for their preparation. The microemulsions prepared with methyl oleate present a short range order compared to the microemulsions prepared with tetradecane. The difference in the range of ordering between both microemulsion systems has been associated with the degree of interaction between the oil molecules and the surfactant membrane.

5.1 Introduction

Sugar surfactant based microemulsions are thermodynamically stable and optically transparent colloidal liquids composed by polar and non-polar nanodomains, which are stabilized by a surfactant membrane.[6–8] The difference in polarity of the nanodomains, in addition to their high interfacial area, favors the solubilization and transport of substances of a wide range of polarity and at the same time enhances the ability of the microemulsions to wet and penetrate into different kind of solid surfaces. Due to these unique properties, sugar surfactant based microemulsions are receiving considerable attention for the decontamination of indoor and outdoor surfaces under a wide range of conditions. Owing to

*Adapted from Journal of colloid and interface science, Vargas Ruiz, S., Schulreich, C., Kostevic, A., Tiersch, B., Koetz, J., Kakorin, S., von Klitzing, R., Jung, M., Hellweg, T. Wellert, S, 2016, 471, pages 118-126, Extraction of model contaminants from solid surfaces by environmentally compatible microemulsions, Copyright (2017), with permission from Elsevier. Adapted with permission from Langmuir, Vargas-Ruiz, S., Solwedel, O., Micciulla, S., Sreij, R., Feoktystov. A., von Klitzing, R., Hellweg, T. Wellert, S. Sugar Surfactant based microemulsions at solid surfaces: Influence of the oil type and surface polarity, DOI 10.1021/acs.langmuir.6b03441, Copyright (2017). American Chemical Society.

the multiple advantages of sugar surfactant based microemulsions and their increasing importance as a potential decontamination medium, the complete characterization of these colloidal systems must be carried out to evaluate the influence of the microemulsion composition on its structural properties in bulk. The relationship between the composition and structure of the sugar surfactant based microemulsions is the key to understanding the efficiency of these complex fluids on the decontamination processes.

In the present chapter, the sugar surfactant based microemulsion systems used in the current investigation are introduced. The microemulsion systems were prepared by using tetradecane (nonpolar) and methyl oleate (polar) as the oil components. The phase tetrahedrons of the microemulsion systems: water/ tetradecane/ $C_{12/13}G_{1.3}$(SL 55)/ pentanol (TD-microemulsion) and water/ methyl oleate/ $C_{12/13}G_{1.3}$(SL 55)/ pentanol (MO-microemulsion) were studied at different sections between $\alpha = 0.1$ and $\alpha = 0.7$. The structural properties of the prepared microemulsions were determined by means of three complementary methods: small-angle neutron scattering (SANS), diffusion neutron magnetic resonance (NMR) spectroscopy, and cryogenic scanning electron microscopy (Cryo-SEM). The obtained results show a clear correlation between microemulsion composition (the type of oil and its content) and its structural properties in the bulk phase.

5.2 Results

5.2.1 Phase diagrams of sugar surfactant based microemulsions

Figure 5.1 depicts the phase diagrams of the quaternary system of the sugar surfactant based microemulsion systems using tetradecane and methyl oleate as the non-polar phase, water as the polar phase and pentanol as the cosurfactant. The phase behavior of both tetradecane based microemulsions (TD-microemulsions) and methyl oleate microemulsions (MO-microemulsions) was evaluated at a constant ratio of oil and water (α), while the content of surfactant (γ) and co-surfactant (δ) was systematically varied[†].

The phase diagrams created for each ratio of oil and water content (α) are characterized by their inversion point or x point. The inversion points indicate the minimum content of surfactant (γ) required to obtain one phase microemulsions (see section 2.1.1). For both microemulsion systems, the variation of (α) induces a shifting of the inversion point in a parabolic fashion. At low oil content ($\alpha = 0.1$) a minimum surfactant content is required

[†]The phase diagrams were created by C. Schulreich and R.Sreij. Physikalische Chemie III, Universität Bielefeld, Germany.

for microemulsion formation. The amount of surfactant and co-surfactant needed to form a microemulsion is maximum when the oil and water contents are symmetric ($\alpha = 0.5$). At high oil content ($\alpha = 0.7$), the inversion point shifts once more to low surfactant contents. The shifting of the inversion point in a parabolic fashion can be explained considering that microemulsions with equal amount of oil and water ($\alpha = 0.5$) have larger interfacial areas in comparison to microemulsions with an asymmetric composition; thereby, a high surfactant content is required to stabilize the microemulsions with $\alpha = 0.5$.[117]

Interestingly, some differences in the phase diagrams of both microemulsion systems can be observed. In general, the inversion points of the TD-microemulsions shifted toward higher contents of surfactant and co-surfactant for all α in comparison to inversion points of MO-microemulsions, except for the TD-microemulsion $\alpha = 0.1$ where a lower amount of surfactant than in MO-microemulsion $\alpha = 0.1$ is required.

The TD- and MO-microemulsions at each α were prepared in correspondence with the phase diagrams by adjusting the surfactant (γ) and co-surfactant (δ) contents in the one phase region, close to the inversion point of the phase diagrams. In this area, the spontaneous curvature of the surfactant membrane is nearly zero such that microemulsions with a bicontinuous structure can be formed.[23] In this investigation, the formation of single phase microemulsions with bicontinuous structures was highly desired as it favors high interfacial areas between the oil and water domains, which in turn enhances the ability of the microemulsions to wet solid surfaces of different polarity and the transport of the contaminants between different nanodomains. Furthermore, a robust formulation is obtained in this region, because small differences in the composition and the purity of the technical grade substances do not considerably influence the properties and stability of the prepared microemulsions.

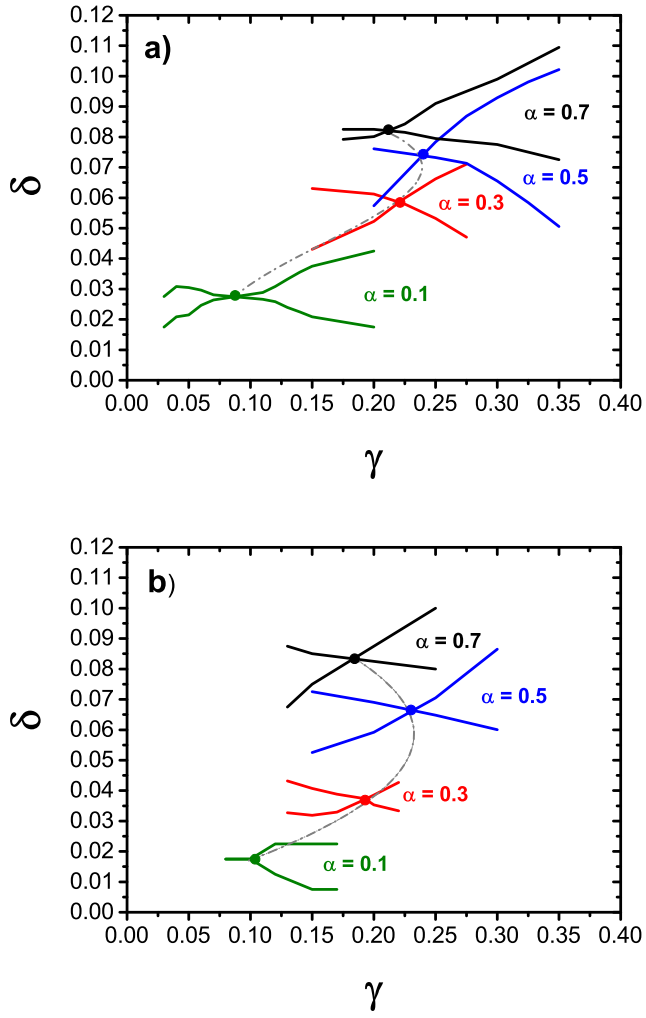

Figure 5.1: Phase diagrams of a) water/ tetradecane/ $C_{12/13}G_{1.3}$(SL 55)/ pentanol (TD-microemulsion) and b) water/ methyl oleate/ $C_{12/13}G_{1.3}$(SL 55)/ pentanol (MO-microemulsion) at different sections along the oil-water axis between $\alpha = 0.1$ and $\alpha = 0.7$

5.2.2 Structural characterization of microemulsions in bulk

Structural characterization by SANS

The mesoscopic structure of TD- and MO-microemulsions was investigated by means of SANS. In particular, the structural changes of the microemulsions at each α were investigated. For each α, the content of co-surfactant (δ) was kept constant, whereas the surfactant content (γ) was systematically varied. The scattering curves of both microemulsion systems are depicted in Figures 5.2 and 5.3, respectively.

In all data sets of the two microemulsion systems, a distinct correlation peak is observed.

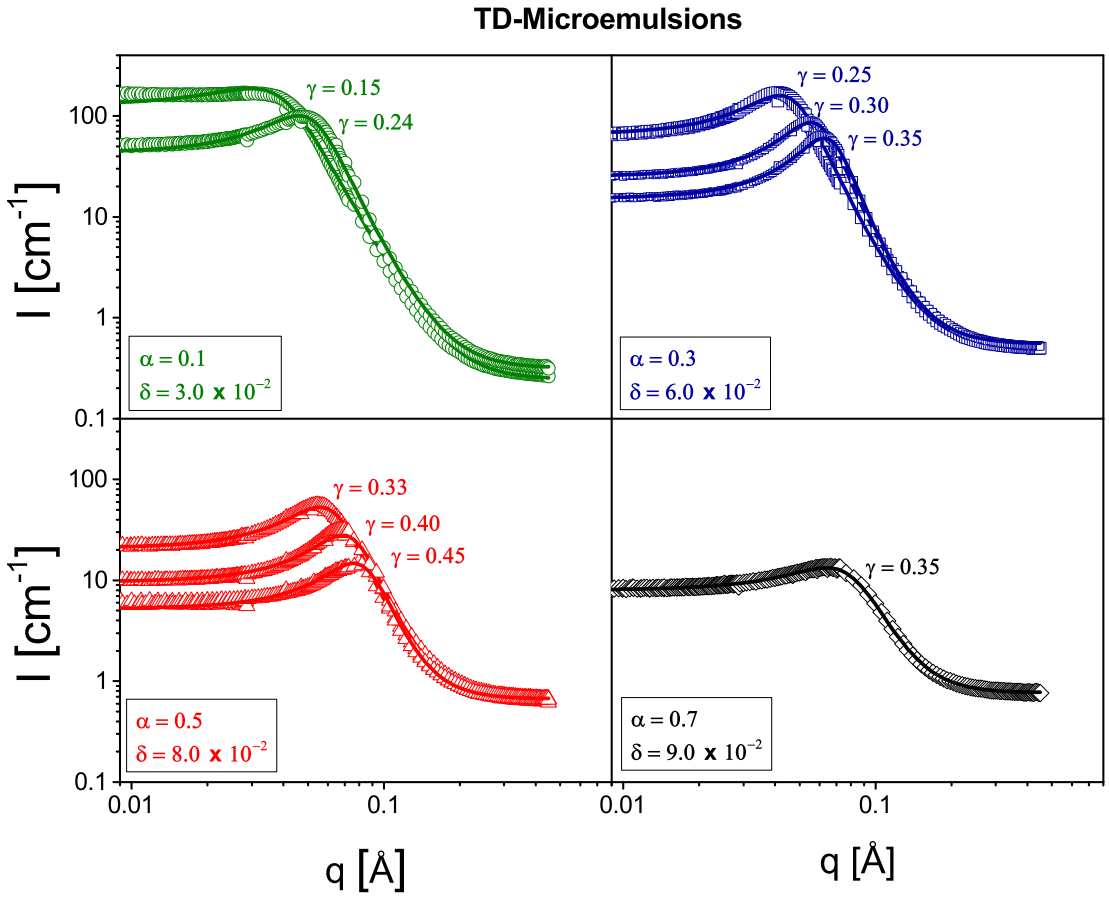

Figure 5.2: Scattering curves of tetradecane based micromulsions. Solid lines correspond to the fits of the scattering data by the Teubener-Strey model (Section 4.1.1)

This peak shifts to larger Q values when the content of surfactant (γ) increases at each series of α, indicating the formation of smaller domains. In addition, the scattering peaks vanish with α. The vanishing of the peak can be associated with the formation of more elongated nanodomains. The qualitative evaluation of the scattering peaks also reveals that the TD-microemulsions have more ordered structures in bulk as their scattering peaks are more pronounced in comparison to the MO-microemulsions.

In order to gain quantitative information of the scattering curves, the scattering intensities were fitted by means of the Teubner-Strey model (Section 4.1.1).[83,84] Although the Teubner-Strey model was developed for analyzing bicontinuous microemulsions with equal amounts of oil and water, it yields a good estimation of the domain size (d_{TS}) and the correlation length (ξ_{TS}) for bicontinuous microemulsions with α deviating from 0.5. Besides, the prepared microemulsions are also characterized by the amphiphilicity factor (f_a), the

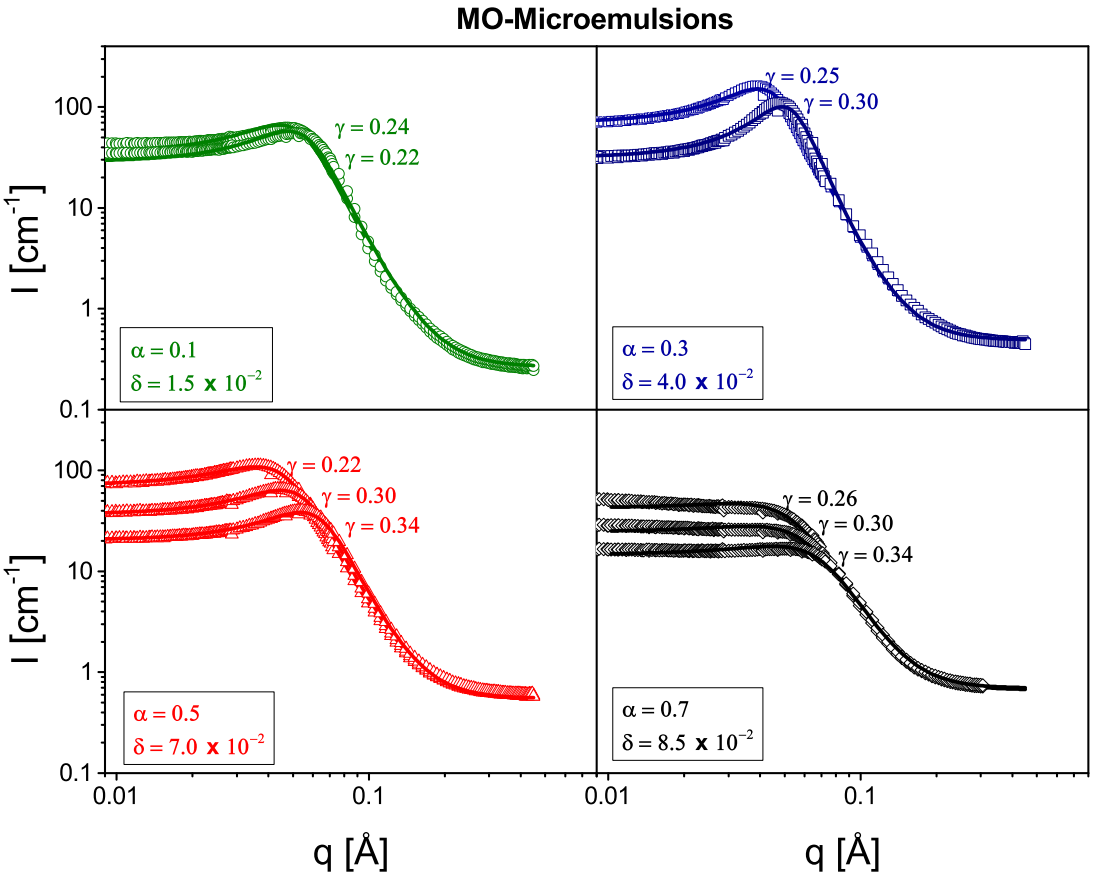

Figure 5.3: Scattering curves of methyl oleate based micromulsions. Solid lines correspond to the fits of the scattering data by the Teubener-Strey model (Section 4.1.1)

renormalized (κ_{SANS}) and bare bending moduli (κ_{bare}). These parameters are calculated according to the equations Eq.4.4, 4.5 and 4.6. All the structural parameters of the TD- and MO-microemulsions as well as their amphiphilicity factor and bending moduli at different α and γ are summarized in Table 5.1.

The domain sizes of both microemulsion systems are mainly dependent on the surfactant content (γ) and oil content (α), a decrease of the domain sizes is observed when γ and α increase. In addition, the TD-microemulsions present smaller domain sizes than the MO-microemulsions when they are prepared at the same α and γ. For example at $\alpha = 0.3$ and $\gamma = 0.30$, the domain sizes for TD-microemulsion and MO-microemulsion are 108 Å and 122 Å, respectively.

In contrast to the domain sizes, the increase of γ in each series of α on both microemulsion

Table 5.1: Structural parameters (domain size (d_{TS}), correlation length (ξ_{TS}), bending modulus (renormalized (κ_{SANS}) and bare (κ_{bare})) of the tetradecane and methyl oleate based microemulsions

Tetradecane based microemulsion

Sample			d_{TS}	ξ_{TS}	κ_{SANS}	κ_{bare}	f_a
α	δ	γ	(Å)	(Å)	(K_BT)	(K_BT)	
0.1	3.0 x 10^{-2}	0.15	178.6 ± 3.3	53.1 ± 0.5	0.25 ± 0.02	0.68 ± 0.02	-0.60
0.1	3.0 x 10^{-2}	0.24	126.8 ± 5.7	54.0 ± 0.9	0.36 ± 0.03	0.71 ± 0.03	-0.71
0.3	6.0 x 10^{-2}	0.25	140.5 ± 7.5	61.7 ± 1.1	0.37 ± 0.03	0.74 ± 0.03	-0.79
0.3	6.0 x 10^{-2}	0.30	108.5 ± 10.2	59.7 ± 1.6	0.46 ± 0.05	0.77 ± 0.05	-0.86
0.3	6.0 x 10^{-2}	0.35	96.8 ± 11.2	58.2 ± 2.2	0.51 ± 0.06	0.79 ± 0.06	-0.88
0.5	8.0 x 10^{-2}	0.33	105.6 ± 5.5	48.3 ± 0.8	0.39 ± 0.03	0.69 ± 0.03	-0.80
0.5	8.0 x 10^{-2}	0.40	86.7 ± 5.4	43.8 ± 1.0	0.43 ± 0.06	0.68 ± 0.06	-0.84
0.5	8.0 x 10^{-2}	0.45	78.3 ± 6.1	40.0 ± 1.2	0.43 ± 0.06	0.66 ± 0.06	-0.80
0.7	9.0 x 10^{-2}	0.35	87.2 ± 1.2	30.1 ± 0.2	0.29 ± 0.01	0.54 ± 0.01	-0.65

Methyl oleate based microemulsion

Sample			d_{TS}	ξ_{TS}	κ_{SANS}	κ_{bare}	f_a
α	δ	γ	(Å)	(Å)	(K_BT)	(K_BT)	
0.1	0.7 x 10^{-2}	0.22	128.1 ± 3.3	47.0 ± 0.5	0.31 ± 0.02	0.66 ± 0.02	-0.58
0.1	0.7 x 10^{-2}	0.24	119.3 ± 3.4	45.9 ± 0.5	0.33 ± 0.02	0.67 ± 0.02	-0.63
0.3	4.0 x 10^{-2}	0.25	147.8 ± 6.1	60.0 ± 1.0	0.35 ± 0.03	0.73 ± 0.03	-0.76
0.3	4.0 x 10^{-2}	0.30	122.6 ± 7.1	64.2 ± 2.0	0.45 ± 0.03	0.78 ± 0.03	-0.85
0.5	7.0 x 10^{-2}	0.26	151.6 ± 2.6	47.7 ± 0.4	0.27 ± 0.01	0.65 ± 0.01	-0.60
0.5	7.0 x 10^{-2}	0.30	125.7 ± 3.0	44.3 ± 0.5	0.30 ± 0.02	0.64 ± 0.02	-0.66
0.5	7.0 x 10^{-2}	0.34	106.6 ± 3.0	40.5 ± 0.5	0.32 ± 0.02	0.62 ± 0.02	-0.70
0.7	8.5 x 10^{-2}	0.26	144.9 ± 3.6	31.4 ± 0.4	0.19 ± 0.03	0.56 ± 0.03	0.24
0.7	8.5 x 10^{-2}	0.30	126.7 ± 2.5	28.1 ± 0.3	0.19 ± 0.02	0.53 ± 0.02	-0.01
0.7	8.5 x 10^{-2}	0.34	107.8 ± 2.0	26.4 ± 0.2	0.21 ± 0.02	0.53 ± 0.02	-0.26

systems does not have a significant impact on the correlation length and amphiphilicity factor. In this case, the variation of α in the microemulsions has a major influence on those parameters. A maximum values of the correlation length and amphiphilicity factor are obtained at $\alpha = 0.3$ and minimum values at $\alpha = 0.7$. This trend independent of the type of oil used in the preparation of the microemulsions. Similarly to the results of the correlation length, the renormalized and bare bending energies of both microemulsion systems also varied with α, reaching a maximum when the content of oil in the microemulsions is α = 0.3. Altough, the bending moduli of both microemulsions follow the same trend, it is noticeable that the renormalized bending moduli of the MO-microemulsion are smaller than the renormalized bending moduli of the TD-microemulsions within the range of α from 0.5 to 0.7. These data suggest that the chemical composition of the oil has an influence on the elasticity of the surfactant membrane in the microemulsions.

Structural characterization by diffusion NMR spectroscopy

Figure 5.4 depicts the normalized self-diffusion coefficients of water, tetradecane, and methyl oleate in the TD- and MO-microemulsions in the range from α =0.1 to α = 0.7. In this experiment, we focused on the microemulsions samples with the same composition as the samples employed in the evaluation of the wetting and extraction process (Table 3.2)[‡].

The measurement of the diffusion coefficient of the microemulsion components gives indirect information about the structure and connectivity of the oil and water nanodomains in the bulk of the microemulsions.[118,119] The self-diffusion coefficients were normalized with respect to the self-diffusion coefficient of pure liquids. In both microemulsion systems, the self-diffusion coefficient of water decreases continuously with α, while the self-diffusion coefficient of tetradecane and methyl oleate increases. Both water and oil components reach the same value of the self-diffusion coefficient when the composition of the microemulsion is nearly symmetrical, around $\alpha = 0.45$ and $\alpha = 0.35$ for the TD- and MO-microemulsions, respectively. Moreover, the self-diffusion coefficient of the surfactant (not shown here) changes continuously over the investigated range of α and becomes similar to the value of the oil, perhaps due to the better monomeric solubility of the sugar surfactant in oil. It is important to point out that the self-diffusion coefficient of water could not be estimated in the microemulsion samples with $\alpha = 0.7$ due to the weak NMR signal of water in these samples.

[‡]The diffusion coefficients were measured by Dr S. Kemper at NMR Messzentrum OC, TU-Berlin, Germany.

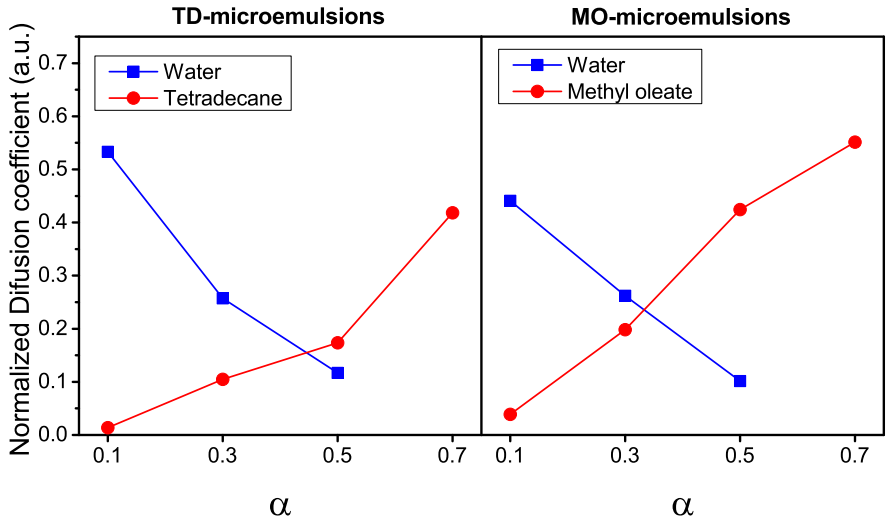

Figure 5.4: Normalized self-diffusion coefficients of water (red squares) and oil (blue squares) of the water and oil component of the microemulsions as a function of α determined by NMR.

Structural characterization by Cryo-SEM

Figure 5.5 presents the cryo-SEM images of MO-microemulsion structures (the composition of these samples is given in Table 3.2) .[§] Image a) shows the structure of MO-microemulsion with $\alpha = 0.1$. The structure of this microemulsion is characterized by the presence of irregular and branched domains of oil and water with sizes in the range from 15 to 20 nm. The increase of the oil content to $\alpha = 0.3$ induces a significant change in the structure (image b). At $\alpha = 0.3$, the oil and water domains are more interconnected than at $\alpha = 0.1$ such that resemble a typical bicontinuous structure. The bicontinuous structure is completely developed when the composition of the microemulsion is symmetric ($\alpha = 0.5$, image c). At this symmetric composition, more defined channels of oil and water are visible. These channels are highly interconnected, and the repeating distance between these channels is in the range from 15 to 20 nm. In image d), larger domains with fewer junctions can be observed at $\alpha = 0.7$.

[§]The cryo-SEM images were taken by Dr B. Tiersch at the Kolloidchemie Institute, Potsdam Universität

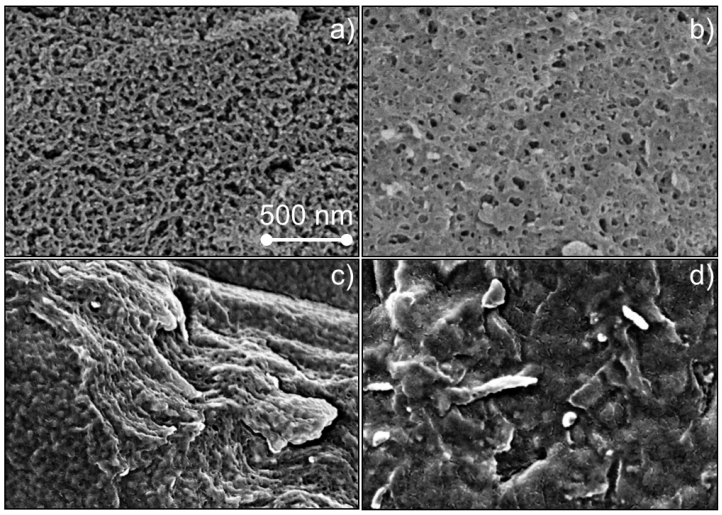

Figure 5.5: Cryo-SEM images of four samples from the bicontinuous region of a) $\alpha = 0.1$, b) $\alpha = 0.3$, c) $\alpha = 0.5$ and d) $\alpha = 0.7$.

5.3 Discussion

The phase diagrams for TD- and MO-microemulsion systems resemble typical Kahlweit fish-type diagrams obtained for model microemulsions and based on pure sugar surfactants and pure alkanes.[120] These results indicate that the technical grade quality of the sugar surfactant does not significantly influence the properties and structure of the surfactant interface. Therefore, the phase behavior of these microemulsions can be compared with data from model systems. Moreover, it was also observed that the inversion points of the TD-microemulsions shifted toward higher contents of surfactant and co-surfactant than the inversion points of MO-microemulsions. The shift of the inversion point is a result of the difference in polarity between the two oils involved in the preparation of the microemulsions. The sugar surfactant could be preferentially located at the methyl oleate/water interface than the less polar tetradecane/water interface.[121] This does not only have implication on the surfactant content required to establish the one-phase microemulsion, but also influences the elastic properties of the surfactant membrane.

The characterization of both microemulsion systems by means of SANS indicates that their structural properties are highly affected by their composition. A decrease of the domain sizes by increasing γ and α has been observed in both microemulsion systems. The formation of smaller domain sizes with γ is caused by an increase of the total the oil/water interface. The formation of the smaller domains with α can be considered as an indirect result of the need to increase the amount surfactant and co-surfactant contents

to solubilize the additional oil in one-phase microemulsions (shift of the phase diagrams to larger γ and δ with α). It has also been observed that domain sizes are smaller in the TD-microemulsions than in the MO-microemulsions with the same composition (α and γ). The domain size differences between both microemulsion systems could be attributed tentatively to the packing of the molecules in the oil domains. Tetradecane molecules could be densely packed in the nanodomains due to their linear structure, which is preferentially adopted as the trans-conformation of the alkane chain has the lowest energy.[122] In contrast, the methyl oleate molecule has a bent structure due to the presence of a cis-double bond. This structural conformation reduces the degree of packing of methyl oleate and thus induces an increase in domain sizes.

The elasticity of the surfactant membrane in both microemulsion systems is characterized by the renormalized bending modulus and the bare bending modulus. The values of the renormalized and bare bending moduli for both series of microemulsions are between 0.3 k_BT and 0.8 k_BT. These values are in the range of the bending moduli commonly reported in the literature for non-ionic microemulsions system, such as microemulsions stabilized with C_iE_j or sugar surfactants.[1,20,117] This suggests that the amphiphilic interface is highly flexible in both microemulsion systems. However, the degree of flexibility of the surfactant membrane depends on the oil content (α) in both microemulsion systems. Microemulsions with $\alpha = 0.3$ show larger bending moduli, indicating the formation of a stiffer surfactant membrane. Although the bending moduli of both systems show the same trend in terms of the α variation, it is important to point out that the renormalized bending moduli of TD-microemulsions are comparatively larger than those of MO-microemulsions, particularly at $\alpha = 0.5$ and $\alpha = 0.7$. Considering that the composition of the surfactant membrane is the same for both microemulsion systems (sugar surfactant and pentanol as co-surfactant), the differences of renormalized bending moduli could be related to the interaction between the oil molecules and the amphiphiles. In this respect, it has been probed via diffusion NMR spectroscopy that the unsaturated fatty acid ethyl oleate can penetrate into the surfactant membrane of non-ionic microemulsions.[123] In a similar fashion, the methyl oleate could penetrate into the sugar surfactant membrane. This could enhance the fluidity of the membrane, which in turn would result in a more flexible membrane represented by the lower elastic constants. Furthermore, a more flexible surfactant membrane can have a direct impact on the degree of ordering of the nanodomains in the bulk of microemulsions.

The degree of ordering of the oil and water nanodomains in the bulk of microemulsions can be indirectly evaluated by means of the correlation length (ξ_{TS}) and the amphiphilicity factor (f_a). The correlation length (ξ) is a parameter related to the distance at which

the quasi-periodicity of the oil and water domains are maintained in the bulk phase. The amphiphilicity factor (f_a) quantifies the amphiphilic strength of a surfactant, and its value also is related to the degree of organization of the microemulsions in the bulk phase.[87,88] A value of f_a close to 1 is characteristic for disordered systems and -1 for more organized systems (i.e., lamellar phases).[87,88] It has been proposed that within this range the values of f_a of well-defined bicontinuous structures should be between -0.7 and -0.9.[124] According to the values of correlation length (ξ) and the amphiphilicity factor (f_a) reported in Table 5.1, it is evident that both microemulsion systems are highly structured when their composition is symmetric ($\alpha = 0.3$ and $\alpha = 0.5$), particularly at $\alpha = 0.3$, where the correlation length reaches maximum values and their amphiphilicity factors are in the range from -0.70 to -0.90, which are typical values for microemulsion systems with a bicontinuous structure. For microemulsions with an asymmetric composition ($\alpha = 0.1$ and $\alpha = 0.7$), the lower values of the correlation length (ξ) indicate the formation of less organized structures in the bulk phase. These microemulsions also differ from the well-defined bicontinuous structure due to their amphiphilicity factor (f_a). Interestingly, the correlation length (ξ) and the amphiphilicity factor (f_a) of TD-microemulsions are larger than those of MO-microemulsions at $\alpha = 0.5$ and $\alpha = 0.7$, indicating that the preparation of microemulsions with tetradecane induce the formation of more organize structure than the microemulsions prepared with methyl oleate. This fact can be associated with differences in the elasticity of the surfactant membrane between both microemulsion systems such that the higher the flexibility of the surfactant membrane, the lower the degree of organization of the microemulsion nanodomains in bulk.

As mentioned before, the amphiphilicity factor (f_a) suggests the formation of a well-defined bicontinuous structure when the composition of the microemulsion is symmetric ($\alpha = 0.3$ and $\alpha = 0.5$) and the formation of a less-defined structure at the asymmetrical compositions ($\alpha = 0.1$ and $\alpha = 0.7$). These structural transitions in both microemulsion systems by the variation of α are also corroborated by the evaluation of the diffusion coefficient of their components (Figure 5.4) and the direct imaging of the nanodomains via cryo-SEM (Figure 5.5). The evaluation of the diffusion coefficient of oil and water in both microemulsion systems shows a restriction of the mobility of each component in the water and oil-rich regions. In contrast to the restrictions in diffusion at high and low α, water and oil can equally diffuse at symmetrical composition. This change in the mobility of the microemulsion components with the variation of α clearly indicates the formation of segregated and smaller domains in the water and oil-rich regions, and the formation of highly interconnected or continuous structures at the intermediate oil and water contents or symmetrical composition.[118,119] The grade of the nanodomain connectivity can be easily

visualized for all α by cryo-SEM in the images of MO-microemulsions. These images show the formation of the oil/water channels in the entire range of α. At symmetric composition ($\alpha = 0.3$ and $\alpha = 0.5$), these channels are highly interconnected.

In this study, the complementary results of the three employed techniques suggest that the structure of both MO- and TD-microemulsions is bicontinuous at all investigated α. This bicontinuous structure is characterized by the formation of elongated nanodomains with an irregular interface due to the high elasticity of the sugar surfactant membrane. The degree of connectivity of these nanodomains is determined by the water and oil content in the microemulsions. A diluted bicontinuous and less interconnected structure is formed at the asymmetric composition, whereas at the symmetric composition a well-defined bicontinuous structure is developed.[125]

5.4 Conclusion

The phase tetrahedrons of the quaternary microemulsion systems water/ tetradecane/ $C_{12/13}G_{1.3}$(SL 55)/ pentanol (TD-microemulsion) and water/ methyl oleate/ $C_{12/13}G_{1.3}$(SL 55)/ pentanol (MO-microemulsion) were studied at different sections along the oil-water axis between $\alpha = 0.1$ to $\alpha = 0.7$. The structure of the chosen microemulsions in bulk was characterized by SANS, diffusion NMR, and cryo-SEM. The complementary results obtained by these three techniques allowed to determine the structure of the TD-microemulsions and MO-microemulsions as bicontinuous across the whole α. This bicontinuous structure is characterized by the formation of elongated and highly deformable oil and water nanodomains. The size of these nanodomains is highly influenced by the surfactant content (γ), the oil and water content (α), and the type of oil used in the preparation. Furthermore, the degree of connectivity of the oil and water nanodomains is influenced by the oil and water content (α). Well-defined bicontinuous structures are formed when the composition of the microemulsion is symmetric ($\alpha = 0.3$ and $\alpha = 0.5$), whereas diluted and less connected bicontinuous structures are developed at asymmetric compositions ($\alpha = 0.1$ and $\alpha = 0.7$). Importantly, the formation of the bicontinuous structure in the whole α in both microemulsion systems is supported by the high flexibility of the sugar surfactant membrane.

It has also been demonstrated that the bending moduli of the sugar surfactant based microemulsions highly depend on the type of oil used in the preparation of microemulsions.

The estimated bending moduli of TD-microemulsion are larger than those of the MO-microemulsion. The variation between the surfactant membrane bending moduli of both microemulsion systems has been associated tentatively with the interaction between the oil molecules with the surfactant membrane. It has been proposed that, unlike tetradecane oil molecules, the methyl oleate molecules can easily penetrate into the sugar surfactant membrane. The penetration of the oil molecules into the membrane enhances its fluidity, therefore reducing the bending moduli. The reduction of the bending elasticity has a direct impact on the degree of organization of the nanodomains in the bulk of the microemulsions. In this case, the MO-microemulsions present short length ordering in bulk in comparison to the TD-microemulsions as it is evaluated by means of the correlation length and amphiphilicity factor.

The present study of the structural properties of the sugar surfactant based microemulsions involving tetradecane (nonpolar) and methyl oleate (polar) as the oil phase yields a good estimation on the relation between the composition and the structure of microemulsions.

Chapter 6

Structure of microemulsions at hydrophilic and hydrophobic solid planar surfaces*

The structure of sugar surfactant based bicontinuous microemulsions at hydrophilic and hydrophobic solid planar surfaces was studied by means of neutron scattering techniques. Particularly, the influence of the type of oil (tetradecane and methyl oleate) on the microemulsion structural properties in the vicinity of surfaces was investigated at different oil-to-water ratios. The obtained results revealed that the structure of the microemulsions near the surface is maintained, and the presence of the surface induces an ordering of the nanodomains in the perpendicular direction to the interface. The near-surface ordering is influenced by microemulsion composition and surface polarity.

6.1 Introduction

The presence of solid surfaces can influence the microemulsion structure as constraints imposed by the surface favor the ordering of complex fluids at the interface.[68,69] A deeper insight into the structuring of microemulsions at the solid-liquid interfaces is essential for this study, since the composition and the structuring properties of microemulsions near the interface have a strong impact on the wetting of surfaces and the transport of the contaminants from the solid to the liquid phase.

Previous work studied the near-surface structure of bicontinuous microemulsions on planar surfaces via neutron reflectometry, grazing incidence scattering, and computer simulations.[74–76] These studies have shown that the presence of the solid surface induces a structural transition in the microemulsion from bicontinuous to well-defined alternating channels of oil and water (lamellar structure) in the vicinity of the solid-liquid interface. These studies on the near-surface structure of microemulsions were focused on non-ionic C_iE_j-type and alkane oil-based microemulsions. The composition of those microemulsions were symmetric (equal water and oil contents, $\alpha = 0.5$), and the lengths of the alkyl chain of the surfactant and the alkane oils were similar (C10, C12).[74–76] Studies related to the structuring of microemulsions with a less symmetric composition based on sugar

*Adapted with permission from Langmuir, Vargas-Ruiz, S., Solwedel, O., Micciulla, S., Sreij, R., Feoktystov. A., von Klitzing, R., Hellweg, T. Wellert, S. Sugar Surfactant based microemulsions at solid surfaces: Influence of the oil type and surface polarity, DOI 10.1021/acs.langmuir.6b03441, Copyright (2017). American Chemical Society.

surfactants and biocompatible oils have not been reported according to the best of our knowledge. Such experiments are essential, as they could give a deeper insight into the interplay between microemulsion and surface properties on the structure of those complex fluids near to the surface.

In this chapter, the effect of planar surfaces of different polarity on the inner structure of TD- and MO-microemulsions is investigated. The structural conformation of the microemulsion near and at the solid-liquid interface was investigated by neutron reflectometry (NR) and grazing-incidence small-angle neutron scattering (GISANS). The comparison of the structural properties measured in bulk (Chapter 5) and near-interface allows correlating the structural changes due to the effects arising from (I) variation in the composition of the microemulsion and (II) surface polarity.

6.2 Results

6.2.1 Structure of microemulsions perpendicular to the solid surface

Figure 6.1 shows the reflectivity curves of TD-microemulsions at different α in contact with a hydrophilic (Figure 6.1a) and a hydrophobic (Figure 6.1b) surface. The reflectograms of the TD-microemulsions reveal a distinct Bragg peak, which broadens and shifts to higher Q_z at increasing α in the microemulsion. The Bragg peak originates from the structuring of the microemulsion at the solid/liquid interface. The broadening of the Bragg peak is interpreted as the deorientation of the microemulsion structure in the direction perpendicular to the surface.

The reflectivity curves can be described by the equation 4.8. This equation represents the oscillating variation of the scattering length densities (SLD) related to alternating oil- and water-rich regions of the TD-microemulsions in the vicinity of the hydrophilic (Figure 6.1c) and hydrophobic (Figure 6.1d) surfaces, respectively[†]. Before the oscillation of SLD takes place, the SLD show a constant value due to the silicon substrate (situated at negative z-values), followed by a layer of SiO_2 with a thickness of 15 Å and an SLD value of 3.47 x 10^{-6} $Å^{-2}$.

[†]The fitting of the neutron reflectometry data was done in cooperation with Dr Soltwedel, Max-Planck-Institute for Solid State Research, Outstation at MLZ, Garching, Germany.

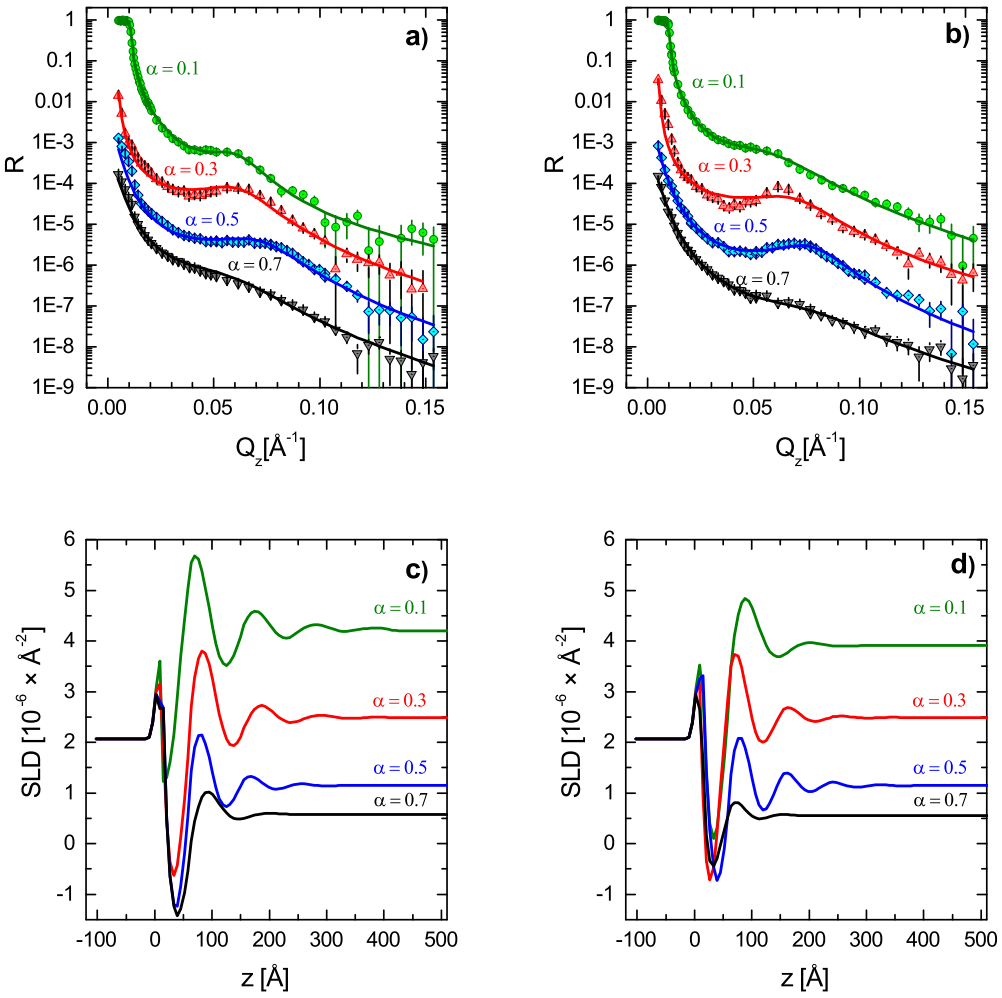

Figure 6.1: Reflectivity curve of tetradecane-based microemulsions at (a) hydrophilic surface and (b) hydrophobic surface. Solid lines correspond to the fit of the scattering data according to Eq.4.8, the corresponding SLD profiles for the hydrophilic and hydrophobic surfaces are presented in Figure (d) and (c).

Figure 6.2 depicts the reflectivity curves and the corresponding SLD profiles of MO-microemulsions at a hydrophilic (Figure 6.2 a,c) and a hydrophobic (Figure 6.1 b,d) surface. The reflectivity curves of the MO-microemulsions show the same features as the reflectivity curves of the TD-microemulsions. However, the SLD profile of the MO-microemulsions indicates a difference in the near-surface structure when the surface polarity is varied. In particular, the MO-microemulsions show well-defined oscillations for all α at the hydrophilic surface, while the oscillations are strongly damped at the hydrophobic surface at increasing α.

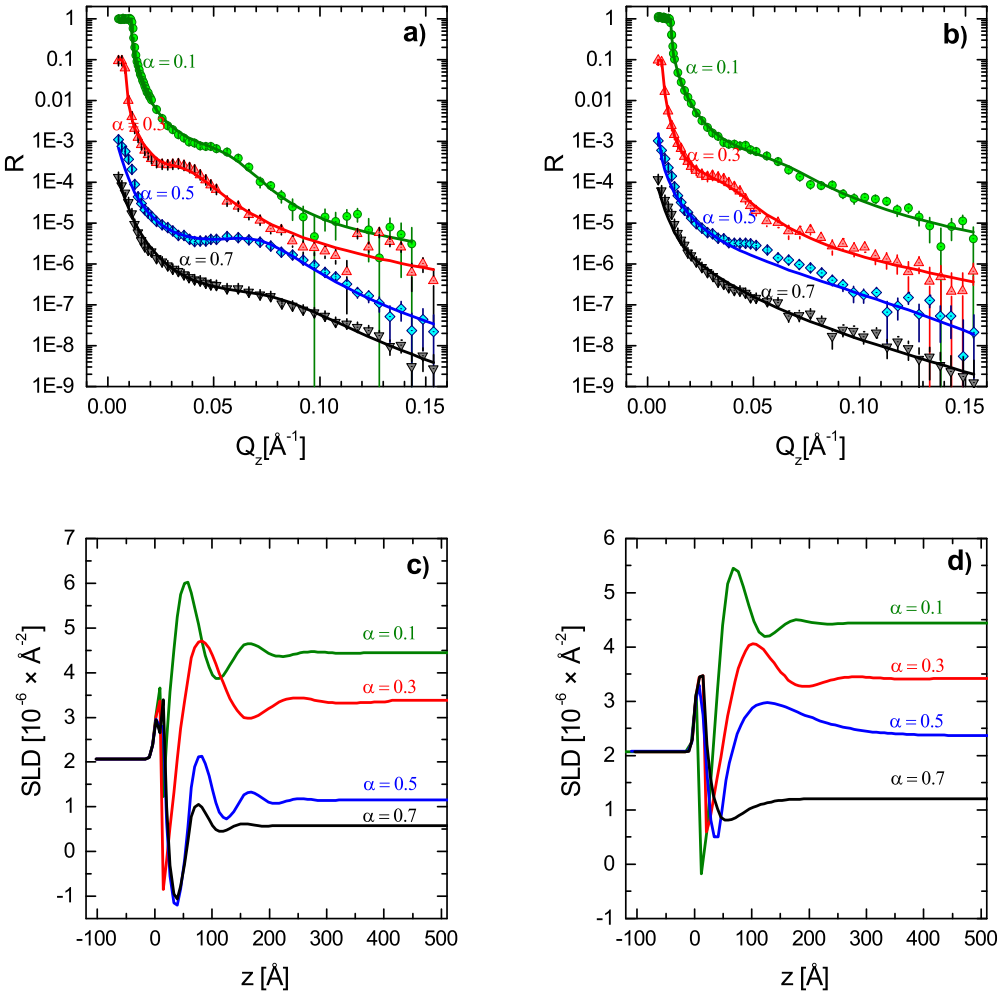

Figure 6.2: Reflectivity curves of methyl oleate-based microemulsions at (a) hydrophilic surface and (b) hydrophobic surface. Solid lines correspond to the fit of the scattering data according to Eq.4.8, the corresponding SLD profiles for the hydrophilic and hydrophobic surfaces are presented in Figure (c) and (d).

The domain size and correlation length ξ_z of microemulsions at the surface can be estimated from the SLD profiles (Eq.4.8). These structural parameters near the surface plotted in Figures 6.3 and 6.4 are compared to their structural parameters determined in bulk (Tables 5.1). The structural parameters of the microemulsions at the hydrophilic and hydrophobic surfaces are in the same range as their corresponding structural parameters in bulk. In general, the domain size and correlation length decrease with increasing α for the TD-microemulsions. For the MO-microemulsions, a maximum in both structural parameters was found when the content of oil in the microemulsion is equal to $\alpha = 0.3$. The structural parameters for the MO-microemulsions with higher oil content at the hydrophobic surface could not be computed due to the extremely thin surface layer and the subsequent fast transition of the SLD to the corresponding bulk-phase properties (Figure 6.2d).

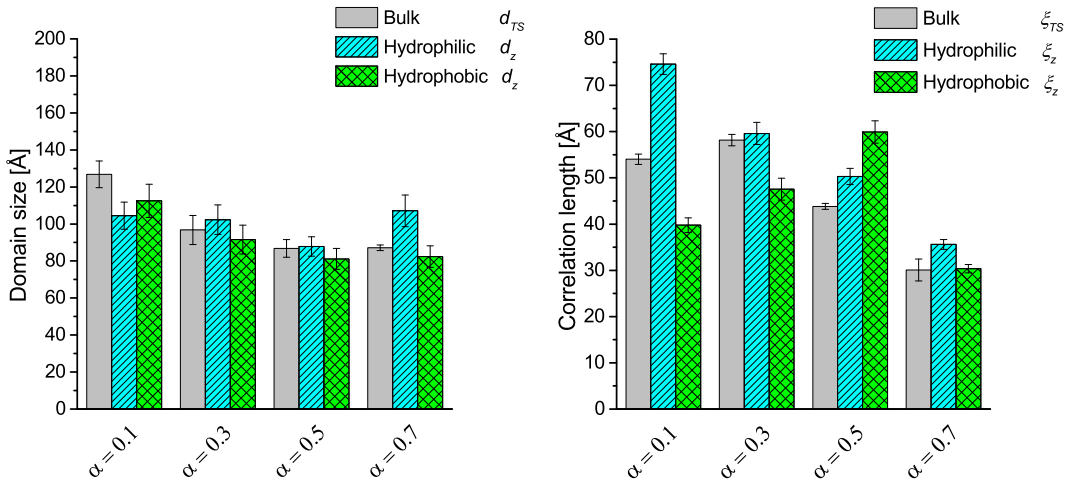

Figure 6.3: Comparison of the structural parameters domain size d_{TS} and correlation length ξ_{TS} of tetradecane-based microemulsions in bulk (Table 5.1) with their structural properties (d_z and correlation length ξ_z) at the hydrophilic and hydrophobic solid surfaces.

Furthermore, the SLD profile also gives qualitative information about microemulsion composition near the solid-liquid surface. Figure 6.5 shows the first SLD minimum values after the SLD range corresponding to the SiO_2 layer. The SLD minimum values are plotted as a function of α for both microemulsion systems at the hydrophilic and hydrophobic surfaces.

In general, the SLD values of both microemulsion systems presents the same trend at the hydrophilic solid-liquid interface, where the SLD value decreases with increasing α and reaches a plateau value at a higher oil content. The change of the surface polarity from

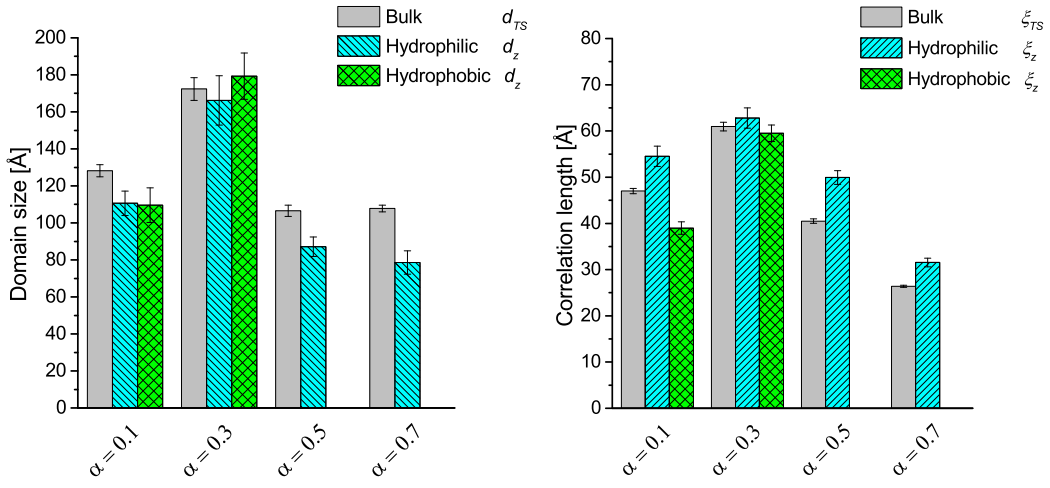

Figure 6.4: Comparison of the structural parameters domain size d_{TS} and correlation length ξ_{TS} of methyl oleate-based microemulsions in bulk (Table 5.1) with their structural properties (d_z and correlation length ξ_z) at the hydrophilic and hydrophobic solid surfaces.

hydrophilic to hydrophobic results in a change of the SLD values close to the interface. The SLD values of the TD-microemulsions at the hydrophobic surface slightly decrease, while the SLD values of the MO-microemulsions increase with α.

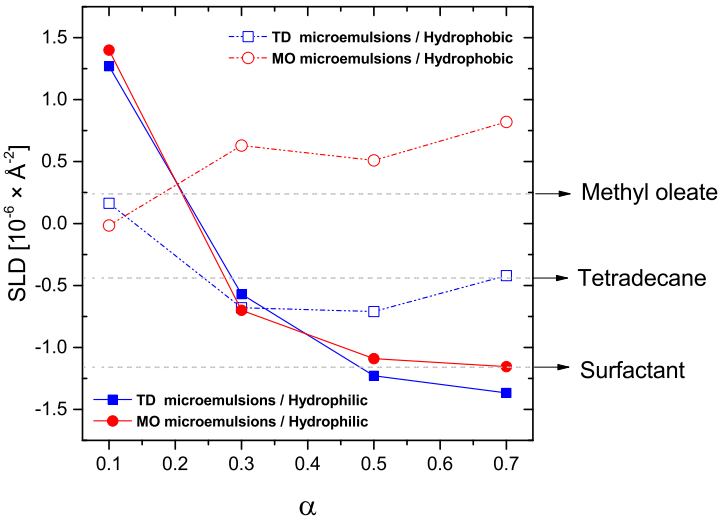

Figure 6.5: SLD values close to the solid-liquid interface for tetradecane-based microemulsions (squares) and methyl oleate-based microemulsions (circles) at the hydrophilic (closed symbols) and hydrophobic (open symbols) surfaces.

6.2.2 Structure of microemulsions parallel to the solid surface

The upper row of Figure 6.6 shows the scattered intensity distributions measured for TD microemulsions at the hydrophilic surface at different oil-to-water ratios α. The scattered intensity is mapped as a function of Q_z and Q_{xy}. At low Q_z and Q_{xy}, the transmitted and specular reflected beams are visible. Additionally, a broad Bragg Peak between Q_z = 0.03-0.04 $Å^{-1}$ is slightly visible. This enhanced scattering is ring-like distributed. This feature of the scattered intensity distributions becomes clearly visible in the transformation of the scattered intensity distribution shown in the lower row of Figure 6.6. Here, the scattered intensity is mapped as a function of Q with $\left(Q = \sqrt{{Q_{xy}}^2 + {Q_z}^2}\right)$ and the polar angle ϕ with ϕ=atan(Q_{xy}/Q_z). In this representation, the enhanced ring-like scattering transforms into a smeared but nearly horizontal distribution. This illustrates that the same structure is observed in all lateral directions.

Figure 6.7 plots the enhanced scattering as a function of Q, with ($Q = (Q_{xy}^2 + Q_z^2)^{1/2}$). The resulting intensity distributions show broad scattering peaks in the Q-range between 0.05$Å^{-1}$ and 0.08$Å^{-1}$. Qualitatively, they correspond to the features observed in the small angle scattering in bulk.

The solid lines in Figure 6.7 are fits of the Teubner-Strey model to the averaged diffuse-

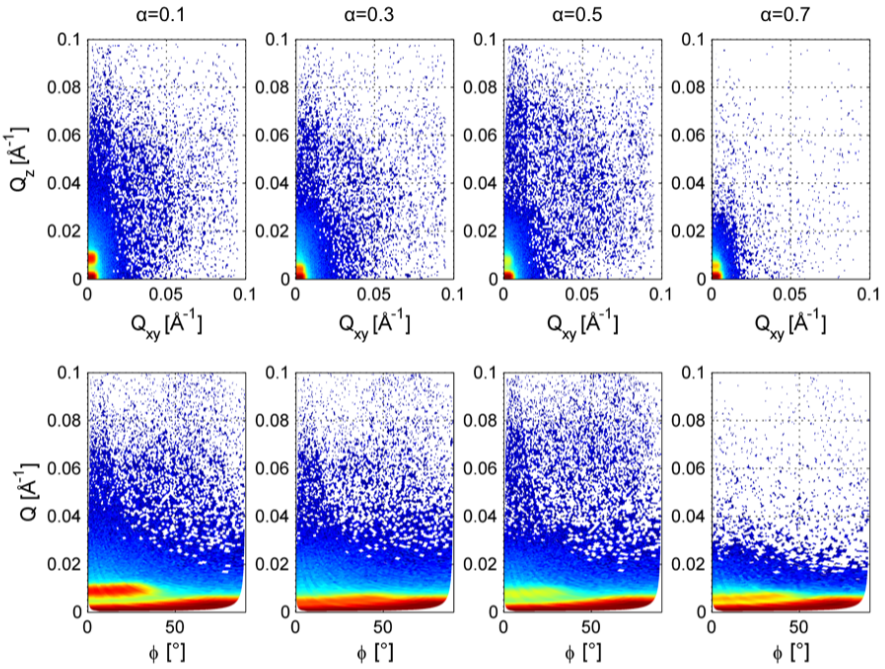

Figure 6.6: Upper row: GISANS pattern of tetradecane-based microemulsions at the hydrophilic surface at different oil to water ratios α. The scattered intensity is mapped as a function of Q_z and Q_{xy}. Lower row: Polar coordinate representation of the same scattered intensity distributions as a function of Q and ϕ (ϕ=atan(Q_{xy}/Q_z)).

scattered intensity profiles. The analysis focuses on the peak region, which is well described by the fits. At larger Q, the intensity decreases. The background level is not described by the model due to the limited precision of the background correction. However, the domain size d and the correlation length ξ were extracted from the fits.

Table 6.1: Summary of the resulting structural parameters from fitting of the Teubner-Strey model to the data in Figure 6.7

Sample	$\boldsymbol{d}$ (Å)	ξ (Å)
$\alpha = 0.1$	131	20
$\alpha = 0.3$	108	21
$\alpha = 0.5$	90	-

The resulting structural parameters are summarized in Table 6.1. The quality of the fits limits the precision of the estimation to about 20 %.

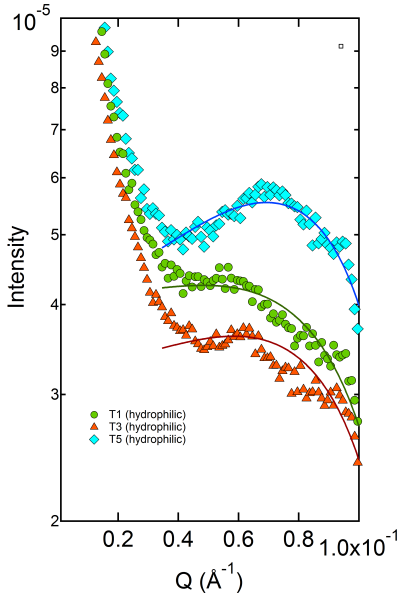

Figure 6.7: Radially-averaged diffuse-scattered intensity as a function of Q of tetradecane based microemulsions ($\alpha = 0.1$ to $\alpha = 0.5$) at the hydrophilic surface. The solid lines are fits of the Teubner-Strey model to the data.

6.3 Discussion

6.3.1 Structure of microemulsions perpendicular to the solid surface

The neutron reflectivity curves of both systems were fitted using the SLD-profile given by the equation 4.8. The oscillations in the derived SLD are related to the near-surface ordering of the oil and water domains perpendicular to the interface. According to the SLD profiles, the degree of ordering is highly dependent on the surface polarity and microemulsion composition. The SLD profiles reveal the similar ordering of the TD- and the MO-microemulsions at the hydrophilic surface. At this surface, the oscillations of both microemulsion systems damped over a distance up to 400 Å from the hydrophilic solid surface towards the microemulsion bulk phase. In contrast to this, the hydrophobic surface only supports the near-surface ordering of the TD-microemulsions, whereas the ordering of the MO-microemulsion is suppressed at higher oil content.

The variation on the surface ordering when changing surface polarity could be due to differences in the preferentially adsorbed molecules at the solid-liquid interfaces. Figure 6.5 suggests the adsorption of the same kind of molecules close to the hydrophilic interface for both microemulsion systems. Possibly, the surfactant molecules can be preferentially adsorbed at the hydrophilic interface and the surface coverage depends on the oil content.

At low oil contents, the hydrophilic solid-liquid interface is assumed to be covered by patches of surfactant and water, and the increasing oil content results in an enrichment of the surfactants at the interface. In contrast, the SLD values suggest the adsorption of tetradecane and methyl oleate close to the hydrophobic surface (Figure 6.5). In this respect, it is likely that wetting properties and the orientation of the oil molecules at the hydrophobic solid-liquid interface affect the ordering of the two microemulsions systems. This is corroborated by dynamic contact angle measurements, where it was found that TD-microemulsions can preferentially wet the hydrophobic surfaces in comparison to the MO-microemulsions across the whole range of α (Chapter 7). Additionally, the arrangement of the TD and MO molecules at the hydrophobic surface might have a significant influence on the near-surface ordering. It was shown via force-distance measurements that the symmetry of liquid molecules determines their ability to pack and orient themselves at solid surfaces.[126] For example, n-alkane molecules can easily pack and orient parallel to bare solid surfaces, while asymmetric molecules, (e.g., introduction of the methyl groups in the backbone), cannot. Possibly, the adsorption of tetradecane at the surface favors the near-surface ordering of these microemulsions. In contrast, the different arrangement of the methyl oleate molecules at the hydrophobic solid interface could increase the roughness of the interface, which in turn hinders the effective ordering of the nanodomains at the hydrophobic solid-liquid interface.

Importantly, both structural parameters of microemulsion systems, domain size and correlation length, are similar in bulk and at the hydrophilic and hydrophobic surface, as shown in Figure 6.3 and Figure 6.4. This is in line with previous experimental and numerical results describing the structuring of symmetric bicontinuous microemulsions containing the non-ionic surfactant $C_{10}E_4$ at planar surfaces.[74–76] These studies attributed the SLD oscillations to the structural transitions of the bicontinuous microemulsions to a lamellar phase close to interface (oil- and water-rich regions), where both lamellar and bicontinuous phases present similar structural parameters. In contrast to this results, on less symmetric microemulsions systems, oil droplets dispersed in water, it was found that the presence of the air/liquid interface induces the ordering of oil droplets. However, the identity of the droplets is maintained and their degree of ordering depends on their volume fraction. Furthermore, the conservation of characteristic bulk structural lengths under confinement is also in good agreement with observations on other colloidal systems, such as polyelectrolytes and colloidal particles.[71–73] As discussed in Section 2.3.2, the presence of the surface induces only the ordering of dispersed medium into a layer perpendicular to the surface in order to favor their mobility in the normal direction of their alignment, where the structural properties of those complex systems are maintained as compared to

bulk.[68,69]

In the present study, the SLD profiles give a clear indication of the oil and water nanodomain ordering in both microemulsion systems close to the solid-liquid interface. Furthermore, it was possible to identify a relationship between the degree of ordering and the microemulsion composition and surface properties. Nevertheless, the SLD profiles do not give a clear indication whether the identity of the nanodomains is preserved or whether there is a restructuring of those nanodomains into a lamellar structure close to the interface. In order to distinguish between both possibilities, structural information about the microemulsions parallel to the solid surface is needed.

6.3.2 Structure of microemulsions parallel to the solid surface

The measurements in grazing-incidence scattering geometry have been used to detect off-specular scattering at small and also virtually infinite penetration depths Λ (Table 4.2). The first case applies to the TD-microemulsions with $\alpha = 0.1$ and $\alpha = 0.3$. For these microemulsions, the lateral structure was probed at a penetration depth corresponding to a few domain sizes of the bicontinuous structure in bulk. The second configuration was given to the TD-microemulsions with larger oil contents. The penetration depth for these samples was determined by the damping of the penetrating neutron wave by, e.g., absorption processes. The reason for evaluating different penetration depths is related to the neutron contrast in the TD-microemulsions. Since D_2O is the dominant component, a critical angle of total external reflection (i.e., critical wave vector transfer $Q_{z,c}$) is only detectable at the lowest oil concentration.

In both configurations, the experimental results shown in Figures 6.6 and 6.7 show no scattering feature that corresponds to a lamellar structure. This indicates either no or only very few lamellar in the vicinity of the surfaces. Moreover, the observed enhanced off-specular scattered intensity distribution shows no spot-like features as in the case of crystalline order but a ring-like distribution, which qualitatively corresponds to the bulk scattering of bicontinuous microemulsions. From the scattering intensity, the structural parameters of the TD-microemulsions in the lateral direction are obtained from fitting the Teubner-Strey model (Table 6.1). The structural parameter in the lateral direction compare well to the obtained results by neutron reflectromety and SANS (Figure 6.3 and Figure 6.4) These suggest a conservation of the bicontinuous structure parallel to the substrate.

In contrast to these results, Kercher et al. found a clear indication of a structural transition of bicontinuous microemulsions closest to the interface.[76] The bicontinuous microemulsions were symmetric in composition ($\alpha = 0.5$) and stabilized with the non-ionic surfactant $C_{10}E_4$. Their lateral structure was investigated via GISANS, where the penetration depth was systematically changed by contrast variation of microemulsions using mixtures of D_2O/H_2O. In those experiments, the GISANS results showed a well-defined scattering peak in the range of penetration depth from 400 and 660 Å, followed by a ring scattering partner at the penetration depth of 800 Å. The peak on the scattering partner confirmed that the presence of surface induces the formation of well-defined lamellar structures. The degree of structuring of the lamellar structure decays with the increase in distance to the bulk structure (ring-like scattering partner). In this study, the TD-microemulsion does not show the formation of lamellar structures, particularly for the TD-microemulsions with $\alpha = 0.1$ and $\alpha = 0.3$, where the penetration depth was 320 and 190 Å, respectively. This could suggest only a weak influence of the lamellar ordering and a fast transition into the bulk structure or, as theoretically predicted, a non-wetting of the surface by the lamellar phase.[127] Instead of an extended oil or D_2O lamellar structure, a rather patchy arrangement of oil and D_2O with domain sizes comparable to the bulk values seems to develop on both types of surfaces at the penetration depths probed in the experiment. The fast decay of the scattering profiles shown in Figures 6.1 and 6.2 is in good agreement with the results of the GISANS measurements. Since most of the effects have been found in both microemulsion systems, we assume that the surfactant properties are of importance for the near-surface structuring. We attribute these observations to the amphiphilicity of the sugar surfactants and their tendency to form comparatively small domains with low ordering as indicated by the low correlation lengths.

6.4 Conclusion

Knowledge about the near-surface ordering of complex liquids is of utmost importance when applications require contact between these liquids and solid surfaces. In this study, the near-surface ordering of TD- and MO-microemulsions at hydrophilic and hydrophobic surfaces were studied. The structure of these microemulsions at solid surfaces was investigated using neutron scattering techniques. Neutron scattering in reflectometry and GISANS mode were applied to investigate bulk structure changes when the microemulsion gets in close contact with a hydrophilic and hydrophobic solid surface. The neutron reflectometry data indicate that the bulk structure continuously deforms into a more layered structure in the vicinity

of the substrates. The presence of one to four oscillations in the vertical scattering length density profile supports the assumption of a transition over small vertical distances of less than 100 nm. This corresponds to the observation of small domain sizes and correlation lengths in bulk. Moreover, a quantitative comparison of the structural parameters shows no difference between bulk and near-surface region. Additionally, GISANS data give no indication of a lateral ordering in addition to the propagation of the bicontinuous structure. The same domain sizes were also observed in the lateral direction within the precision of the experiment. Therefore, it is assumed that bicontinuous structure appears at the substrate, where a weak contribution of the lamellar phase to the near-surface structure can be presented.

Furthermore, a difference in the ordering was found between the apolar tetradecane and the polar methyl oleate at the hydrophobic surface. The different oil components in the two microemulsion systems also influence the near-surface structure of the solid-liquid interface. Here, the scattering length density profiles reveal that both tetradecane- and methyl oleate-based microemulsions develop a well-defined structure in the direction perpendicular to the hydrophilic solid-liquid interface. This result is in good agreement with previous experimental findings. In contrast, the structuring of the methyl oleate microemulsions is hindered at the hydrophobic solid-liquid interface, while the structuring of the tetradecane-based microemulsion is preserved. This effect at the hydrophobic surfaces is related to the polarity and adsorption behavior of the used oils.

Chapter 7

Wetting of model surfaces by microemulsions

Abstract

Understanding of the wetting behavior of different types of surfaces by microemulsions is crucial in order to control surface processes. The wettability of model planar and porous surfaces by microemulsions was determined by evaluating the dynamic contact angles. The main parameters evaluated in the wetting processes were: (1) the composition of the sugar surfactant microemulsion, in particular, the type of oil used in the preparation and its content, and (2) the surface polarity. In this investigation, it is shown that wetting of the model surfaces is highly dependent on the type of oil used in the preparation of microemulsions and its adsorption on the model surfaces.

7.1 Introduction

The wetting of any surfaces by microemulsions is a critical issue for many applications, for example, decontamination,[128] cosmetics and personal care,[129] food science,[130] oil recovery,[131] and drug delivery systems.[132] Despite the significant importance of wetting and considering the fact that microemulsions have been thoroughly studied over the last 40 years, only a few studies have been done on the relationship between microemulsion composition, solid properties, and wettability. One particular study evaluated the advancing and receding contact angles of the microemulsions with an oil phase constituted by isoparaffins on surfaces of different polarities using the goniometer method. It was found that the advancing and receding contact angles of microemulsions are independent of the surface polarity and there is no hysteresis between both angles.[133] More recently, the wetting of varnished metal sheets by perchlorethylene-based microemulsions has been investigated.[134] It was found that the formulated microemulsions can partially wet the hydrophobic metal surfaces in a bicontinuous region at different oil-to-water ratios. The average static contact angles ranges from 40° for the microemulsion with an equal content of oil and water to 25° for the oil-rich microemulsions. Nevertheless, these two studies did not present any clear correlation between the microemulsion properties close to the interface and the wetting behavior of the surface. As mentioned in Section 2.3.1, the structuring and composition of any complex fluid near the interface has a strong influence on surface wetting. Therefore,

an extensive investigation is needed to understand the interplay between surface wetting and the structure and composition of microemulsions.

This chapter deals with the ability of microemulsions to wet model planar and porous surfaces of different polarities. For model planar surfaces, silicon wafers were employed because their chemical surface properties can be easily modified by the reaction with organosilane reagents. In particular, etched silicon wafers were used as planar model hydrophilic surfaces and dichlorochlorodimethylsilane functionalized silicon wafers as planar model hydrophobic surfaces. The capacity of the two microemulsion systems to wet the model planar surfaces was evaluated by determining the dynamic contact angles using two different methods: Wilhelmy plate method and tilted plate method. The reason for applying these two methods is that it allows to obtain complementary results to have a better understanding of how microemulsion systems wet the model solid planar surfaces. The capacity of the two microemulsion systems to penetrate and wet porous solid surfaces was additionally evaluated on porous surfaces with different pore sizes and polarities. As model porous surfaces, standard glass filters with pore sizes between 10 and 250 μm were employed. The advantage of these glass filters is that the surface polarity can be easily tuned by a reaction with dichloromethylsilane reagent while keeping their structural properties unchanged. The wetting of the porous surfaces by the microemulsion systems was investigated using the Washburn method.

7.2 Results

7.2.1 Model surfaces and microemulsions

Silicon wafers as planar model surfaces

Figure 7.1 presents AFM images of the planar model surfaces, including information about the surface roughness calculated in an area of 1 μm^2 and the layer thickness measured by ellipsometry. The AFM images show homogenous silicon surfaces whose roughness increases from 1.1 Å to 8.0 Å after their functionalization with dichlorodimethylsilane. The layer thickness of (1.5 ± 0.3) nm, estimated for the hydrophilic surface, corresponds to the native silicon oxide layer of freshly cleaned silicon wafers. The thickness of dichlorodimethylsilane-functionalized silicon wafer layer is (1.0 ± 0.1) nm. This thickness indicates the formation of multilayers during the functionalization process as the thickness of a single dichlorodimethylsilane layer is approximately 0.35 nm.[135] The formation

of multilayers during functionalization process is a common phenomenon due to the polymerization of the silane molecules with already chemisorbed layers.[136] However, the formed multilayers remain homogenous throughout the surfaces due to the absence of agglomerates and the low surface roughness (see Fig 7.1).

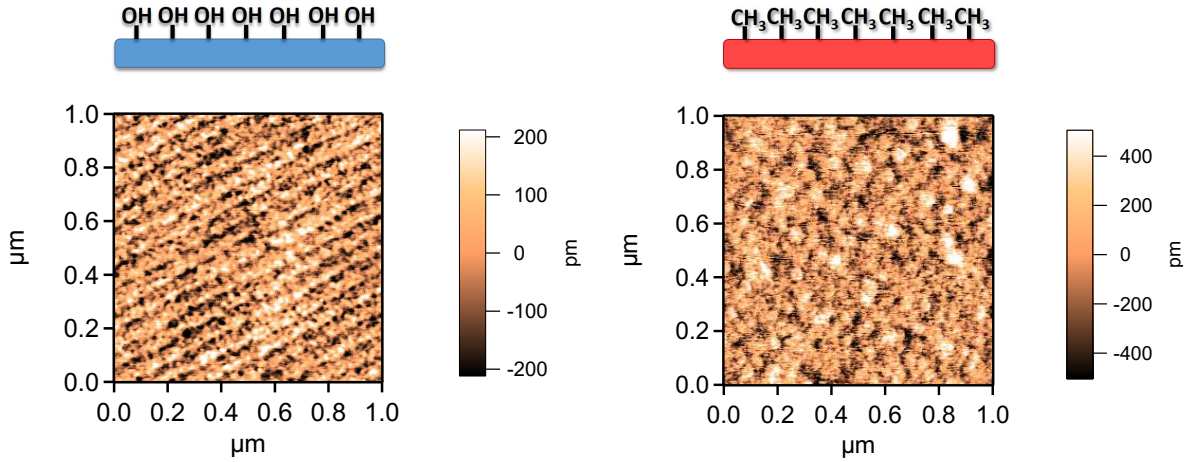

Roughness	(1.1 ± 0.1) Å	(8.8 ± 0.1) Å
Thickness	(1.5 ± 0.3) nm	(1.0 ± 0.1) nm

Figure 7.1: AFM images of model planar surfaces, and the roughness and thickness of the surfaces determined by the AFM and ellipsometry, respectively.

The surface energies of the model surfaces were estimated by means of the Owens-Wendt-Rabel-Kaelble (OWRK) method (Eq. 4.14). Figure 7.2 shows the OWRK plots for the two model planar surfaces. The estimated surface energy estimated by the OWRK method and the corresponding dispersive and polar components are presented in Table 7.1.

Table 7.1: Total surface energy of the etched silicon surface (hydrophilic) and silicon surfaces functionalized with dichlorodimethylsilane (hydrophobic) and their corresponding dispersive and polar components estimated by the OWRK method

Surface	**Total energy** (γ_s) $mN\ m^{-1}$	**Dispersive component** (γ_s^d) $mN\ m^{-1}$	**Polar component** (γ_s^p) $mN\ m^{-1}$
Hydrophilic	63.5 ± 0.8	29.7 ± 0.6	33.7 ± 0.6
Hydrophobic	27.0 ± 0.7	23.1 ± 0.2	3.9 ± 0.5

As expected, a transition from high to low surface energy was achieved by functionalizing the silicon wafers with dichlorodimethylsilane. The functionalization with dichlorodimethylsilane induces the hydrophobization of the surface, where the dispersive components account

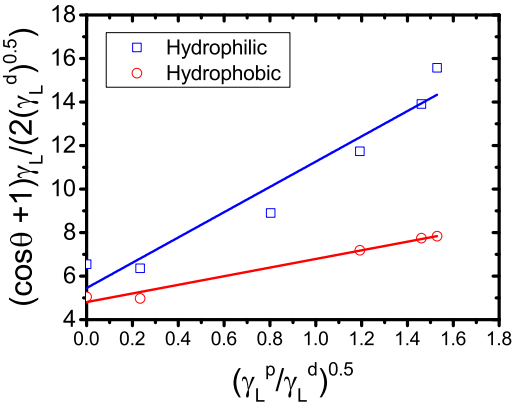

Figure 7.2: OWRK plots of the etched silicon surface (hydrophilic) and the silicon surfaces functionalized with dichlorodimethylsilane (hydrophobic).

for the largest share of its surface energy due to the presence of methyl alkyl chains. The surface energy of the etched silicon wafer is dominated by the polar component provided by the hydroxy groups on the surfaces. The surface energy of these model surfaces is in the same surface energy range as reported in the literature.[137]

According to the analysis of the silicon wafers by the OWRK method, a change of the energy and thus the polarity of surface is achieved by its functionalization with methyl alkyl chains. Moreover, it has been verified by the AFM that, although surface roughness increases after the functionalization of silicon wafers, the roughness is still too small to influence the dynamic contact angles.[138] Therefore, homogeneous functionalization of silicon wafers with their low surface roughness allows to use them as model planar surfaces to evaluate the variation of dynamic contact angles of microemulsions as a function of their composition and surface polarity.

Glass filters as porous model surfaces

Figure 7.3 displays hydrophilic and hydrophobic glass filters with different pore sizes. The figure shows that water drops on porous hydrophobic surfaces have static contact angles larger than 100°. In contrast, water droplets can easily penetrate hydrophilic porous surfaces (not shown in the figure).

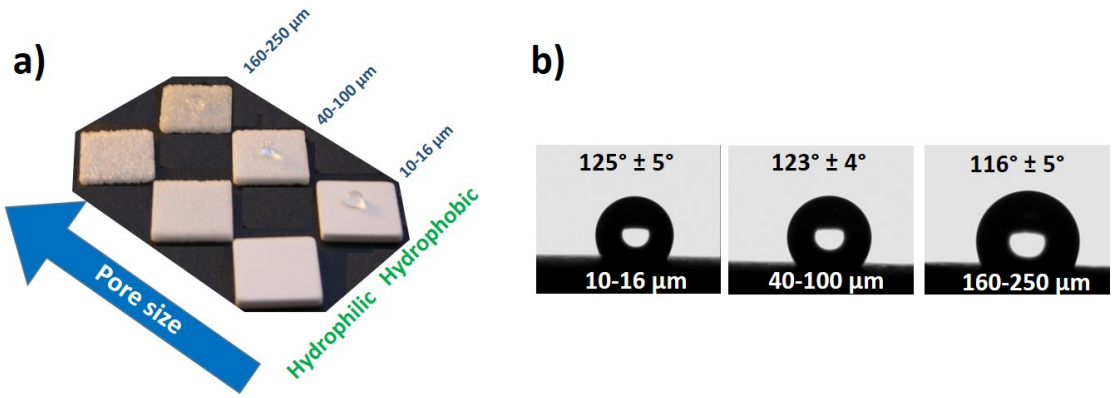

Figure 7.3: a) Hydrophilic (bottom) and hydrophobic (top) glass filters with different pore sizes, and b) evaluation of the static contact angles of hydrophobic porous surfaces with the reference liquid water.

Macroscopic properties of the TD-microemulsions and MO-microemulsions

The density, surface tension, dynamic viscosity, and capillary number of the TD- and MO-microemulsions play an important role in the wetting of the model surfaces and are therefore presented in this chapter (Table 7.2). The density of both microemulsion systems slightly decreased with increasing α. The dynamic viscosity of the prepared microemulsions was within the range of 20 to 50 mPa s and it tends to increase with α in both systems. In contrast, the variation of α had little impact on the surface tension of the microemulsion systems. The average surface tensions throughout the whole range of α were (25.24 ± 0.44) mN m^{-1} and (27.65 ± 0.34) mN m^{-1} for the TD- and MO-microemulsions, respectively. The dynamic viscosity (μ), the surface tension (γ), and the spreading or contact velocity between the liquid and the solid allow us to calculate the capillary number (Ca):

$$Ca = \frac{V\mu}{\gamma} \tag{7.1}$$

where contact velocity (V) is the dipping velocity of planar surfaces into the microemulsion when performing the dynamic contact angle measurements by the Wilhelmy plate method. In this study, the dipping velocity was set to 5 mm/min (see Section 4.2.3).

The capillary number is a dimensionless number given as the ratio between viscous and capillary forces. This dimensionless number allows distinguishing which of these two forces has a larger impact on the displacement of the liquid on a surface. In this case, the

calculated capillary numbers of microemulsions at the dipping velocity speed of the plates are less than one, indicating the capillary force as the dominant force during wetting.

Table 7.2: Density, surface tension, dynamic viscosity, and capillary number of tetradecane- and methyl oleate-based microemulsions

Pure components				
sample	**Density** ($g\ mL^{-1}$)	**Surface tension** ($mN\ m^{-1}$)	**Dynamic viscosity** (mPa s)	**Capillary number**
Surfactant Sln.	0.99889 ± 0.00001	28.12 ± 0.02	1.25	2.23×10^{-5}
Tetradecane	0.75679 ± 0.00415	26.13 ± 0.01	2.72	5.20×10^{-5}
Methyl oleate	0.87567 ± 0.00002	30.29 ± 0.01	5.32	8.78×10^{-5}
Tetradecane-based microemulsions				
$\alpha = 0.1$	1.01196 ± 0.00024	24.65 ± 0.06	24.07	4.88×10^{-4}
$\alpha = 0.3$	0.98838 ± 0.00081	25.52 ± 0.24	46.95	9.20×10^{-4}
$\alpha = 0.5$	0.95562 ± 0.00068	25.13 ± 0.22	34.18	6.80×10^{-4}
$\alpha = 0.7$	0.92765 ± 0.00033	25.64 ± 0.20	50.28	9.80×10^{-4}
Mehthyl oleate-based microemulsions				
$\alpha = 0.1$	1.03147 ± 0.00006	27.87 ± 0.14	22.80	4.09×10^{-4}
$\alpha = 0.3$	1.00692 ± 0.00023	27.96 ± 0.09	34.98	6.26×10^{-4}
$\alpha = 0.5$	0.99689 ± 0.00026	27.57 ± 0.06	40.05	7.26×10^{-4}
$\alpha = 0.7$	0.97789 ± 0.00079	27.20 ± 0.10	54.40	1.00×10^{-3}

7.2.2 Evaluation of the dynamic contact angles of microemulsions on planar model surfaces

Evaluation of the dynamic contact angles of TD-microemulsions

Figure 7.4 depicts the dynamic contact angles and their hysteresis of the TD-microemulsions evaluated by the Wilhelmy plate method (WPM) and the tilted plate method (TPM). This figure also displays the dynamic contact angles of the sugar surfactant aqueous solution (1 wt%) and tetradecane presented as horizontal lines for comparison.

Determined by the WPM, the advancing contact angle (θ_{adv}) of the TD-microemulsion with $\alpha = 0.1$ shows a remarkable difference when the polarity of the planar surface is changed: the θ_{adv} increases from 10° to 35° when the surface polarity is decreased. However, the variation of the surface polarity barely influences the θ_{adv} of the TD-microemulsions with higher oil contents: the θ_{adv} of the $\alpha = 0.5$ and $\alpha = 0.7$ TD-microemulsions increase just by

*The dynamic contact angles measured by the TPM were carried out by Jana Lutzki at Stranski-Laboratorium für Physikalische und Theoretische Chemie, TU-Berlin, Germany.

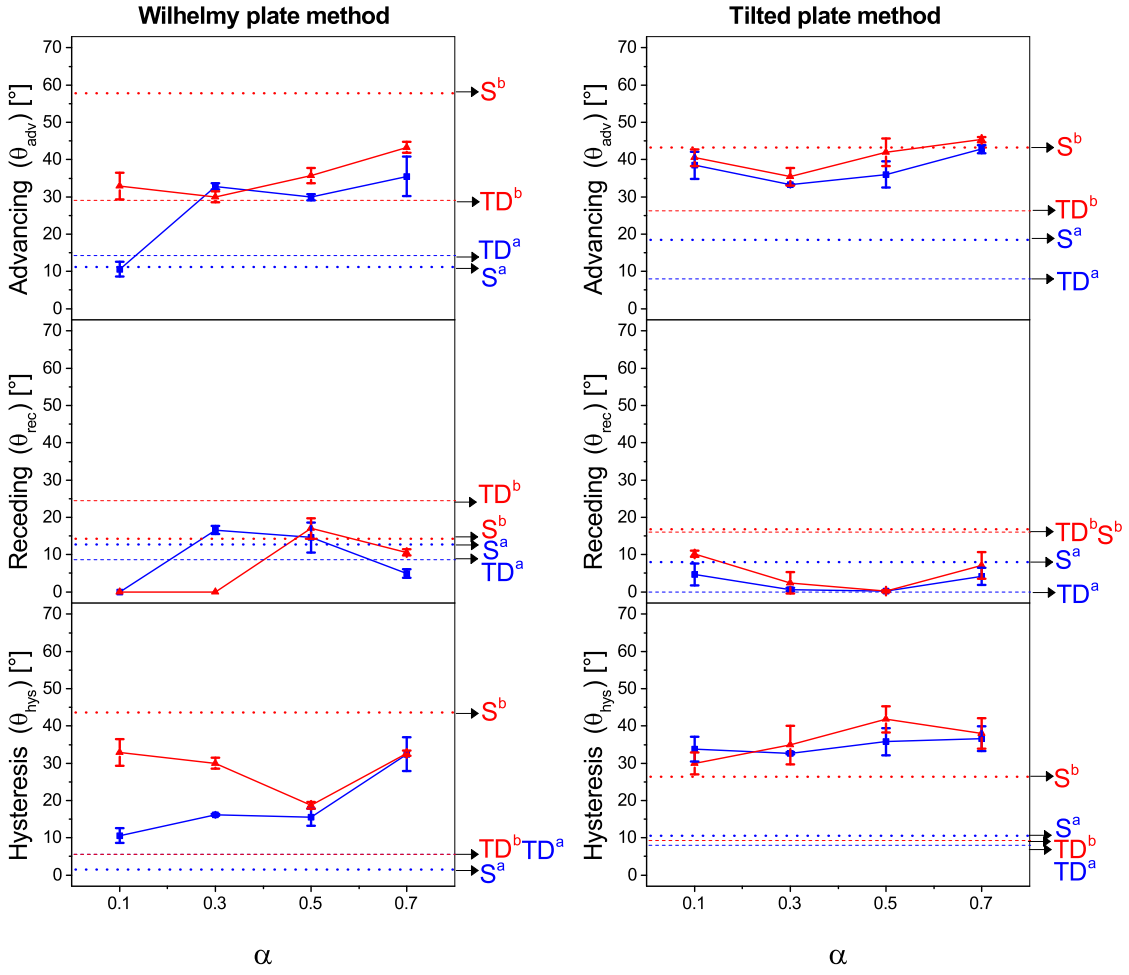

Figure 7.4: Dynamic contact angles of tetradecane-based microemulsions on model surfaces evaluated by the Wilhelmy plate method and the tilted plate method on hydrophilic (squares) and hydrophobic (triangles) planar surfaces. In this figure, the dynamic contact angles of tetradecane (TD, dashed lines) and the surfactant solution (S, dotted lines) on hydrophilic (blue, superscript "a") and hydrophobic (red, superscript "b") planar surfaces are also displayed for reference. The error of the dynamic contact angle measurement of tetradecane and the surfactant solution is in the range between 3° and 5°.

5 ° when the surface polarity is decreased. Moreover, the θ_{adv} of the TD-microemulsions are larger than the θ_{adv} of their components (tetradecane and the surfactant solution) on the hydrophilic surface, except for the TD-microemulsions with $\alpha = 0.1$, where θ_{adv} is similar to the θ_{adv} of the surfactant solution. Conversely, the θ_{adv} of the TD-microemulsions on the hydrophobic surface falls within the same range as the θ_{adv} of tetradecane.

According to the results obtained by the WPM, the receding contact angles (θ_{rec}) of the TD-microemulsions are approximately 10° to 20° smaller than the θ_{adv} on both hydrophilic and hydrophobic surfaces. The θ_{rec} of the TD-microemulsions are in the same range as the θ_{rec} of the surfactant solution and tetradecane. The difference between θ_{adv} and θ_{rec} gives the hysteresis of the dynamic contact angles (θ_{hys}). The θ_{hys} increases around 15° to 20° by decreasing the surface polarity for the TD-microemulsions with low oil content ($\alpha = 0.1$ and α =0.3). The TD-microemulsions with higher oil content yield the same θ_{hys} values on both hydrophilic and hydrophobic surfaces. Regarding θ_{hys} of the oil and surfactant solution, tetradecane also displays the same θ_{hys} on both surfaces. In contrast, the θ_{hys} of the surfactant solution increases by 40° when the surface polarity is decreased.

The dynamic contact angles of the TD-microemulsions and the surfactant solution evaluated by the TPM vary significantly compared to the results obtained by the WPM, whereas the dynamic contact angles of tetradecane are within the same range. In general, the dynamic contact angles of the TD-microemulsions determined by the TPM do not show any significant dependency of the surface polarity, especially the TD-microemulsion with $\alpha = 0.1$. Moreover, the θ_{rec} of the TD-microemulsions estimated by the TPM are between 0° and 5°, which are lower values than those obtained by the WPM. Due to lower θ_{rec} obtained by the TPM, the differences between the θ_{adv} and θ_{rec} lead to higher θ_{hys} than the values calculated by the WPM.

Evaluation of the dynamic contact angles of MO-microemulsion

Figure 7.5 shows the dynamic contact angles and their hysteresis of the MO-microemulsions evaluated by the WPM and TPM. In contrast to the TD-microemulsions, for the MO-microemulsions the WPM yields a significantly higher θ_{adv} for the hydrophobic surface than for the hydrophilic ones. A more pronounced increase can be seen in the MO-microemulsion with low oil content ($\alpha = 0.1$). An increase in the θ_{adv} from 15° to 65° occurs when the surface polarity is decreased. For the MO-microemulsions with higher oil content, the decrease on the surface polarity induces an increase in θ_{adv} of 20°. By comparing θ_{adv} of the MO-microemulsion and θ_{adv} of the surfactant solution and methyl oleate, one can observe that the θ_{adv} of the MO-microemulsions are close to the θ_{adv} values of methyl oleate, except for the MO-microemulsion with $\alpha = 0.1$. For the MO-microemulsion $\alpha =$ 0.1, a similar θ_{adv} as the surfactant solution was observed.

The results obtained by the WPM indicate that variation of the surface polarity also influences the θ_{rec} of the MO-microemulsions: the θ_{rec} of the MO-microemulsions at the

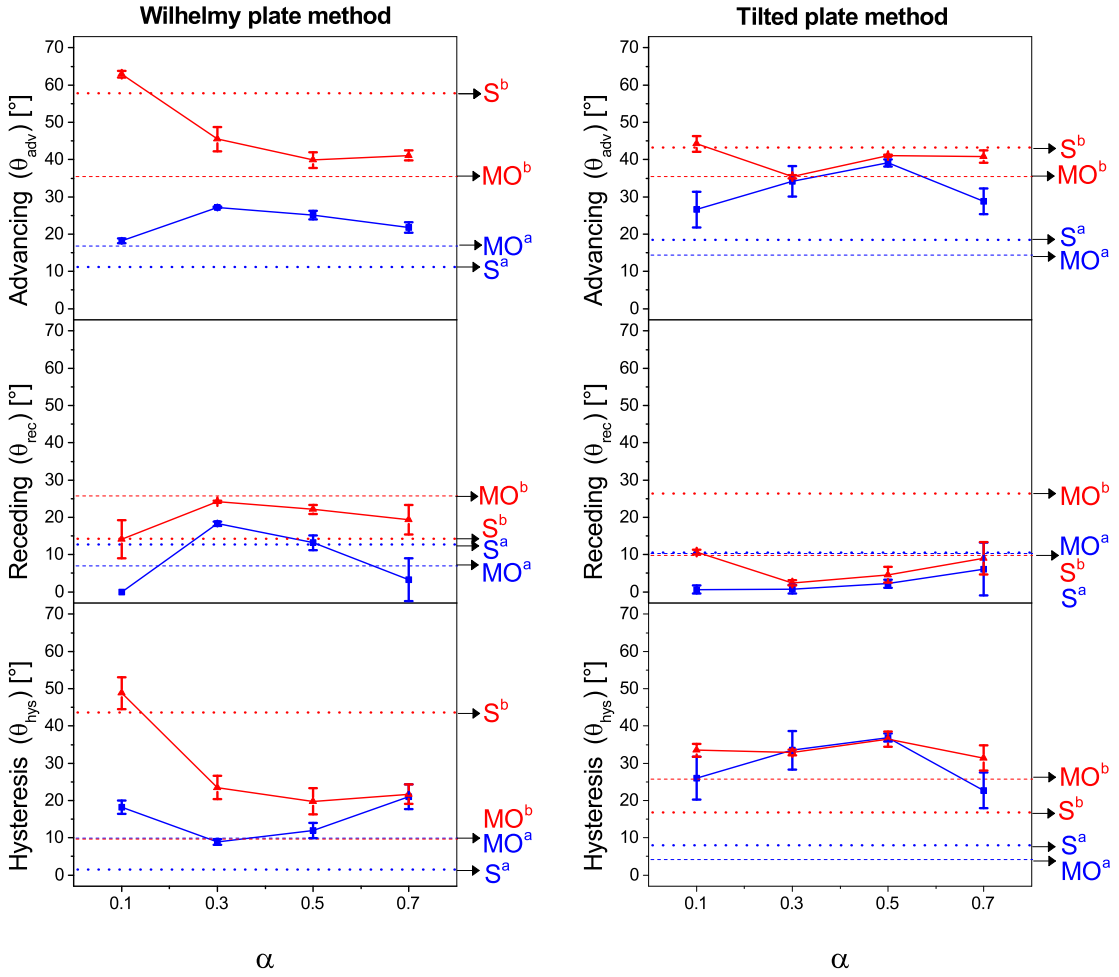

Figure 7.5: Dynamic contact angles of methyl oleate-based microemulsions evaluated by the Wilhelmy plate method and the tilted plate method on hydrophilic (squares) and hydrophobic (triangles) planar surfaces. The dynamic contact angles of methyl oleate (MO, dashed lines) and the surfactant solution (S, dotted lines) on hydrophilic (blue, superscript "a") and hydrophobic (red, superscript "b") planar surfaces are also displayed for reference. The error of the dynamic contact angle measurement for methyl oleate and the surfactant solution is between 3° and 5°.

hydrophobic surface is approximately 5° higher than the θ_{rec} measured on the hydrophilic surface. It was also observed that the MO-microemulsions on the hydrophobic surface have similar θ_{rec} to the θ_{rec} of methyl oleate, except for the MO-microemulsion with α = 0.1 which shows a θ_{rec} close to the θ_{rec} of the surfactant solution. Moreover, the θ_{hys} values of the MO-microemulsions depend on both: the polarity of the surface and the oil

content (α) of the microemulsions. The surface polarity has a particularly large impact on the θ_{hys} of the MO-microemulsions with low oil content ($\alpha = 0.1$ and $\alpha = 0.3$).

Similarly to the results presented in the case of TD-microemulsions, those obtained by the TPM do not show a strong influence of the surface polarity on the dynamic contact angles of the MO-microemulsions. The θ_{adv} remains constant for the MO-microemulsions with a symmetrical composition ($\alpha = 0.3$ and $\alpha = 0.5$), while those with an asymmetric composition ($\alpha = 0.1$ and $\alpha = 0.7$) display an increase of approximately 10° to 15° when the surface polarity decreases. Moreover, the θ_{rec} of the MO-microemulsions evaluated by the TPM are lower than the values obtained by the WPM. For example, there is a relative difference of 20° between the θ_{rec} determined by the two methods on the hydrophobic surface. As expected, θ_{hys} of the MO-microemulsions determined by the tilted plate method does not show any influence of the surface polarity either.

Comparison of the dynamic contact angles of the TD-microemulsions and MO-microemulsions evaluated by the Wilhelmy plate method

The WPM shows a stronger response on the dynamic contact angles of the microemulsions than the TPM due to surface polarity variations. Hence, the results obtained by this method for the TD- and MO-microemulsions on the two model planar surfaces are compared in Figure 7.6. According to the obtained results, the dynamic contact angles are strongly influenced by the type of oil used in the microemulsion preparation and the polarity of the surface. On the hydrophilic surfaces, the θ_{adv} of the two microemulsion systems reaches its minimum at the lowest oil content of $\alpha = 0.1$. At higher α, the θ_{adv} of both microemulsions increases and remains constant from $\alpha = 0.3$ to $\alpha = 0.7$. In this range of α, the θ_{adv} of the TD-microemulsions are approximately 5° higher than the θ_{adv} of the MO-microemulsions. The θ_{rec} of the two microemulsion systems on the hydrophilic surface do not differ throughout the whole α. The microemulsions with a symmetric composition ($\alpha = 0.3$ and $\alpha = 0.5$) display a maximum on the θ_{rec} of 15°, while the θ_{rec} of the microemulsions with an asymmetric composition ($\alpha = 0.1$ and $\alpha = 0.7$) are close to zero. Furthermore, the θ_{hys} increases with the oil content (α) in the microemulsions.

On the hydrophobic surfaces, the TD-microemulsions show lower θ_{adv} values compared to the MO-microemulsions throughout the whole α. Interestingly, there are larger differences between both microemulsion systems at low oil contents ($\alpha = 0.1$ and $\alpha = 0.3$). At higher oil contents, there are no significant differences in the θ_{adv} between both microemulsion

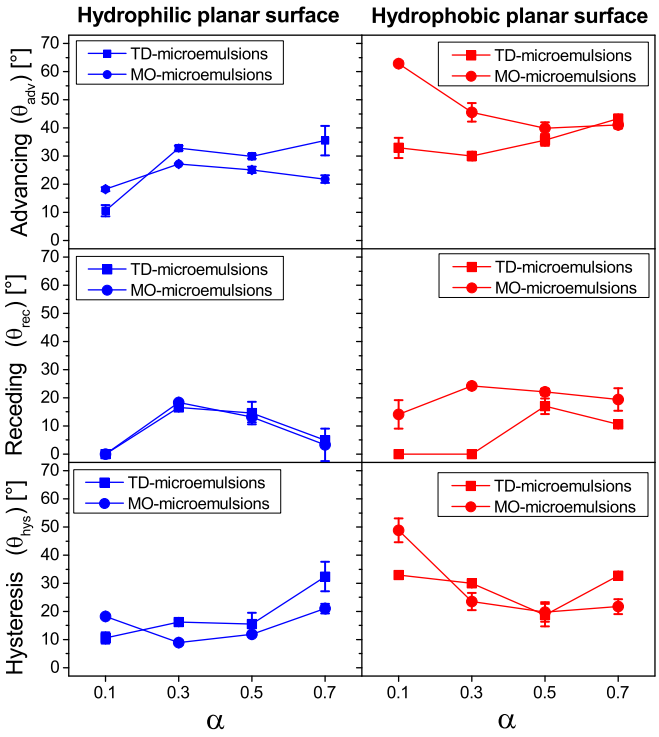

Figure 7.6: Dynamic contact angles of tetradecane- and methyl oleate-based microemulsions on model planar surfaces evaluated by the Wilhelmy plate method.

systems. Furthermore, θ_{rec} values of the MO-microemulsions on the hydrophobic surface are higher than the those of the TD-microemulsions in the whole range of α. It is also noticeable that θ_{hys} for both microemulsion systems on the hydrophobic surface tends to decrease when their oil content (α) increases.

7.2.3 Evaluation of the contact angles of tetradecane- and methyl oleate-based microemulsions on porous model surfaces

The ability of the microemulsions to wet and penetrate the hydrophilic and hydrophobic model porous surfaces has been evaluated by means of the Washburn method (Eq.4.18). Exemplary imbibition curves of the TD- and MO-microemulsions into the hydrophilic and hydrophobic porous surfaces with pore size distribution beteween 40-100 μm are shown in Figure 7.7. The imbibition curves of both microemulsion systems into the porous surfaces are characterized by a fast increase of the mass due to the wicking of the microemulsions, followed by a decrease of the imbibition speed, which is associated with either the saturation of the porous surface or the establishment of the equilibrium state

between the capillary and hydrostatic pressure.[80]

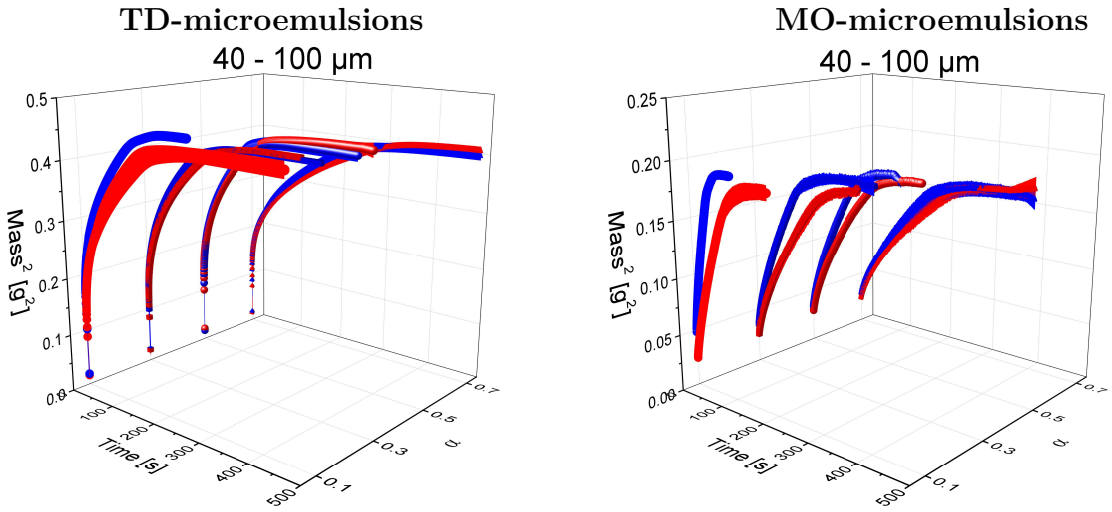

Figure 7.7: Imbibition curves of tetradecane and methyl oleate based microemulsions on hydrophilic (blue curves) and hydrophobic (red curves) porous surfaces with a distribution of pore sizes between 40-100 μm.

Figure 7.8 presents the slopes of the imibibtion curves of the TD- and MO-microemulsions into the hydrophilic and hydrophobic porous surfaces. In this figure, the imbibition slopes of tetradecane, methyl olate, and the surfactant solution are also included for reference. The initial analysis of the slopes of the imbibition curves allows us to estimate the flow rate as a function of the microemulsion composition and porous surface properties. The polarity of the porous surface with the pore sizes ranging from 10-16 μm does not influence the flow rate of the microemulsion systems. However, the flow of the microemulsions into the porous surfaces is influenced by their oil content. The microemulsions with oil content α = 0.7 permeated the surface slower than the microemulsions with oil content $\alpha = 0.1$. The increase of the solid surface pore sizes to 40-100 μm favors the flow of the microemulsions into the material such that the speed of the microemulsion imbibition increases by almost one order of magnitude. Moreover, the polarity of the surfaces starts to play a role in the microemulsion imbibition process. The imbibition of the MO-microemulsions is faster in the hydrophilic porous surfaces in comparison to the hydrophobic surfaces. A further increase in the solid surface pore sizes to 160-250 μm range, as expected, enhances the imbibition of the microemulsions. In addition, it leads to an accentuated difference in the microemulsion imibibiton when changing the surface polarity: all prepared microemulsions are imbibed faster by the hydrophilic porous surface. In comparison to the microemulsion systems, tetradecane, methyl oleate, and the surfactant solution were imbibed faster by the

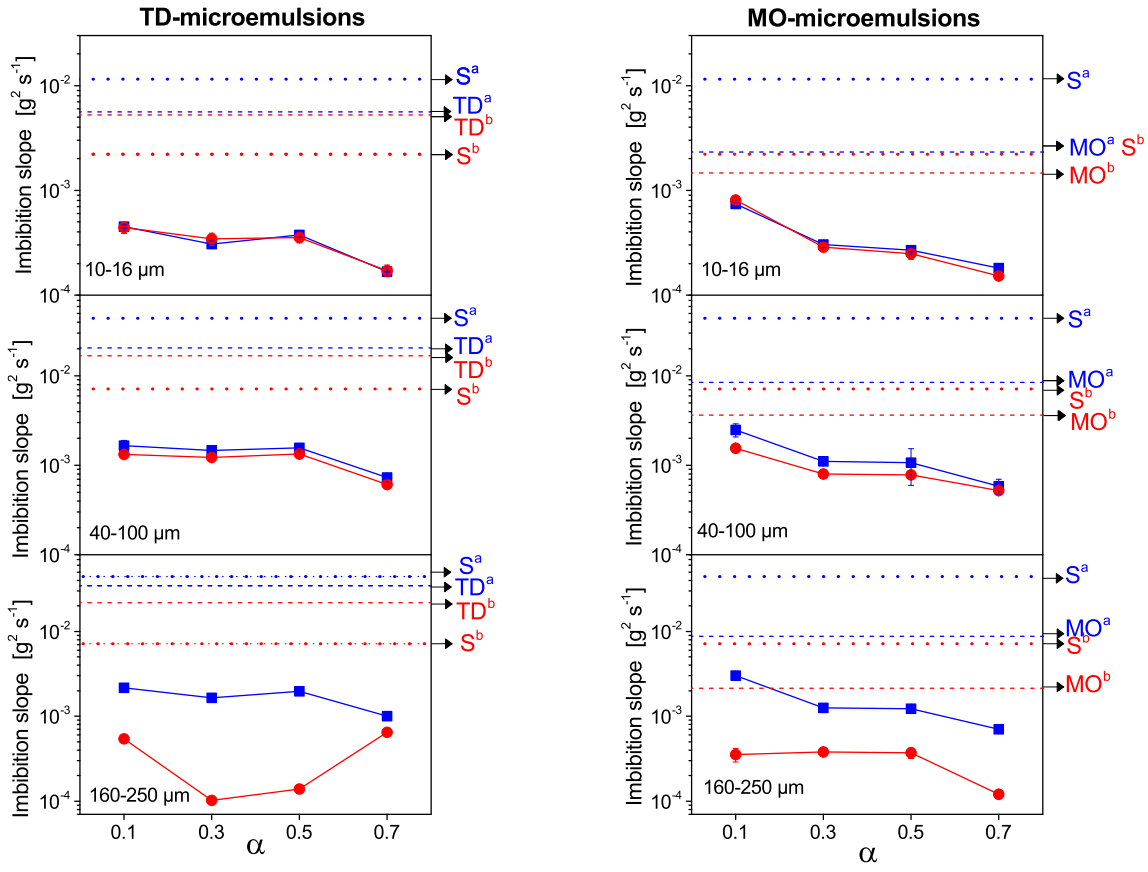

Figure 7.8: Slope of the imbibition curves of tetradecane- and methyl oleate-based microemulsions by hydrophilic (blue squares) and hydrophobic (red circles) porous surfaces evaluated by the Washburn method. In this figure, the slope of the imbibition curves of methyl oleate and tetradecane (MO and TD, dashed lines), and the surfactant solution (S, dotted lines) on hydrophilic (blue, superscript "a") and hydrophobic (red, superscript "b") planar surfaces are also displayed for reference

three sets of porous surfaces. Furthermore, the polarity of the porous surfaces plays a role in the imbibition speed of these components. The oils were imbibed two times faster by the hydrophilic porous surfaces than by the hydrophobic porous surfaces (considering the logarithmic scale), whereas the surfactant solution was imbibed one order of magnitude faster by the hydrophilic surface than by the hydrophobic one.

The contact angle of both microemulsion systems on the model porous surfaces were calculated according to Eq.4.18 and using decane as a reference liquid (See section 4.2.4). The contact angles of both microemulsion systems as a function of their composition for each set of porous surfaces are shown in Figure 7.9. In this study, the contact angles of

the oils and surfactant solution are not reported as their estimated $\cos\theta$ values are larger than one (Eq.4.18).

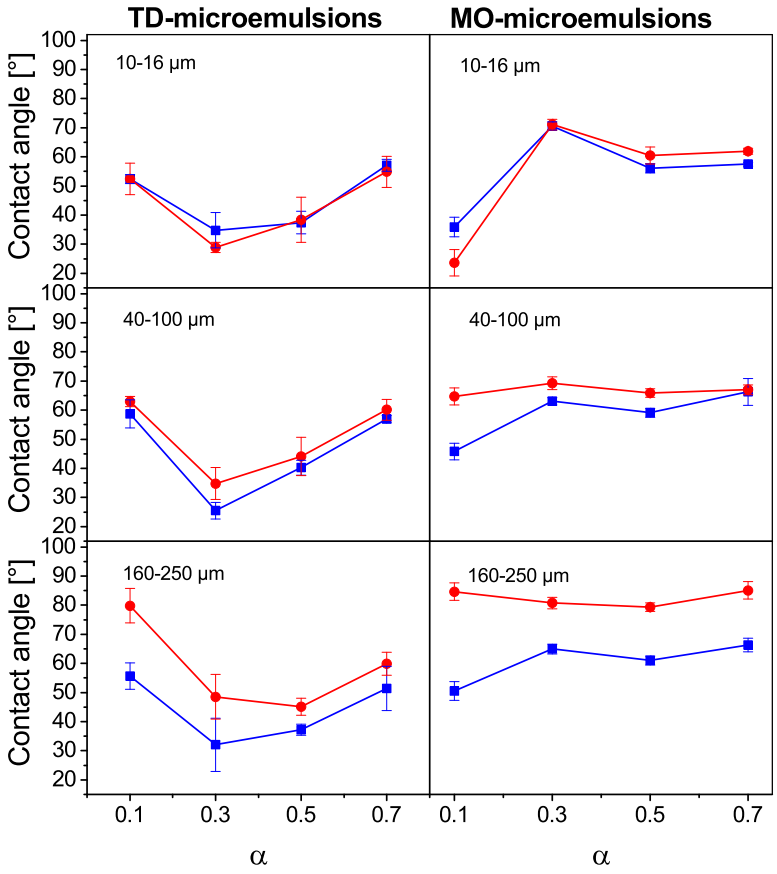

Figure 7.9: Contact angles of tetradecane and methyl oleate-based microemulsions on hydrophilic (blue squares) and hydrophobic (red circles) porous surfaces evaluated by the Washburn method.

Although the range of pore sizes shows a strong influence on the microemulsion imbibition rate, the influence of this parameter on the surface wetting is not significant. At the hydrophilic porous surfaces, the contact angle of both microemulsion systems remains within the same range despite the pore size variation. The polarity of the porous surfaces starts to play a role on the microemulsion contact angle when the pore size of the model surfaces is increasing. When the pore size ranges from 10-16 μm, the contact angles of both microemulsion systems are independent of the polarity of the porous surface. At intermediate pore sizes (40-100 μm), a decrease of the surface polarity induces a shift to large contact angles values in the MO-microemulsion. This shift of the contact angles is

around 5°. The effect of the surface polarity is even more pronounced with large pore sizes (100-250 μm), where the shift in the contact angle value is around 15° for both microemulsion systems when the polarity of the porous surfaces is decreased.

It is important to point out that the contact angles determined by the Washburn method have been associated with advancing contact angles due to the advancing of the liquids through the porous surfaces during the measurements. In this study, the contact angles determined by the Washburn method are between 55° and 80° for both microemulsion systems on the hydrophilic and hydrophobic porous surfaces. This range of contact angles is larger than that of the advancing contact angles evaluated on the model planar surfaces, where the range of advancing contact angles is between 15° and 55°. Moreover, the contact angles for the TD-microemulsions yield show lower values in both hydrophilic and hydrophobic porous surfaces in comparison to the contact angles of the MO-microemulsions.

7.3 Discussion

7.3.1 Dynamic contact angles of microemulsions on planar model surfaces

The dynamic contact angles of microemulsions often show discrepancy between the results obtained by the WPM and TPM. The dynamic contact angles determined by the WPM are strongly influenced by changing microemulsion composition and the surface polarity, whereas the angles evaluated by the TPM are nearly independent of the properties of both the microemulsion and the surface. Krishnan et al. examined the dynamic contact angle by both methods using a variety of surfaces with a broad range of polarities and water as reference liquid.[139] They found a good agreement between the θ_{adv} measured by the WPM and the TPM. However, the resulting θ_{rec} were found to be lower in the TPM in comparison to the values obtained by the WPM. The systematic difference in the θ_{rec} between both methods was attributed to the deformation of the drop during the TPM measurements due to its adhesion to the surface, therefore causing the estimation of a lower θ_{rec}.[140] Furthermore, it has been mentioned in the study carried out by Vogler that a similar result of the dynamic contact angles estimated by the WPM or the goniometry (tilted plate) method can only be obtained if there is no significant adsorption of the liquid molecules on the tested surface.[141] In this sense, the divergence in the dynamic contact angles of the TD- and MO-microemulsions between the results obtained by both methods is not only due to the deformation of the drop but also to the structural properties of microemulsions and the strong adsorption of their components at the solid-liquid interface.

This fact is further supported by considering the properties of the microemulsions: both microemulsion systems have capillary numbers of the order of 10^{-4} in the whole α such as the wetting of the model surface is not dependent on the microemulsion viscosity but rather on capillary forces.[100] If the capillary forces play a major role, then it also important to point out that the surface tension of the microemulsions does not change significantly with α variations. Thereby, the observed changes of the microemulsion dynamic contact angles are indeed mainly associated with the adsorption of their components at the interface.

A difference in the adsorption processes at the interface could occur when using both methods due to changes in the contact areas and contact times between the solid surfaces and the microemulsions. The measurements carried out by the TPM imply contact areas of a few millimeters, where the measurements take place in a couple of seconds. In contrast, the WPM requires a larger contact area between the microemulsions and the surface for a prolonged time. This could lead to a higher adsorption of the microemulsion components at the interface, which therefore enhances the sensitivity of WPM in the determination of the dynamic contact angles. Given that the WPM provides a higher sensitivity in the determination of the dynamic contact angles, the influence of the microemulsion composition and the surface polarity on the wetting is discussed in the next section according to the results obtained by this method.

Wetting of hydrophilic planar surfaces by microemulsions

Both microemulsion systems show similar dynamic contact angles on the hydrophilic surface in the whole range of α. According to the results of θ_{adv}, the microemulsions with $\alpha = 0.1$ have the highest efficiency to wet the hydrophilic surface in comparison to the microemulsions with a higher oil content ($\alpha = 0.3$ to $\alpha = 0.7$). Although both microemulsion systems present the same trend in the θ_{adv}, the TD-microemulsions have θ_{adv} just 5° larger than the MO-microemulsions between $\alpha = 0.3$ and $\alpha = 0.7$. In order to discuss these results, it should be pointed out that the most polar components of the microemulsions, water and sugar surfactant, can be preferentially adsorbed at the hydrophilic planar surface as it was shown in Section 6.2.1. This adsorption of the microemulsion polar components at the interface could explain the reason why microemulsions with $\alpha = 0.1$ are the most efficient media to wet the hydrophilic surface, as these are the microemulsion samples with the highest water content. Nevertheless, the adsorption of the polar components is not homogenous due to the formation of a patchy microemulsion structure at the interface (Chapter 6), particularly when the microemulsions have intermediate or high oil contents

($\alpha = 0.3$ to $\alpha = 0.7$). Hence, differences in the θ_{adv} between both microemulsion systems with the higher oil contents can be explained by a variation in the degree of the interaction between the oil molecules and the hydrophilic surfaces. Compared to the tetradecane, methyl oleate can interact strongly with the hydrophobic surfaces due to the presence of the polar group (ester group) in its structure, which could favour the reduction of the energy of the solid-liquid interface.

As in the case of θ_{adv}, both microemulsion systems present the same trend in θ_{rec} with the variation of α. On the hydrophilic planar surface, lower θ_{rec} are measured when the composition of the microemulsion is asymmetric ($\alpha = 0.1$ and $\alpha = 0.7$), and higher values when its composition is symmetric ($\alpha = 0.3$ and $\alpha = 0.5$). It is important to point out that the discussion of the receding contact angles is challenging, as these angles depend on the microemulsion structure and the molecules that have been previously adsorbed on the surfaces during the advance stage. On the one hand, it can be explained that low θ_{rec} are favored due to the pre-adsorbed water and sugar surfactant molecules from the microemulsions during the advance stage, particularly for the microemulsions with a low oil content ($\alpha = 0.1$). On the other hand, the structure of the microemulsion could play a role in the sliding mechanism during the receding stage. For instance, it has been discussed that the formation of lamellar structures close to the interface could enhance the sliding of the microemulsions in the lateral direction of the surface, which in turn favors the wetting of the surface.[75,77] In our study, it has demonstrated a weak contribution of the lamellar phase on the near surface structure of microemulsions (Chapter 6). Therefore, the wetting of the planar surfaces in not influenced by a lamellar structure. The variation of θ_{rec} could be tentatively explained by the degree of connectivity of the oil and water nanodomains in the microemulsions. As it was shown in Chapter 5, the oil and water nanodomains are less connected in the microemulsions with an asymmetric composition ($\alpha = 0.1$ and $\alpha = 0.7$) than the nanodomains in the microemulsion with a symmetric composition ($\alpha = 0.3$ and $\alpha = 0.5$). Speculatively, the less connected nanodomains could favour the sliding of the microemulsions during the receding stage, and thus lower θ_{rec} are obtained. Conversely, the more interconnected the structure of the microemulsions are ($\alpha = 0.3$ and $\alpha = 0.5$), restrictive their sliding on the surface can be. This could lead to an increase of the friction between the liquid and solid surfaces, which in turns yields an increase in the θ_{rec}.

Furthermore, the θ_{hys} could indicate the strength of the microemulsion component adsorption at the solid-liquid interface. On the hydrophilic surfaces, both microemulsions systems show that θ_{hys} increases along with α such that the adsorption of the microemulsion polar components is less favored at higher oil content, and therefore the wetting of the

hydrophilic planar surfaces preferentially takes place at low α.

Wetting of the planar hydrophobic surfaces by microemulsions

In contrast to the dynamic contact angles of both microemulsion systems at the hydrophilic surface, there is a clear difference between the dynamic contact angles of both microemulsion systems at the hydrophobic surface. In particular, the TD-microemulsions show lower θ_{adv} than the MO-microemulsions across the whole range of α. This result can be explained by considering that tetradecane and methyl oleate are preferentially adsorbed at the hydrophobic surface (see Section 6.2.1), where the tetradecane could interact more strongly with the hydrophobic surface than with methyl oleate due to its low surface tension (Table 7.2). This can also be observed by the increase of θ_{adv} on both microemulsion systems when decreasing the surface polarity (Figures 7.4 and 7.5). The θ_{adv} of TD-microemulsions with high oil content ($\alpha = 0.5$ and $\alpha = 0.7$) increases 5° , whereas θ_{adv} increases 20° for the MO-microemulsions with $\alpha = 0.5$ and $\alpha = 0.7$, when decreasing surface polarity. Moreover, the favored adsorption of tetradecane oil molecules on hydrophobic surfaces is also reflected by θ_{rec}, which is lower for the TD-microemulsions than for the MO-microemulsions across the whole range of α.

A detailed analysis of the results also reveals differences on the dynamic contact angle between both microemulsion systems that arises with increasing oil content. The θ_{adv} of TD-microemulsions become higher along with α, whereas the MO-microemulsions show a decrease in θ_{adv} with an increase in α. For the MO-microemulsions, the reduction of θ_{adv} along with α can be related to a better surface coverage by the oil molecules, which can be also translated into a better wettability. The same behavior should also be expected for the TD-microemulsions, where a better wetting of the surface should take place for high oil contents (α). However, the results indicate that the wetting ability of the TD-microemulsions on the hydrophobic surfaces decreases along with the increase of α. A similar trend has also been observed on the hydrophilic surface and surfaces functionalized with APTES (results not shown here). Therefore, it may be inferred that the variation of the dynamic contact angles of TD-microemulsions with α is associated with a change in their structural or macroscopic properties (e.g., viscosity). A detailed explanation behind this phenomenon is still an open question.

7.3.2 Wetting of hydrophilic and hydrophobic porous model surfaces

The ability of both microemulsion systems to wet and to penetrate into the porous surfaces was evaluated by means of the Washburn method. The transport of the two microemulsion systems into the model porous surfaces is clearly related to the pore size, where the increase of the pore size enhances the speed of imbibition by one order of magnitude. Importantly, the polarity of the porous surfaces does not significantly influence the imbibition speed of the microemulsions, whereas the imbibition of the oils and surfactant solution is indeed strongly influenced by this parameter. This can be accounted by differences in the viscosity between the microemulsions and their components (Table 7.2). The viscosity values of the microemulsions are one order of magnitude higher than the viscosity of pure oils and surfactant solutions. A higher microemulsion viscosity does not only influence their imbibition speed, but also it would become important in the wetting of the porous surfaces.

In this respect, it has been established in the previous section that the viscosity of the microemulsion does not play a significant role in the establishment of the dynamic contact angles on the planar surface. This was explained considering that the capillary number was in the order of 10^{-4} when calculated with the dipping velocity of 5 mm/min. However, the speed of imbibition of the microemulsion into the porous surfaces should be faster than the dipping velocity of the planar surface, such that the viscous forces become important on the imbibition and wetting of porous surfaces. The effect of viscosity on the wetting of planar and rough surfaces was investigated by Grewal et al.[142] They found that the viscosity of glycerol aqueous solutions has a negligible effect on their contact angles on planar surfaces of different chemical nature. However, on textured surfaces (rough surfaces), the resulting contact angles are strongly dependent on the viscosity of the solution. This fact was associated with the increment of the viscous forces by the displacement of the liquid on the rough surface. These findings confirm that the wetting of porous surfaces is dominated by the viscous forces. Moreover, this could be the reason why the change of polarity on porous surfaces does not influence the contact angles, particularly on the porous surfaces with small and intermediate pore sizes.

Furthermore, the microemulsion contact angles are in the same range irrespectively of pore size. These results are in agreement with the wettability studies of materials with different particle sizes packed in columns (e.g. glass, quartz, or sphalerite particles).[143–146] It was found in these studies that the variation in the particle size (or pore size) influences the

transport of the test liquid but not its wettability as the contact angles remain constant when particle sizes are changed.

It was also found in our study that the contact angles of the microemulsions at porous model surfaces are larger than the advancing contact angles on planar surfaces. This difference in the contact angles could be explained by two main factors. First, the increase of viscous forces on the porous surfaces (also considered as a rough surface) could induce an increase in the contact angle values. Second, the porous solid constants calculated using a reference liquid could induce a systematic error on the determination of the contact angles (Section 4.2.4). In this calculation, it is assumed that the reference liquid can wet the porous surface completely.[147] If the reference liquid does not completely wet the solid surface, it would lead to an overestimation of the porous surface constant, which in turn would affect the calculated contact angles.

It can also be noted that the TD-microemulsions can wet the hydrophilic and hydrophobic porous surfaces better than the MO-microemulsions. This result is in contrast to what was found on planar surfaces, where the MO-microemulsions can preferentially wet the hydrophilic planar surface, whereas the TD-microemulsions wet stronger the hydrophobic planar surface. The fact that the TD-microemulsions can stronger wet the hydrophilic and hydrophobic porous surfaces could be associated with a difference between the two microemulsion systems in the transport mechanisms through the porous surfaces. However, the mechanism of the microemulsion transport cannot be fully clarified at this stage of the research.

7.4 Conclusion

This study evaluated the wettability of solid model surfaces by microemulsions. The polarity and porosity of the solid surfaces were varied in order to evaluate the effect on their wetting by the sugar surfactant microemulsion systems. The wetting of planar surfaces of different polarity by the sugar surfactant-based microemulsion systems was determined by evaluating the dynamic contact angles using two different methods: the tilted plate and the Wilhelmy plate method. Both methods shows divergences on the estimated dynamic contact angles. It has been concluded that the Wilhelmy plate method shows a higher sensitivity in the determination of dynamic contact angles than the tilted plate method. The reason for the high sensitivity of the Wilhelmy plate method is a stronger interaction and adsorption of the microemulsion components on the planar surfaces

during the measurements carried out using this method. It was identified on the basis of the dynamic contact angles estimated by the Wilhelmy plate method that the adsorption of microemulsion components and microemulsion structure play a significant role in the wetting of planar surfaces. Sugar surfactant and water molecules are preferentially adsorbed at the hydrophilic solid-liquid interface. As these are the common components of both microemulsion systems, the hydrophilic planar surface is wetted in a similar fashion by the TD- and MO-microemulsions with α variation. This surface was strongly wetted by the microemulsion with a high water content ($\alpha = 0.1$). The oil components of the tetradecane and methyl oleate microemulsions are adsorbed preferentially on the hydrophobic surface. The change of the adsorbed molecules at the solid-liquid interface leads to a change in the capabilities of microemulsion systems to wet the hydrophobic surface. In this case, the hydrophobic surface is wetted preferentially by the TD-microemulsions across the whole range of α.

The wetting of porous model surfaces of different polarity by microemulsion systems was evaluated using the Washburn method. The imbibition rate of both microemulsion systems into the porous surface is determined by the pore size of the surfaces and the viscosity of the microemulsions. In particular, the viscosity of the microemulsions plays an important role in the wetting of the porous surfaces as the viscous forces start to dominate the displacement of the microemulsions through the rough surface. The variation of the pore size does not influence the wettability of the porous surfaces as the evaluated contact angles are constant for both microemulsion systems independently from the pore size. Furthermore, the TD-microemulsions can strongly wet the hydrophilic and hydrophobic porous surfaces compared to the MO-microemulsions. These results have been tentatively associated with a difference in the transport mechanism between both microemulsion systems through the porous surfaces.

Chapter 8

Extraction of model contaminants from solid surfaces by microemulsions*

Abstract

The efficiency of methyl oleate and sugar surfactant based microemulsions to decontaminate solid surfaces was investigated by monitoring the extraction of non-toxic model molecules of sulfur mustard out of model surfaces. The extraction process of the non-toxic simulants was monitored by means of spectroscopic and chromatographic techniques. The kinetics of the removal process was analyzed by different empirical models. The analysis of kinetics further allowed us to assess the influence of the amounts of oil and water and the microemulsion structure on the extraction process.

8.1 Introduction

In view of a potential emergency caused by accidental or intentional release of highly toxic substances, it is of utmost importance to understand how effective decontamination media can be implemented in order to mitigate the impact of these toxic substances on the environment and the public health.[26,148] In the study of decontamination processes of hazardous solid surfaces, the most common substance used as contaminant is sulfur mustard agent.[149]The main reason for using this highly toxic substance is its low volatility and low solubility in water, which induces an increases its persistence in the environment and the challenges to remove it from the affected area.[149] For example, It has been found that the half-life time of the sulfur mustard agent on different substrates is in the range from 75 hours up to 54 weeks.[150–152]

It is important to point out that the persistence and toxicity of any toxic substance are dramatically enhanced when they are mixed with thickening agents.[153] The most commonly used thickening agents are methyl methacrylate and chlorinated rubber with molecular weights in the range from 40 to 50 thousand daltons. Mixing chemical warfare agents with approximately 5 % thickener induces an increase in viscosity in the range

*Adapted from Journal of colloid and interface science, Vargas Ruiz, S., Schulreich, C., Kostevic, A., Tiersch, B., Koetz, J., Kakorin, S., von Klitzing, R., Jung, M., Hellweg, T. Wellert, S, 2016, 471, pages 118-126, Extraction of model contaminants from solid surfaces by environmentally compatible microemulsions, Copyright (2017), with permission from Elsevier.

from 30 to 600 cp. In this range of viscosity, the adhesiveness of the mixture to different surfaces is improved and the persistence of the contaminant is thereby increased. At the same time, the employment of thickeners can hamper the decontamination processes as the thickener exhibits low solubility in most environmentally friendly solvents (e.g., biodiesel or food grade oils). To the best of our knowledge, no reports on the half-life time of the highly toxic substances mixed with thickening agents have been available to the public up to date.

Considering that the half-life time of the most persistent chemical warfare agents on solid surfaces are in the range from days to months, it is necessary to develop decontamination methods that are capable of extracting these contaminants from the affected surface within the range of hours and can at the same time guarantee further functionality of the surface after the decontamination processes. In this chapter, the efficiency of environmentally compatible microemulsions to extract and remove model contaminants from sorptive surfaces is evalatuated. The evaluation of the extraction processes was carried out with the MO-microemulsions, as the microemulsions prepared with methyl oleate are more biodegradable and biocompatible than the microemulsions prepared with tetradecane. Three harmless model lipophilic substances were employed as model contaminants: Sudan III, methyl salicylate, and 2-chloroethyl ethyl sulfide (CEES). Sudan III dye is a lipophilic molecule that can easily be monitored by spectroscopic techniques. Methyl salicylate and CEES are two lipophilic models for the highly toxic and water-insoluble sulfur mustard agent (Table 8.1). Moreover, the kinetics of the removal processes of the lipophilic contaminants was quantitatively analyzed by comparing four often used empirical models. The analysis of the kinetics allows us to obtain a correlation between the efficiency of the microemulsions to extract lipophilic contaminants and their structural properties.

Table 8.1: Physicochemical properties of the compounds employed as model contaminants. The parameter Log P is an indication of the compound hydrophobicity and is expressed as the logarithm of the partition coefficient of the molecule between octanol and water

Property	Sudan III	Methyl Salicylate
Chemical Structure	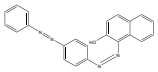	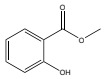
Molecular Weight	352.29 g mol^{-1}	152.05 g mol^{-1}
LogP	7.51±0.47	7.51±0.47
Vapor Pressure	——	0.0343 Torr at 25 âC
Property	**2-Chloroethyl ethyl sulfide CEES**	**Mustard agent**
Chemical Structure	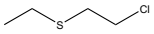	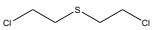
Molecular Weight	124.63 g mol^{-1}	159.07 g mol^{-1}
LogP	1.86±0.47	2.23±0.47
Vapor Pressure	3.4 Torr at 25° C	0.11 Torr at 25° C

All physicochemical parameters shown in the table were estimated with ChemDraw Pro program.

8.2 Results

8.2.1 Extraction of Sudan III from a porous polymeric surface

In the evaluation of the efficiency of MO-microemulsions to extract Sudan III, the polymeric surface poly(butylmethacrylate-co-ethylendimethacrylate) was used as porous model surface. The pore sizes of porous polymeric surfaces range from 100 to 1000 nm.[154–156] These porous surfaces can easily retain lipophilic contaminants due to their highly hydrophobic nature. This hydrophobic character is indicated by the high static water contact angle at the surface as demonstrated in Figure 8.1a). Hence, a non-polar medium capable to wet such a surface which would also favor the extraction of the contaminant is required.

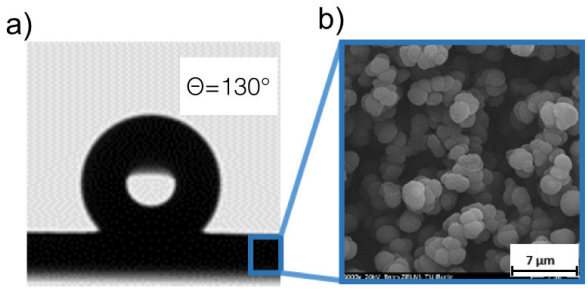

Figure 8.1: a) Contact angle of a drop of water in the hydrophobic porous polybutylmethacrylate-co-ethylendimetacrylate) and b) SEM image of the surface illustrating its porous nature.

Glass filters were also used as model surfaces to evaluate the extraction processes of Sudan III and methyl salicylate. Nevertheless, the extraction curves were not reproducible when they were evaluated on the porous glasses with the same pore sizes and polarity (data not shown here). The low reproducibility was associated with the lack of control of the contaminant distribution in the surface due to the high thickness of the glass filters (2.5 mm). Despite the lack of reproducibility, it was observed that the overall rate of transfer of the methyl salicylate into the microemulsions is highly dependent on the range of pore size. This relation is associated with the rate of transport or imbibition of the microemulsions into the porous surfaces. These preliminary results show the need to investigate the role of the pore size distribution of the surfaces in the decontamination processes.

In contrast to the glass filters, highly reproducible extraction curves were obtained using porous polymeric surfaces due to their low thickness (0.50 mm) and the homogenous distribution of the contaminant across the whole surface. Figure 8.2 presents the kinetics of the extraction of Sudan III out of the porous polymeric surfaces by the MO-microemulsions at different α as a function of the time. The extracted amount of Sudan III is given in percentage E, where E denotes the amount of extracted dye relative to the total amount deposited on the surface.

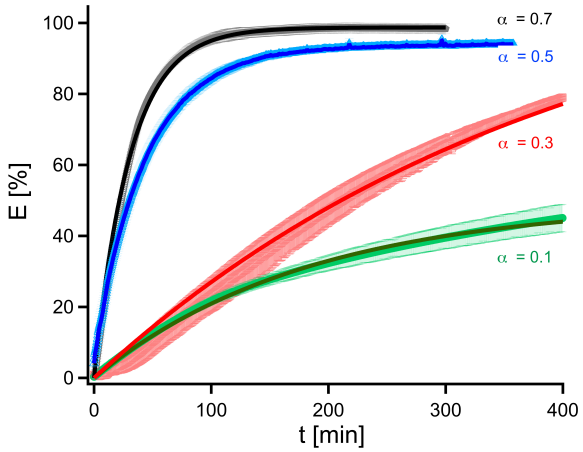

Figure 8.2: Extracted percentage E of Sudan III from porous polymeric surfaces as a function of time monitored by UV-vis spectroscopy. The thickness of the curves refers to the error of three repeated measurements. Solid lines are fits of the first order model, Eq.4.24 to the data.

The extraction curves of Sudan III show a distinctive behavior determined by α of the microemulsions. The MO-microemulsion with $\alpha = 0.1$ extracts Sudan III from the porous surfaces comparatively slowly. It tends to reach saturation level when only 40 % of the dye have been extracted. The extraction curve for the MO-microemulsion with α=0.3

has a sigmoidal shape. After an initial phase of 30 minutes, the extraction of Sudan III increases such that the MO-microemulsion with $\alpha = 0.3$ is able to extract 80 % of the dye after 7 hours. In contrast, the MO-microemulsions formulated at $\alpha = 0.5$ and $\alpha = 0.7$ are the most effective decontamination media as they can extract the dye from the porous surfaces comparatively fast. The extracted amount reached 80 % and 90 % of the dye in the first 100 minutes, respectively.

8.2.2 Extraction of methyl salicylate from porous polymeric surface

The efficiency of the microemulsions to extract methyl salicylate from the porous polymeric surfaces was monitored via high pressure liquid chromatography (HPLC)[†]. This technique has a low detection limit, leading to a higher sensitivity for the methyl salicylate in comparison to the IR and UV-Vis spectroscopic techniques.

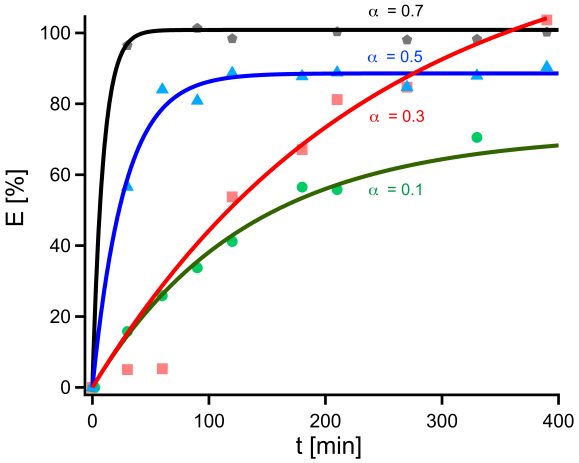

Figure 8.3: Extracted percentage of methyl salicylate from porous polymeric surfaces by the prepared microemulsions as a function of the time (process monitoring via HPLC). The solid lines indicate the fit of the data by the first order model, Eq.4.24.

The extraction curves of methyl salicylate from the porous substrates (Figure 8.3) show similar trends when compared to the extraction curves of Sudan III (Figure 8.2). The main difference between both extraction processes is that the saturation of methyl salicylate is reached in shorter time compared to Sudan III extraction. For instance, the microemulsion with $\alpha = 0.1$ is saturated when 60 % of methyl salicylate have been extracted. In contrast, for the same microemulsion, the Sudan III saturation is already reached at 40 % extraction. The extraction curve of methyl salicylate using the microemulsion with $\alpha = 0.3$ also shows a delay in the extraction process. Nevertheless, the microemulsion with $\alpha = 0.3$ can

[†]The HPLC measurements were carried out by M. Griffel, Analytik des Instituts für Chemie, TU-Berlin.

completely extract methyl salicylate out of the porous polymeric surface after 7 hours, while the microemulsions with $\alpha = 0.5$ and $\alpha = 0.7$ extract 80 % and 100 % of methyl salicylate in the first 50 minutes, respectively.

8.2.3 Extraction of thickened CEES from planar surfaces

Figure 8.4 presents the kinetics of the extraction of CEES from planar surface (the hydrophobic diamond crystal of ATR-IR spectrometer) by microemulsions as a function of time[‡]. Here, the affinity of the contaminant to the diamond surface has been enhanced by thickening the CEES with chlorinated rubber Parlon S before its deposition.[28] Parlon S is a thickener used in chemical warfare agents in order to enhance the persistence of the agent in the medium and to reduce its volatility.

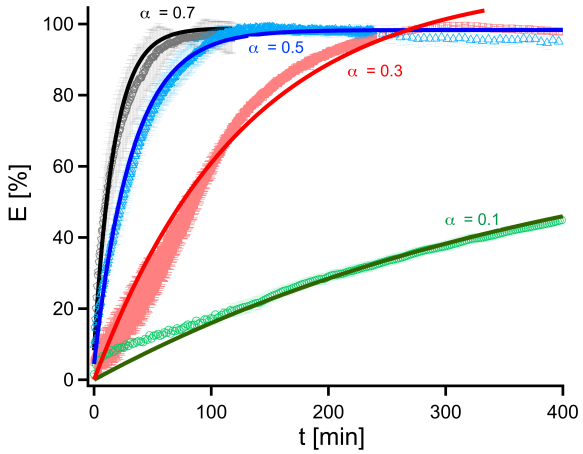

Figure 8.4: Extracted percentage of CEES from a planar diamond by the prepared microemulsions as a function of the time (process on-line monitored via ATR-IR). The thickness of the curves refers to the standard error of three repeated measurements, and the solid line refers to the fit of the data by the first order model, Eq.4.24

The extraction curves of the thickened CEES at the planar surface compare well with the results obtained for Sudan III and methyl salicylate extraction from the porous polymeric surfaces (Figures 8.2 and 8.3). The similarity of the obtained results can be associated with the non-polar character of the porous polymeric surface and the thickening agent Parlon S. Hence, the affinity of the lipophilic contaminant as well as the interaction of the microemulsion with both media are comparable. It is important to point out that the microemulsions should be able to wet and penetrate the porous polymeric surface,

[‡]The CEES extraction experiments were carried out by A. Kostevic and Dr M. Jung Wehrwissenschaftliches Institut für Schutztechnologien, Germany.

whereas on the planar surface they should be able to dissolve the thickening agent in order to favor the extraction of the contaminant.

8.2.4 Evaluation of extraction kinetics

The extraction curves were fitted using four models: the two-site kinetic model, the modified Gompertz model, the Pelegs model, and the first-order model (Appendix 1)[§]. The first-order model, Eq. 4.24, showed the highest accuracy to describe the removal curves of the microemulsions. In the first order model, the constant k denotes the overall extraction rate coefficient of the contaminated from the surface to the microemulsion, E_c indicates the percentage of extraction of the contaminant at the equilibrium stage. The efficiency of the extraction process can be discussed in terms of the rate constant k and the maximum amount E_c that can be solubilized in the oil reservoir of the microemulsion. The overall transfer rate constant k and the percentage of extraction E_c at the equilibrium stage for each evaluated process are listed in Table 8.2.

	Sudan III UV-Vis		**Methyl salicylate (HPLC)**		**CEES (ATR-IR)**	
α	k ($min^{-1} * 10^{-3}$)	E_c (%)	k ($min^{-1} * 10^{-3}$)	E_c (%)	k ($min^{-1} * 10^{-3}$)	E_c (%)
0.1	5.4 ± 0.5	50 ± 1	7.6 ± 0.7	72 ± 3	3.4 ± 0.5	64 ± 1
0.3	2.5 ± 0.5	122 ± 1	4.2 ± 0.5	130 ± 30	8 ± 1	112 ± 12
0.5	25 ± 1	93 ± 1	36.4 ± 0.5	89 ± 1	31 ± 1	98 ± 1
0.7	32 ± 1	99 ± 1	110 ± 15	101 ± 1	58 ± 1	100 ± 1

Table 8.2: The overall extraction rate constant k and the percentage of extracted Sudan III, methyl salicylate, and CEES at the equilibrium stage E_c determined for the extraction processes by the prepared microemulsions. The kinectic parameters were calculated according to the first order model, Eq.4.24

The kinetic parameters determined for the extraction processes of Sudan III, methyl salicylate, and CEES are highly comparable between the microemulsions with the same composition or α. In the three processes studied, the microemulsion with $\alpha = 0.1$ has a limited extraction capacity such that it saturates when only 40 % to 70 % of the contaminants have been extracted. Moreover, the overall rate of extraction for the microemulsion with $\alpha = 0.1$ is significantly lower than the overall rate constant obtained for the microemulsions with higher oil content. The extraction of the three lipophilic model

[§]The fitting of the extraction curves was done in cooperation with Dr S. Kakorin, Physikalische Chemie III, Universität Bielefeld, Germany.

molecules by the microemulsion with $\alpha = 0.3$ has an overall extraction rate in the same order of magnitude as the microemulsion at $\alpha = 0.1$. However, the results for E_c using the first-order model overestimate the maximum amount of contaminant that can be extracted. This is associated with the fact that the model does not perfectly fit the experimental data. This in turn can also affect the calculated overall extraction rate constant. Nevertheless, it is clear that the increment of the oil content from $\alpha = 0.1$ to $\alpha = 0.3$ enhances the removed amount of the three contaminants at the end of the processes.

The extraction processes performed by using the microemulsions with $\alpha = 0.5$ and $\alpha = 0.7$ are well described by the first-order model. For these microemulsions, the overall extraction rate constant is 10 times higher than the overall extraction rate constant calculated for the microemulsion with $\alpha = 0.1$ and $\alpha = 0.3$. The increase of the removed amount is most likely related to the connectivity of the oil domains and the increasing oil content. This favors the transport and solubilization of the lipophilic substances in the bulk of the microemulsion. At slightly shorter times, a higher amount of contaminants can be removed.

8.3 Discussion

The MO-microemulsion system was employed as a decontamination medium for the extraction of model contaminants Sudan III, methyl salicylate, and thickened CEES out of porous and planar surfaces. A comparison of the results for the three test substances shows strong similarities that are independent from test substances and surfaces. According to the removal curves and their kinetic parameters, we can establish two main characteristics of the lipophilic compound removal process by the MO-micoremulsions: (i) the removal capacity of the microemulsion is dominated by its oil content, for instance, the MO-microemulsion $\alpha = 0.1$ can only remove around 50 to 60 % of the lipophilic molecule deposited on the surface, and this microemulsion also shows the overall lowest rate of extraction, and (ii) a 10-fold increase on the extraction rate is achieved by increasing the oil content from $\alpha = 0.3$ to $\alpha = 0.5$. These general trends allow to infer that the composition and structure of the microemulsion play a major role in the decontamination of the sorptive surfaces since the kinetics of the removal process is hardly influenced by the physicochemical properties of the model contaminants and the morphology and chemical nature of the sorptive surface, in which these lipophilic molecules are embedded.

As discussed in Chapter 5, the used MO-microemulsions in the range from $\alpha = 0.1$ to

$\alpha = 0.7$ are formulated in the bicontinuous region. The variation of α induces a change in the connectivity of the oil and water nanodomains. The structure of the microemulsions at $\alpha = 0.1$ is a diluted network of oil domains in an aqueous environment. The rate of extraction of the contaminants by this microemulsion is limited by the fact that the transport of the lipophilic substance to the bulk of the microemulsion is hindered by the high water content in the medium. Whereas the low saturation capacity of the MO-microemulsion with $\alpha = 0.1$ is associated with the limited oil content available for the solubilization of the contaminant. Furthermore, the hydrophobic solid surfaces are not wetted efficiently by the MO-microemulsion with $\alpha = 0.1$ (see Chapter 7), which can also be a parameter limiting the rate of transfer of the contaminant into the bulk phase of the microemulsion.

The increase of the oil content in the MO-microemulsion from $\alpha = 0.1$ to $\alpha = 0.3$ induces a growth in the oil nanodomain size and improves its connectivity. Hence, the increase of the oil content in the microemulsion to $\alpha = 0.3$ considerably enhances the solubilization capacity of the microemulsion, in turn favoring the overall rate of extraction. A further increase of the oil content in the MO-microemulsion from $\alpha = 0.3$ to $\alpha = 0.5$ promotes the connectivity of the oil and water nanodomains, such that at $\alpha = 0.5$ a well-defined bicontinuous structure is developed. It is remarkable that in this study a higher connectivity of the oil and water nanodomains dramatically enhances the extraction efficiency of the microemulsion. The enhancement on the extraction process is associated with the continuity of the oil domains as interconnected channels. This favors the transport and solubilization of the lipophilic substances in the bulk phase; thereby, the overall removal rate constant increases by a factor of 10 folds compared to the rate constant of the microemulsions $\alpha = 0.1$ and $\alpha = 0.3$.

The efficiency of the microemulsion in the removal process by increasing the oil content from $\alpha = 0.5$ to $\alpha = 0.7$ does not significantly influence the efficiency of the MO-microemulsion in the extraction process. Taking into account that the structure in the microemulsion $\alpha = 0.7$ could correspond to the less connected water nanodomains in an oil medium, it can be assumed the high inter-connectivity of the oil nanodomains in the MO-microemulsions with $\alpha = 0.5$ are as efficient as the continuous medium oil in transporting the lipophilic substances from the solid-liquid interface to the bulk phase. Moreover, the increase of the overall extraction rate constant and extraction percentage at the equilibrium from $\alpha = 0.5$ to $\alpha = 0.7$ is associated with the increase of solubilization capacity of the MO-microemulsions.

For Sudan III, the extraction capacity of the aqueous surfactant solution (without oil) and

the pure oil (methyl oleate) was investigated (See appendix 1). The rate constants and yields of surfactant solution and the MO-microemulsions with $\alpha = 0.1$ and $\alpha = 0.3$ are in good agreement. The extraction by the pure oil is in the same order of magnitude as the MO-microemulsions with $\alpha = 0.5$ and $\alpha = 0.7$ but up to a factor of 2 smaller. Speculatively, the wetting properties and viscosity of the microemulsions could be beneficial in this case.

Qualitatively, the observed extraction effect and the obtained yields are in a good agreement with the findings from experiments with microemulsions prepared with different surfactant and oils but mainly with a droplet phase structure.[33,35,36]

8.4 Conclusion

The extraction kinetics of the MO-microemulsions was investigated using three test substances (Sudan III, methyl salicylate, and thickened CEES) and detection methods (UV VIS spectroscopy, liquid chromatography, and FTIR-ATR spectroscopy). The kinetics was quantified by using four empirical models. A comparison of fit quality and results showed that a first order model is best suited to describe the data. It has been established that the structure and composition of the microemulsion play a major role in the removal of the lipophilic contaminants out of the solid surfaces, as the efficiency of the process is not significantly influenced by the physicochemical properties of the lipophilic molecule removed or by the nature and morphology of the solid surfaces on which these molecules have been deposited. The MO-microemulsions $\alpha = 0.5$ with a well-defined bicontinuous structure show the best performance in the removal of lipophilic contaminants out of the solid surfaces due to the high interconnectivity of the oil domains in the structure, which facilitates the transport and solubilization of the lipophilic contaminant into the bulk phase. In terms of the role of the surface in the decontamination process, further studies will concentrate on the investigation of the influence of porosity and polarity of the solid surface on the removal of deposited lipophilic contaminant by microemulsions.

Chapter 9

Summary and outlook

The presented thesis aims to gain a better understanding of the structural properties of sugar surfactant based microemulsions at solid-liquid interfaces, focusing on the correlation between the structural properties of the microemulsions, their ability to wet the substrate, and the transport of the contaminant from the wetted surface to the bulk of the microemulsion. The motivation behind this study is the demand for new decontamination media that can simultaneously extract and decompose toxic lipophilic compounds deposited onto different types of surfaces.

The first part of this work was dedicated to studying the structural properties of sugar surfactant-based microemulsions in bulk prepared by using tetradecane (nonpolar) and methyl oleate (polar) oils. The structural properties of both microemulsion systems were characterized by means of three complementary techniques: SANS, diffusion NMR, and cryo-SEM. The results indicate that well-defined bicontinuous structures were formed at symmetric compositions ($\alpha = 0.3$ and $\alpha = 0.5$), whereas diluted and less connected bicontinuous structures were formed at asymmetric compositions ($\alpha = 0.1$ and $\alpha = 0.7$). Moreover, it was demonstrated that the bending moduli of the sugar surfactant-based microemulsions highly depended on the type of oil employed. The estimated bending moduli of the TD-microemulsions are larger than those of the MO-microemulsions, particularly in the range from $\alpha = 0.5$ to $\alpha = 0.7$. Differences in the bending moduli have a direct impact on the degree of organization of the nanodomains in the bulk. The MO-microemulsions present short length ordering of the bicontinuous structures in comparison to the TD-microemulsions.

In the second part of the study, the structural properties of microemulsions in contact with substrates of different polarity were investigated using neutron reflectometry and GISANS. The contact between sugar surfactant-based microemulsions and solid surfaces leads to a reconfiguration of their structural properties. A quantitative comparison of the structural parameters (domain size and correlation length) showed no difference between the bulk and the near-surface region. This fact is supported by the results obtained by GISANS, which indicate that the bulk structure of microemulsions is preserved along the lateral direction. These findings suggest that the structure of the microemulsions near the surface is maintained, and the presence of the surface only induces the organization of oil and water nanodomains into a more layered structure in the vicinity of planar surfaces, where a weak contribution of the lamellar phase to the near-surface structure has been assumed. More importantly, the extension of the microemulsion structuring perpendicularly to the

solid-liquid interface was highly influenced by surface polarity. At the hydrophilic surface, both TD- and MO-microemulsion systems developed a distinct structure perpendicular to the hydrophilic solid-liquid interface. Conversely, at the hydrophobic solid-liquid interface the structuring of the MO-microemulsions was hindered, while the ordering of the TD-microemulsion was preserved. This effect was attributed to differences in the adsorption behavior of the microemulsion components at the solid-liquid interface, a fact that also has a strong impact on the wetting of the surfaces. The wetting of surfaces by microemulsions was investigated by dynamic contact angle measurements. In this study, the morphology of solid model surfaces (planar or porous) and their polarity (hydrophilic and hydrophobic) was controlled to verify their effect on the wetting processes. It has been suggested that the composition of the microemulsions and the adsorption of their components on solid surfaces plays a significant role during the wetting process. Hydrophilic planar surfaces are wetted in a similar fashion by both MO- and TD-microemulsions. The similar wetting behavior has been associated with the fact that in both systems the sugar surfactant is preferentially adsorbed at the hydrophilic planar surface. In contrast, the TD-microemulsions are more efficient in wetting hydrophobic planar surfaces than the MO-microemulsions. The difference on the hydrophobic surface wetting by the two microemulsions systems can be related to the adsorption of the oil molecules on this surface, where tetradecane is more efficient in reducing the interfacial tension of the solid-liquid interface than methyl oleate.

This study also established that the microemulsion structuring in bulk and at the interface has a high impact on the extraction of contaminants out of planar and porous surfaces. The extraction kinetics was evaluated for three hydrophobic substances deposited onto hydrophobic and porous polymeric substrates and hydrophobic planar surfaces: Sudan III, methyl salicylate, and thickened CEES. The MO-microemulsion system was chosen as the extraction media since this microemulsion system is more compatible with the current environmental regulations. The extraction and solubilization processes are strongly affected by the structure of the microemulsion. The extraction rate of the contaminants by the MO-microemulsion with $\alpha = 0.1$ is limited because of two parameters: (I) the hydrophilic surfaces are not efficiently wetted by this microemulsion, and (II) the transport of the contaminant from the solid surface to the bulk of the microemulsion is hindered by the high water content in the medium. In contrast, an efficient extraction of the contaminants is achieved by means of symmetric bicontinuous MO-microemulsions ($\alpha = 0.5$). The high extraction efficiency is due to the high connectivity of the oil and water nanodomains and the ability of this sample to wet the hydrophobic surface. These two properties enhance the transport of the molecules from the solid surface to the bulk of the microemulsion.

This knowledge allows us to optimize the efficiency of decontamination processes by up to 80 % by applying environmentally compatible microemulsions.

Overall, a strong correlation between microemulsion structuring at the solid-liquid interface, the wetting of the surface, and the transport of the contaminant has been established in this thesis.

Future work in the field of decontamination with environmentally compatible microemulsions can be done by two different approaches. The first approach can be based on a combination of experimental studies. It has been observed that the adsorption of the microemulsion components on solid surfaces has a substantial impact on the structuring at the interface as well as on the wetting processes. Therefore, a quantitative evaluation of the interfacial adsorption is required to estimate the real impact of this phenomenon on the adsorption-related processes. In order to have a complete picture of the adsorption onto solid surfaces, the use of complementary techniques such as neutron reflectometry and quartz-crystal microbalance with dissipation (QCM-D) is highly recommended. Neutron reflectometry experiments could allow a quantitative estimation of the composition of the solid-liquid interface by using contrast variation of the bulk phase of microemulsions, which would allow to be more precise on the estimation of the scattering length density profile at the interface and thus on its composition. QCM-D as a surface-sensitive technique allows monitoring real-time changes in the surface mass that arise from the adsorption of microemulsion components. Although QCM-D cannot distinguish the identity of the molecules adsorbed at the interface, it allows to monitor the adsorption process when the composition of the microemulsion and the polarity of the surface are changed. Furthermore, changes in the resonance frequency and the dissipation, two parameters measured by this technique, can provide new insights into the viscoelastic properties of the microemulsion close to the interface, and their relation to the structural properties of the oil and water nanodomains near to the solid-liquid interface. The second approach could be based on computer simulation studies. Computer simulation can provide means to understanding the interaction and adsorption of microemulsion components at solid-liquid interfaces. These simulations can be further extended to model the structural ordering of the oil and water nanodomains at both vertical and lateral direction of the solid-liquid interface. In addition, computer simulations can also support the investigation of the transport of molecules from the surface to the microemulsions based on (I) the structural properties of the microemulsion at the solid-liquid interface and in the bulk phase, (II) the diffusion properties of the molecules, and (III) the molecular solubility in the water and oil phases.

Chapter 10

Appendix

Appendix 1

Evaluation of the extraction models

The goodness of the description of the experimental data by the models was analyzed using the Pearson correlation coefficient r and the normalized root mean square error value (Section 4.5.5). The results of the evaluation are presented in Table 10.1.

Kinetics model		α=0.1	α=0.3	α=0.5	α=0.7
Sudan III					
First-order	NRM r	0.014 0.999	0.017 0.999	0.045 0.991	0.012 0.999
Gompertz	NRM r	0.040 0.990	0.020 0.998	0.024 0.996	0.019 0.996
Peleg	NRM r	0.007 1.000	0.023 0.998	0.067 0.974	0.041 0.983
Two-site	NRM r	0.004 1.000	0.017 0.999	0.045 0.9991	0.012 0.999
Methyl salicylate					
First-order	NRM r	0.040 0.994	0.098 0.977	0.033 0.994	0.027 0.996
Gompertz	NRM r	0.096 0.977	0.063 0.989	0.032 0.995	0.027 0.996
Peleg	NRM r	0.051 0.990	0.100 0.976	0.047 0.989	0.030 0.996
Two-site	NRM r	0.040 0.994	0.098 0.978	0.032 0.995	0.028 0.996
CEES					
First-order	NRM r	0.025 0.998	0.048 0.989	0.021 0.996	0.029 0.990
Gompertz	NRM r	0.041 0.988	0.009 1.00	0.021 0.997	0.020 0.992
Peleg	NRM r	0.021 0.998	0.0063 0.980	0.042 0.972	0.020 0.992
Two-site	NRM r	0.01 0.999	0.059 0.989	0.018 0.997	0.010 0.998

Table 10.1: Goodness of fits of the extraction kinetics represented by the Pearson correlation coefficient r and the normalized root mean square error value NRM, for the extraction of Sudan III, methyl salicylate and CEES by microemulsions at different oil to water ratios α.

Kinetic of the extraction process of Sudan III by methyl oleate and surfactant solution

Figure 10.1 presents the kinetics of the extraction of Sudan III out of the porous polymeric surfaces by methyl oleate and surfactant solution. The overall transfer rate constant k and the percentage of extraction E_c at the equilibrium stage are estimated by means of the first order model (Table 10.2).

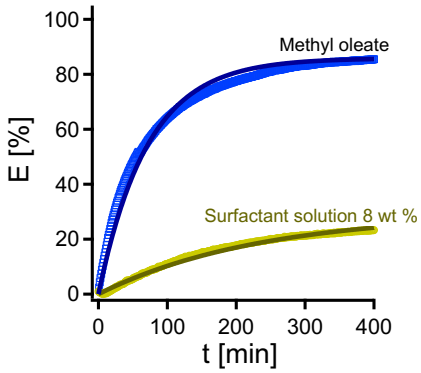

Figure 10.1: Extracted percentage E of Sudan III from porous polymeric surfaces as a function of time monitored by UV-vis spectroscopy. Solid lines are fits using the first order model.

Extraction of Sudan III		
	k $(min^{-1} * 10^{-3})$	E_c (%)
Surfactant solution 8 wt%	4.3 ± 0.1	29.6 ± 0.1
Methyl oleate	14.0 ± 0.1	85.9 ± 0.1

Table 10.2: Overall extraction rate constant k and the extracted percentage at the equilibrium stage E_c determined for the extraction processes of Sudan III by methyl oleate and surfactant solution monitored via UV-Vis spectroscopy. The kinetic parameters were calculated according to the first order model.

Bibliography

[1] Schulreich, C.; Angermann, C.; Höhn, S.; Neubauer, R.; Seibt, S.; Stehle, R.; Lapp, A.; Richardt, A.; Diekmann, A.; Hellweg, T. *Colloids and Surfaces, A: Physicochemical and Engineering Aspects* **2013**, *418*, 39–46.

[2] Wellert, S.; Imhof, H.; Dolle, M.; Altmann, H.-J.; Richardt, A.; Hellweg, T. *Colloid and Polymer Science* **2008**, *286*, 417–426.

[3] Wellert, S.; Tiersch, B.; Koetz, J.; Richardt, A.; Lapp, A.; Holderer, O.; Gaeb, J.; Blum, M.-M.; Schulreich, C.; Stehle, R.; Hellweg, T. *European Biophysics Journal* **2011**, *40*, 761–774.

[4] Hellweg, T.; Wellert, S.; Mitchell, S. J.; Richardt, A. *Decontamination of Warfare Agents*; Wiley-VCH Verlag GmbH & Co. KGaA, 2008; pp 223–251.

[5] Gaeb, J.; Melzer, M.; Kehe, K.; Wellert, S.; Hellweg, T.; Blum, M.-M. *Analytical and Bioanalytical Chemistry* **2010**, *396*, 1213–1221.

[6] Langevin, D. *Annual Review of Physical Chemistry* **1992**, *43*, 341–369.

[7] Strey, R. *Colloid and Polymer Science* **1994**, *272*, 1005–1019.

[8] Hellweg, T.; von Klitzing, R. *PHYSICA A* **2000**, *283*, 349 – 358.

[9] Hoar, T.; Schulman, J. *Nature* **1943**, *152*, 102–103.

[10] Winsor, P. *Transactions of the Faraday Society* **1948**, *44*, 376–398.

[11] Schulman, J. H.; Stoeckenius, W.; Prince, L. M. *The Journal of physical chemistry* **1959**, *63*, 1677–1680.

[12] Salager, J.-L.; Anton, R.; Forgiarini, A.; Marquez, L. *Microemulsions*; John Wiley & Sons, Ltd, 2009; pp 84–121.

[13] Kahlweit, M.; Strey, R.; Firman, P.; Haase, D.; Jen, J.; Schomaecker, R. *Langmuir* **1988**, *4*, 499–511.

[14] Stubenrauch, C. *Current opinion in colloid & interface science* **2001**, *6*, 160–170.

[15] Jakobs, B.; Sottmann, T.; Strey, R.; Allgaier, J.; ; Richter, D. *Langmuir* **1999**, *15*, 6707–6711.

[16] Sottmann, T.; Stubenrauch, C. *Microemulsions*; John Wiley & Sons, Ltd, 2009; pp 1–47.

[17] Thiyagarajan, P.; Chaiko, D.; Hjelm Jr, R. *Macromolecules* **1995**, *28*, 7730–7736.

[18] Kahlweit, M.; Strey, R. *Angewandte Chemie International Edition in English* **1985**, *24*, 654–668.

[19] Pizzino, A.; Molinier, V.; Catté, M.; Salager, J.-L.; Aubry, J.-M. *The Journal of Physical Chemistry B* **2009**, *113*, 16142–16150.

[20] Sottmann, T.; Strey, R.; Chen, S. *Journal of Chemical Physics* **1997**, *106*, 6483–6491.

[21] Helfrich, W. *Zeitschrift für Naturforschung C* **1973**, *28*, 693–703.

[22] Widom, B. *The Journal of chemical physics* **1984**, *81*, 1030–1046.

[23] Arleth, L.; Marcelja, S.; Zemb, T. *J. Chem. Phys* **2001**, *115*, 3923–3936.

[24] Duvail, M.; Dufreche, J.-F.; Arleth, L.; Zemb, T. *Physical Chemistry Chemical Physics* **2013**, *15*, 7133–7141.

[25] Duvail, M.; Arleth, L.; Zemb, T.; Dufreche, J.-F., J.-F.che *The Journal of Chemical Physics* **2014**, *140*.

[26] Altmann, H.-J.; Richardt, A. *Decontamination of Warfare Agents*; Wiley-VCH Verlag GmbH & Co. KGaA, 2008; pp 83–115.

[27] Mercey, G.; Verdelet, T.; Renou, J.; Kliachyna, M.; Baati, R.; Nachon, F.; Jean, L.; Renard, P.-Y. *Accounts of chemical research* **2012**, *45*, 756–766.

[28] Sata, U.; Ramkumar, S. In *Intelligent Textiles and Clothing for Ballistic and NBC Protection*; Kiekens, P., Jayaraman, S., Eds.; NATO Science for Peace and Security Series B: Physics and Biophysics; Springer Netherlands, 2012; pp 177–195.

[29] Carrillo, C.; Saloni, D.; Lucia, L.; Hubbe, M.; Rojas, O. *Journal of Colloid and Interface Science* **2012**, *381*, 171 – 179.

[30] Bagwe, R.; Kanicky, J.; Palla, B.; Patanjali, P.; Shah, D. *Critical Reviews in Therapeutic Drug Carrier Systems* **2001**, *18*, 77–140.

[31] Harwell, J. H.; Sabatini, D. A.; Knox, R. *Colloids and Surfaces A: Physicochemical and Engineering Aspects* **1999**, *151*, 255 – 268.

[32] Acosta, E. J.; Nguyen, T.; Witthayapanyanon, A.; Harwell, J. H.; Sabatini, D. A. *Environmental Science & Technology* **2005**, *39*, 1275–1282, PMID: 15787367.

[33] Zheng, G.; Wong, J. W. Application of microemulsion to remediate organochlorine pesticides contaminated soils. Proceedings of the Annual International Conference on Soils, Sediments, Water and Energy. 2010; p 4.

[34] Do, L. D.; Withayyapayanon, A.; Harwell, J. H.; Sabatini, D. A. *Journal of Surfactants and Detergents* **2009**, *12*, 91–99.

[35] Dierkes, F.; Haegel, F.-H.; Schwuger, M. *Colloids and Surfaces A: Physicochemical and Engineering Aspects* **1998**, *141*, 217 – 225.

[36] Giorgi, R.; Baglioni, M.; Berti, D.; Baglioni, P. *Accounts of Chemical Research* **2010**, *43*, 695–704, PMID: 20205447.

[37] Carretti, E.; Dei, L.; Miliani, C.; Baglioni, P. In *Trends in Colloid and Interface Science XV*; Koutsoukos, P. G., Ed.; Springer Berlin Heidelberg: Berlin, Heidelberg, 2001; pp 63–67.

[38] Scharff, E. I.; Koepke, J.; Fritzsch, G.; Lücke, C.; Rüterjans, H. *Structure* **2001**, *9*, 493–502.

[39] Bonn, D.; Eggers, J.; Indekeu, J.; Meunier, J.; Rolley, E. *Rev. Mod. Phys.* **2009**, *81*, 739–805.

[40] Young, T. *Philosophical Transactions of the Royal Society of London* **1805**, *95*, 65–87.

[41] Kumar, G.; Prabhu, K. N. *Advances in Colloid and Interface Science* **2007**, *133*, 61 – 89.

[42] Yuan, Y.; Lee, T. R. In *Surface Science Techniques*; Bracco, G., Holst, B., Eds.; Springer Berlin Heidelberg: Berlin, Heidelberg, 2013; pp 3–34.

[43] Johnson, R. E.; Dettre, R. H.; Brandreth, D. A. *Journal of Colloid and Interface Science* **1977**, *62*, 205 – 212.

[44] Seebergh, J. E.; Berg, J. C. *Chemical Engineering Science* **1992**, *47*, 4455 – 4464.

[45] Eral, H. B.; 't Mannetje, D. J. C. M.; Oh, J. M. *Colloid and Polymer Science* **2013**, *291*, 247–260.

[46] Wenzel, R. N. *Industrial & Engineering Chemistry* **1936**, *28*, 988–994.

[47] Cassie, A.; Baxter, S. *Transactions of the Faraday Society* **1944**, *40*, 546–551.

[48] Milne, A.; Elliott, J.; Zabeti, P.; Zhou, J.; Amirfazli, A. *Physical Chemistry Chemical Physics* **2011**, *13*, 16208–16219.

[49] Milne, A.; Elliott, J.; Amirfazli, A. *Physical Chemistry Chemical Physics* **2015**, *17*, 5574–5585.

[50] Yaminsky, V.; Nylander, T.; Ninham, B. *Langmuir* **1997**, *13*, 1746–1757.

[51] Starov, V. M.; Kosvintsev, S. R.; Velarde, M. G. *Journal of colloid and interface science* **2000**, *227*, 185–190.

[52] Cachile, M.; Cazabat, A.; Bardon, S.; Valignat, M.; Vandenbrouck, F. *Colloids and Surfaces A: Physicochemical and Engineering Aspects* **1999**, *159*, 47–56.

[53] Paria, S.; Khilar, K. C. *Advances in colloid and interface science* **2004**, *110*, 75–95.

[54] Paria, S.; Manohar, C.; Khilar, K. C. *Industrial & engineering chemistry research* **2005**, *44*, 3091–3098.

[55] Atkin, R.; Craig, V.; Biggs, S. *Langmuir* **2000**, *16*, 9374–9380.

[56] von Bahr, M.; Tiberg, F.; Zhmud, B. V. *Langmuir* **1999**, *15*, 7069–7075.

[57] Venzmer, J. *Current Opinion in Colloid & Interface Science* **2011**, *16*, 335–343.

[58] Lang, P.; Steitz, R.; Braun, C. *Colloids. Surf. A* **2000**, *163*, 91–101.

[59] Klapp, S. H. L.; Zeng, Y.; von KLitzing, R. *Physical Review Letters* **2008**, *100*, 118303(1)–118303(4).

[60] Gerstenberg, M. C.; Pedersen, J. S.; Smith, G. S. *Phys. Rev. E* **1998**, *58*, 8028–8031.

[61] Gerstenberg, M. C.; Pedersen, J. S.; J., M.; Smith, G. S. *Langmuir* **2002**, *18*, 4933–4943.

[62] Gerstenberg, M. C.; Pedersen, J. S. *Langmuir* **2001**, *17*, 7040–7046.

[63] Lang, P. *Journal of Physics: Condensed Matter* **2004**, *16*, R699–R720.

[64] Fragneto-Cusani, G. *Journal of Physics: Condensed Matter* **2001**, *13*, 4973.

[65] Majewski, J.; Kuhl, T. L.; Wong, J. Y.; Smith, G. S. *Rev. Mol. Biotechnol.* **2000**, *74*, 207 – 231.

[66] Müller-Buschbaum, P. *Polymer journal* **2013**, *45*, 34–42.

[67] Petrov, P.; Olsson, U.; Wennerström, H. *Langmuir* **1997**, *13*, 3331–3337.

[68] Bowers, J.; ; Vergara-Gutierrez, M. C.; Webster, J. R. P. *Langmuir* **2004**, *20*, 309–312.

[69] Hamilton, W. A.; Porcar, L.; Butler, P. D.; Warr, G. G. *J. Chem. Phys* **2002**, *116*, 8533–8546.

[70] Gelbart, W. M.; Ben-Shaul, A. *The Journal of Physical Chemistry* **1996**, *100*, 13169–13189.

[71] Zeng, Y.; Schön, S.; von Klitzing, R. *Journal of Colloid and Interface Science* **2015**, *449*, 522 – 529, Liquid Films, Interfaces and Colloidal DispersionsHonoring Professor Darsh T. Wasan.

[72] Zeng, Y.; Grandner, S.; Oliveira, C. L.; Thünemann, A. F.; Paris, O.; Pedersen, J. S.; Klapp, S. H.; von Klitzing, R. *Soft Matter* **2011**, *7*, 10899–10909.

[73] Uzum, C.; Makuska, R.; von Klitzing, R. *Macromolecules* **2012**, *45*, 3168–3176.

[74] Zhou, X.-L.; Lee, L.-T.; Chen, S.-H.; Strey, R. *Phys. Rev. A* **1992**, *46*, 6479–6489.

[75] Lee, D. D.; Chen, S. H.; Majkrzak, C. F.; Satija, S. K. *Phys. Rev. E* **1995**, *52*, R29–R32.

[76] Kerscher, M.; Busch, P.; Mattauch, S.; Frielinghaus, H.; Richter, D.; Belushkin, M.; Gompper, G. *Phys. Rev. E* **2011**, *83*, 030401.

[77] Frielinghaus, H.; Kerscher, M.; Holderer, O.; Monkenbusch, M.; Richter, D. *Physical Review E* **2012**, *85*, 041408.

[78] Berghaus, M.; Paulus, M.; Salmen, P.; Al-Ayoubi, S.; Tolan, M.; Winter, R. *The Journal of Physical Chemistry B* **2016**, *120*, 7148–7153.

[79] Kraska, M.; Domschke, M.; Stühn, B. *Soft Matter* **2013**, *9*, 3488–3496.

[80] Fries, N. *Capillary transport processes in porous materials-experiment and model*; Cuvillier, 2010.

[81] Feoktystov, A. V.; Frielinghaus, H.; Di, Z.; Jaksch, S.; Pipich, V.; Appavou, M.-S.; Babcock, E.; Hanslik, R.; Engels, R.; Kemmerling, G.; Kleines, H.; Ioffe, A.; Richter, D.; Brückel, T. *Journal of Applied Crystallography* **2015**, *48*, 61–70.

[82] Frielinghaus, H.; Feoktystov, A.; Berts, I.; Mangiapia, G. *Journal of large-scale research facilities JLSRF* **2015**, *1*, 28.

[83] Teubner, M. *Journal of Chemical Physics* **1990**, *92*, 4501–4507.

[84] Strey, R.; Winkler, J.; Magid, L. *Journal of Physical Chemistry* **1991**, *95*, 7502–7507.

[85] Gompper, G.; Endo, H.; Mihailescu, M.; Allgaier, J.; Monkenbusch, M.; Richter, D.; Jakobs, B.; Sottmann, T.; Strey, R. *EPL* **2001**, *56*, 683.

[86] Gompper, G.; Kroll, D. *Physical Review Letters* **1998**, *81*, 2284.

[87] Schubert, V.; Strey, R.; Kline, S. R.; Kaler, E. W. *The Journal of Chemical Physics* **1994**, *101*, 5343–5355.

[88] Leitao, H.; Telo da Gama, M. M.; Strey, R. *The Journal of Chemical Physics* **1998**, *108*, 4189–4198.

[89] Pieruschka, P.; Safran, S. *EPL* **1995**, *31*, 207.

[90] Morse, D. C. *Phys. Rev. E* **1994**, *50*, R2423.

[91] Sinha, S. K.; Sirota, E. B.; Garoff, S.; Stanley, H. B. *Phys. Rev. B* **1988**, *38*, 2297–2311.

[92] Lee, D. D.; Chen, S. H.; Majkrzak, C. F.; Satija, S. K. *Phys. Rev. E* **1995**, *52*, R29–R32.

[93] Gompper, G.; Schick, M. *Physical Review Letters* **1990**, *65*, 1116–1119.

[94] Chernov, A. A.; Mikheev, L. V. *Physical Review Letters* **1988**, *60*, 2488–2491.

[95] Charitat, T.; Lecuyer, S.; Fragneto, G. *Biointerphases* **2008**, *3*, FB3–FB15.

[96] Busscher, H.; van Pelt, A.; de Boer, P.; de Jong, H.; Arends, J. *Colloids and Surfaces* **1984**, *9*, 319 – 331.

[97] Janczuk, B.; Biallopiotrowicz, T. *Journal of Colloid and Interface Science* **1989**, *127*, 189 – 204.

[98] Rame, E. *Journal of colloid and interface science* **1997**, *185*, 245–251.

[99] Rupp, F.; Axmann, D.; Ziegler, C.; Geis-Gerstorfer, J. *Journal of Biomedical Materials Research* **2002**, *62*, 567–578.

[100] Keller, A.; Broje, V.; Setty, K. *Journal of Petroleum Science and Engineering* **2007**, *58*, 201 – 206.

[101] Kirdponpattara, S.; Phisalaphong, M.; Newby, B.-m. Z. *Journal of colloid and interface science* **2013**, *397*, 169–176.

[102] Alghunaim, A.; Kirdponpattara, S.; Newby, B.-m. Z. *Powder Technology* **2016**, *287*, 201–215.

[103] Perkampus, H.-H. *UV-VIS Spectroscopy and Its Applications*; Springer Berlin Heidelberg: Berlin, Heidelberg, 1992; pp 3–9.

[104] Edwards, A. A.; Alexander, B. D. UV-visible Absorption Spectroscopy, Organic Application. 2010.

[105] Larkin, P. In *Infrared and Raman Spectroscopy*; Larkin, P., Ed.; Elsevier: Oxford, 2011; pp 7 – 25.

[106] Buergi, T. In *Biointerface Characterization by Advanced {IR} Spectroscopy*; Pradier, C., Chabal, Y., Eds.; Elsevier: Amsterdam, 2011; pp 115 – 144.

[107] Claesson, P.; van der Wal, A.; Fogden, A. *Handbook for Cleaning/Decontamination of Surfaces* **2007**,

[108] McMaster, M. C. *HPLC: A Practical User's Guide*; Wiley, 2006; pp 4–6.

[109] Baier, J.; Koetz, J.; Kosmella, S.; Tiersch, B.; Rehage, H. *Journal of Physical Chemistry B* **2007**, *111*, 8612–8618.

[110] Davidovich, I.; Issman, L.; de Paula, C.; Ben-Barak, I.; Talmon, Y. *Colloid and Polymer Science* **2015**, *293*, 3189–3197.

[111] Lutter, S.; Koetz, J.; Tiersch, B.; Kosmella, S. *Journal of Dispersion Science and Technology* **2009**, *30*, 745–752.

[112] Ly, M.; Margaritis, A.; Jajuee, B. *Biotechnology and bioengineering* **2007**, *96*, 67–79.

[113] PELEG, M. *Journal of Food Science* **1988**, *53*, 1216–1217.

[114] Planinić, M.; Velić, D.; Tomas, S.; Bilić, M.; Bucić, A. *European Food Research and Technology* **2005**, *221*, 446–451.

[115] Zwietering, M.; de Koos, J.; Hasenack, B.; de Witt, J.; van't Riet, K. *Applied and Environmental Microbiology* **1991**, *57*, 1094–1101.

[116] Karacabey, E.; Mazza, G.; Bayindirli, L.; Artik, N. *Food Bioprod. Process.* **2012**, *5*, 359–371.

[117] Stehle, R.; Schulreich, C.; Wellert, S.; Gäb, J.; Blum, M.-M.; Kehe, K.; Richardt, A.; Lapp, A.; Hellweg, T. *Journal of Colloid and Interface Science* **2014**, *413*, 127–132.

[118] Boonme, P.; Krauel, K.; Graf, A.; Rades, T.; Junyaprasert, V. B. *Aaps Pharmscitech* **2006**, *7*.

[119] Tchakalova, V.; Bailly, C.; Fieber, W. *Flavour Frag. J.* **2014**, *29*, 67–74.

[120] Sottmann, T.; Kluge, K.; ; Strey, R.; Reimer, J.; Söderman, O. *Langmuir* **2002**, *18*, 3058–3067.

[121] Panapisal, V.; Charoensri, S.; Tantituvanont, A. *AAPS PharmSciTech* **2012**, *13*, 389–399.

[122] Thomas, L. L.; Christakis, T. J.; ; Jorgensen*, W. L. *Journal of Physical Chemistry B* **2006**, *110*, 21198–21204, PMID: 17048945.

[123] Kaur, G.; Chiappisi, L.; Prévost, S.; Schweins, R.; Gradzielski, M.; Mehta, S. K. *Langmuir* **2012**, *28*, 10640–10652.

[124] Harrar, A.; Zech, O.; Klaus, A.; Bauduin, P.; Kunz, W. *Journal of Colloid and Interface Science* **2011**, *362*, 423 – 429.

[125] Arleth, L.; Marcelja, S.; Zemb, T. *J. Chem. Phys* **2001**, *115*, 3923–3936.

[126] Gee, M. L.; Israelachvili, J. N. *J. Chem. Soc., Faraday Trans.* **1990**, *86*, 4049–4058.

[127] Gompper, G.; Zschocke, S. *Phys. Rev. A* **1992**, *46*, 4836–4851.

[128] Vargas-Ruiz, S.; Schulreich, C.; Kostevic, A.; Tiersch, B.; Koetz, J.; Kakorin, S.; von Klitzing, R.; Jung, M.; Hellweg, T.; Wellert, S. *Journal of Colloid and Interface Science* **2016**, *471*, 118 – 126.

[129] Boonme, P. *J. Cosmet. Dermatol.* **2007**, *6*, 223–228.

[130] Kalaitzaki, A.; Emo, M.; Stébé, M. J.; Xenakis, A.; Papadimitriou, V. *Food Res. Int.* **2013**, *54*, 1448 – 1454.

[131] Bera, A.; Mandal, A. *Journal of Petroleum Exploration and Production Technology* **2014**, *5*, 255–268.

[132] Lawrence, M.; Rees, G. D. *Adv. Drug. Deliv. Rev.* **2000**, *45*, 89 – 121.

[133] Reed, R. L.; Healy, R. N. *Society of Petroleum Engineers Journal* **1984**, *24*, 342–350.

[134] Wellert, S.; Imhof, H.; Dolle, M.; Altmann, H.-J.; Richardt, A.; Hellweg, T. *Colloid and Polymer Science* **2007**, *286*, 417–426.

[135] Lin, Y.; Wang, L.; Krumpfer, J. W.; Watkins, J. J.; McCarthy, T. J. *Langmuir* **2013**, *29*, 1329–1332, PMID: 23327535.

[136] Zhu, M.; Lerum, M. Z.; Chen, W. *Langmuir* **2012**, *28*, 416–423, PMID: 22128807.

[137] Horng, P.; Brindza, M. R.; Walker, R. A.; Fourkas, J. T. *The Journal of Physical Chemistry C* **2010**, *114*, 394–402.

[138] Starov, V. M.; Velarde, M. G. *Journal of Physics: Condensed Matter* **2009**, *21*, 464121.

[139] Krishnan, A.; Liu, Y.-H.; Cha, P.; Woodward, R.; Allara, D.; Vogler, E. A. *Colloids and Surfaces B: Biointerfaces* **2005**, *43*, 95 – 98.

[140] Pierce, E.; Carmona, F.; Amirfazli, A. *Colloids and Surfaces A: Physicochemical and Engineering Aspects* **2008**, *323*, 73 – 82.

[141] Vogler, E. A. *Langmuir* **1992**, *8*, 2013–2020.

[142] Grewal, H.; Kim, H. N.; Cho, I.-J.; Yoon, E.-S. *Scientific reports* **2015**, *5*.

[143] Yang, Y.-W.; Zografi, G.; Miller, E. E. *Journal of Colloid and Interface Science* **1988**, *122*, 35 – 46.

[144] Subrahmanyam, T.; Prestidge, C.; Ralston, J. *Minerals Engineering* **1996**, *9*, 727 – 741.

[145] Subrahmanyam, T.; Monte, M.; Middea, A.; Valdiviezo, E.; Lins, F. *Minerals Engineering* **1999**, *12*, 1347 – 1357.

[146] Brown, S.; Oliveira, R.; Moudgii, B. *Functional Fillers and Nanoscale particles. Colorado, USA: Society for Mining, Metallurgy and Exploration, Inc* **2003**, 105–12.

[147] Carlos Ramirez-Flores, J.; Bachmann, J. *Journal of Plant Nutrition and Soil Science* **2013**, *176*, 19–16.

[148] Duarte-Davidson, R.; Orford, R.; Wyke, S.; Griffiths, M.; Amlôt, R.; Chilcott, R. *Environ. Int.* **2014**, *72*, 3–14.

[149] Gorzkowska-Sobas, A. A. Chemical warfare agents and their interactions with solid surfaces. FFI-Rapport 2013/00574, Norwegian Defence Research Establishment (FFI), 2013.

[150] Brevett, C. A.; Sumpter, K. B.; Wagner, G. W.; Rice, J. S. *Journal of Hazardous Materials* **2007**, *140*, 353 – 360.

[151] Brevett, C. A.; Sumpter, K. B.; Nickol, R. G. *Journal of Hazardous Materials* **2009**, *162*, 281 – 291.

[152] Mizrahi, D. M.; Goldvaser, M.; Columbus, I. *Environmental science & technology* **2011**, *45*, 3466–3472.

[153] Malhotra, R.; Ganesan, K.; Sugendran, K.; Swamy, R. *Defence Science Journal* **1999**, *49*, 97.

[154] Levkin, P. A.; Svec, F.; Frechet, J. M. J. *Advanced Functional Materials* **2009**, *19*, 1993–1998.

[155] Eeltink, S.; Geiser, L.; Svec, F.; Frechet, J. *Journal of Separation Science* **2007**, *30*, 2814–2820.

[156] Peters, E.; Petro, M.; Svec, F.; Frechet, J. *Analytical Chemistry* **1998**, *70*, 2296–2302.